

Analysis of Millimeter Wave Wireless Relay Networks

by

Khagendra Belbase

A thesis submitted in partial fulfillment of the requirements for the degree of

Doctor of Philosophy

in

Communications

Department of Electrical and Computer Engineering

University of Alberta

© Khagendra Belbase, 2019

Abstract

Fifth generation (5G) wireless networks must handle massive data rates given the recent and future demand growth. A solution is the use of millimeter wave (mmW) bands (20–100 GHz) which can leverage massive bandwidths (up to 5 GHz). However, mmW signals experience high path loss, directivity and blockages. Moreover, node locations are becoming increasingly random due to deployment constraints which limits the performance of these networks. To overcome these challenges, this thesis makes several contributions on the deployment of randomly located mmW relays to enhance the coverage and rate. First, an analytical framework is developed for the coverage and rate of a decode-and-forward relay network with a best relay selection by incorporating mmW channel impairments and by using stochastic geometry technique to model the relay locations. Second, a multi-hop network is analyzed in noise-limited and interference-limited regimes to characterize the coverage, error rate, and ergodic capacity by developing the end-to-end signal-to-noise ratio distribution. Third, to improve the relaying spectral efficiency and coverage, two-way relays with two users exchanging their message is analyzed by selecting a best relay from a set of randomly located nodes. Finally, coverage is analyzed when non-orthogonal multiple access is utilized in mmW relaying for several relay selection strategies. This thesis demonstrates that these relaying techniques improve coverage and rate significantly when appropriate relay selection is performed.

~

Preface

This thesis presents the original work by Khagendra Belbase, some parts of which have been published or submitted to journals or conferences, which are listed as follows:

Chapter 3 of this thesis has been published as K. Belbase, Z. Zhang, H. Jiang, and C. Tellambura, “Coverage Analysis of Millimeter Wave Decode-and-Forward Networks With Best Relay Selection,” *IEEE Access*, vol. 6, pp. 22670-22683, April 2018. A part of the contribution of this chapter has been also published as K. Belbase, H. Jiang, and C. Tellambura, “Coverage Analysis of Decode-and-Forward Relaying in Millimeter Wave Networks,” in *Proc. IEEE International Conference on Communications (ICC)*, May 2018.

Chapter 4 of this thesis has been submitted to *IEEE Access* as K. Belbase, C. Tellambura, and H. Jiang, “Coverage, Capacity, and Error Rate Analysis of Multi-Hop Millimeter-Wave Decode and Forward Relaying,”.

Chapter 5 of this thesis has been published as K. Belbase, C. Tellambura, and H. Jiang, “Two-way relay selection for millimeter wave networks,” *IEEE Communications Letters*, vol. 22, no. 1, pp. 201–204, January 2018.

Chapter 6 of this thesis has been submitted to *IEEE Communications Letters* as K. Belbase, C. Tellambura, and H. Jiang, “Coverage Analysis of Cooperative NOMA in Millimeter Wave Networks,”.

~

Dedicated to my parents . . .

Acknowledgements

First of all, I express my deepest gratitude to my co-supervisors, Dr. Chintha Tellambura and Dr. Hai Jiang, for their excellent mentorship and patience during my PhD study. It would not be possible to complete this thesis without their continued support, effective guidance and timely feedback.

I also extend my sincere gratitude to Dr. Yindi Jing for her time and interest to serve as one of my PhD supervisory committee members and for providing valuable feedback during my PhD candidacy and final examinations. I am also grateful to my external examiner Dr. Ha H. Nguyen from University of Saskatchewan for his valuable comments and suggestions during my final examination. Many thanks to Dr. Hao Liang for providing valuable feedback and suggestions during my PhD candidacy and final examinations. I also extend my thanks to Dr. Witold Krzysiecin for providing valuable feedback during my PhD candidacy examination.

My sincere thanks to my seniors: Vesh, Yamuna, Prasanna, and Sachitha for sharing their experiences and creating a conducive environment in the lab. I am also grateful to all my lab-mates in iCore Wireless Communications Lab W5-070 and Advanced Wireless Communications and Signal Processing Lab W5-077 for productive discussions and motivation they provided. I also express my sincere appreciation to all my friends in NESAs for their support and for the joyous time during the PhD years.

Most importantly, I am completely indebted to my parents, my wife, my sisters and other family members for their inspiration and unequivocal support during my PhD journey. Many thanks to my son, who was born just before I started writing this thesis, for providing me with the determination to complete it on time and for bringing joy to our family.

~

Contents

List of Figures	ix
List of Tables	xii
1 Introduction	1
1.1 5G Cellular - Next Generation of Mobile Communication	2
1.1.1 5G Use Cases	2
1.1.2 Enablers of High Data Rates in 5G	4
1.2 Millimeter Wave Communication	5
1.2.1 Standardization of mmW networks	7
1.3 Relays	8
1.4 Non-orthogonal Multiple Access	9
1.5 Motivation and Problem Statements	9
1.6 Outline of the Thesis and Major Contributions	11
2 Background	14
2.1 Key Aspects of Millimeter Communications	14
2.1.1 MmW Channel Modeling	14
2.1.2 Path Loss Modeling	15
2.1.3 Small-scale Fading	16
2.1.4 Directional Beamforming Modeling	17
2.1.5 Blockage Modeling	19
2.2 Relays	21
2.2.1 One-way Relaying	22
2.2.2 Two-way Relaying	23

2.2.3	Multi-hop Relaying	23
2.3	Stochastic Geometry in Wireless Networks	24
2.3.1	Properties of the PPP	28
2.4	Non-Orthogonal Multiple Access (NOMA)	29
3	Coverage Analysis of Millimeter Wave Decode-and-Forward Networks With Best Relay Selection	31
3.1	Introduction and Motivation	31
3.1.1	Problem Statement and Contributions	34
3.2	System Model	35
3.2.1	Network Modeling	35
3.2.2	SNR Model	36
3.3	Performance Analysis	37
3.3.1	Direct Mode	37
3.3.2	Relay Selection	39
3.3.3	Coverage Probability With Random Relay Selection	46
3.4	Some Extensions	48
3.4.1	Coverage Probability With Beam Alignment Errors	48
3.4.2	Effect of power allocation factor	49
3.4.3	Rate Coverage Probability	49
3.4.4	Average Throughput	50
3.5	Simulation and Analytical Results	50
3.6	Summary	59
4	Coverage, Capacity, and Error Rate Analysis of Multi-Hop Millimeter-Wave Decode and Forward Relaying	60
4.1	Introduction and Motivation	61
4.1.1	Performance analysis of sub-6 GHz multi-hop relays	62
4.1.2	Performance analysis of mmW multi-hop networks	62
4.1.3	Problem Statement and Contributions	63
4.2	System Model	64
4.2.1	Network Modeling	64

4.2.2	Path Loss Modeling	65
4.2.3	Received Signal Model	65
4.3	Performance of Noise Limited Network	66
4.3.1	Distribution of the destination SNR	67
4.3.2	SNR Coverage Probability	69
4.3.3	Rate Coverage Probability	69
4.3.4	Ergodic Capacity	70
4.3.5	SER Analysis	72
4.4	Performance of Interference-Limited Network	76
4.4.1	Case 1: Interference powers are i.i.d.	77
4.4.2	Case 2: Interference powers are i.n.i.d.	79
4.4.3	Ergodic Capacity	81
4.4.4	SER Analysis	83
4.5	Results and Discussion	84
4.5.1	Noise-limited Regime	85
4.5.2	Interference-limited Regime	90
4.6	Summary	93
5	Two-Way Relay Selection in Millimeter Wave Networks	95
5.1	Introduction	95
5.2	System Model	96
5.2.1	Network Modeling	96
5.2.2	Path Loss, Directivity and Blockage Modeling	97
5.2.3	SNR Modeling	97
5.3	Relay Selection	99
5.3.1	Coverage Probability	99
5.3.2	CDF expression of γ_z	100
5.3.3	Coverage Probability with Beam Alignment Errors	102
5.4	Numerical Results and Simulations	103
5.5	Summary	104

6	Coverage Analysis of Cooperative NOMA in Millimeter Wave Networks	105
6.1	Introduction	105
6.2	System Model	106
6.3	Coverage Analysis	108
6.3.1	Relay Selection	108
6.4	Numerical Results	113
6.5	Summary	115
7	Conclusion and Future Research Directions	116
7.1	Conclusion and Summary of Contributions	116
7.2	Future Research Directions	118
	Appendices	120
A	Derivations for Chapter 3	120
A.1	Proof of Lemma 4	120
B	Derivations for Chapter 4	122
B.1	Proof of Lemma 7	122
B.2	Proof of Proposition 8	122
B.3	Proof of Lemma 10	123
B.4	Proof of Lemma 11	124
B.5	Proof of Proposition 9	125
	Bibliography	130

List of Figures

1.1	Expected worldwide mobile data demand [1].	2
1.2	Three different use cases of 5G [2].	3
1.3	An overview of spectrum availability in sub-6 GHz and mmW frequency bands in the US.	5
1.4	Millimeter wave cellular network with a base station, relays, blocking objects, and user equipments (UEs).	6
2.1	A sectoral antenna model [3].	17
2.2	Random shape theory model for blockages where the irregular LOS region to a typical user is approximated by a ball in the fixed LOS ball model [4].	19
2.3	LOS probability (2.9) for different blockage densities with $\mathbb{E}[L] = \mathbb{E}[W] = 15$ m.	20
2.4	A basic one way relay operation.	22
2.5	A basic two way relay operation.	23
2.6	A realization of a homogeneous PPP with $\lambda = 10^{-4}$ on $[0, 1000]^2$ area.	26
2.7	A realization of an inhomogeneous PPP with a density function $\lambda(x, y) = (1 + \cos(x)) e^{-\frac{y}{5}}$ on $[0, 20]^2$. As the function indicates, the point density is periodic along x and decreases along y	27
2.8	Two user downlink NOMA using power domain multiplexing.	30
3.1	Geometrical locations of S , D and a typical relay (R).	36
3.2	One snapshot of relay locations with S and D as shown. The potential relays (dots) form a PPP. The decoding set is clustered around S . Its nodes form an inhomogeneous PPP. In the decoding set, the node with minimum path loss to D is selected as the relay.	42

3.3	Size of the decoding set versus SNR threshold for different relay densities, $W = 300$ m.	52
3.4	Association probability of destination (D) with LOS and NLOS relays for different relay densities for $W = 300$ m.	52
3.5	Coverage probability vs. SNR thresholds with direct link, relay selection and random relay for different relay densities when $W = 300$ m.	53
3.6	Association probability of the destination (D) with LOS and NLOS relays versus the $S - D$ distance W ($\lambda = 100/\text{km}^2$).	54
3.7	Coverage probability versus W for different SNR thresholds, $\lambda = 100/\text{km}^2$	55
3.8	Coverage probability versus ξ for different SNR thresholds ($W = 300$ m, $\lambda = 100/\text{km}^2$).	56
3.9	Coverage Probability versus SNR threshold for different beamforming errors when $\lambda = 200/\text{km}^2$ and $W = 300$ m.	57
3.10	Rate Coverage versus rate threshold for different relay densities when $W = 200$ m.	58
3.11	Spectrum Efficiency versus SNR threshold for different relay densities when $W = 300$ m.	58
4.1	A multi-hop wireless relay network.	64
4.2	Co-channel interferences at relay and destination nodes.	77
4.3	CCDF of per hop SIR plotted along x (dB) using <i>Welch-Satterthwaite Approximation</i> (Lemma 9), MGF approach (Lemma 10), and simulation. N_L and N_N denote the number of LOS and NLOS interferers, respectively, which are located at different distance to realize i.n.i.d. interference powers. The CCDF curves also refer to the per hop coverage probability along the SIR threshold of x dB.	80
4.4	Coverage versus SNR thresholds for different K	85
4.5	Outage Probability versus average per hop SNR for different SNR thresholds.	86
4.6	Coverage probability versus blockage density (η) at $\gamma_{\text{th}} = 10$ dB for different number of hops (K), $D = 500$ m.	86
4.7	Rate coverage vs rate threshold ($D = 500$) m.	88

4.8	Ergodic capacity vs $\bar{\gamma}$, $K = 2, 3, 5$	88
4.9	SER versus $\bar{\gamma}$ for DBPSK, BPSK and 4-QAM, $K = 3$	89
4.10	Ergodic capacity vs number of hops (K) for different average per hop SNRs.	90
4.11	Coverage versus SIR thresholds for different K	91
4.12	Outage Probability versus average per hop SIR for different SIR thresholds.	92
4.13	Ergodic capacity vs $\bar{\xi}$, $K = 2, 3$	92
4.14	SER versus $\bar{\xi}$ for BPSK for $K = 2$ and $K = 5$	93
5.1	Two-way relay network. Relay R_j is selected from a set of potential relay nodes (triangles).	96
5.2	Coverage vs. SNR threshold for several relay densities.	102
5.3	Coverage vs. SNR threshold for different beam alignment errors (σ_E), when $\phi = 30^\circ$ and $\lambda = 20/\text{km}^2$	103
5.4	Average user throughput for different SNR thresholds.	104
6.1	Coverage probability vs transmit power for NOMA using $\mathcal{S}_1, \mathcal{S}_2$ and \mathcal{S}_3 and OMA, where the curves (a) are for $\{R_D, R_R\} = \{1, 3\}$ bps/Hz, and (b) for $\{R_D, R_R\} = \{1.9, 6\}$ bps/Hz.	114
6.2	Coverage probability vs relay density for rate thresholds $\{R_D, R_R\} = \{1, 3\}$ bps/Hz with $P_S = P_R = 0$ dB. The curves (a) are for $\mu = 2 \times 10^{-4}/\text{m}^2$, and (b) are for $\mu = 5 \times 10^{-4}/\text{m}^2$	114
B.1	Integration contour.	126

List of Tables

3.1	Simulation Parameters	51
4.1	Notations and Simulation Parameters	84

List of Symbols and Notations

Notation	Definition
$\binom{n}{k}$	binomial coefficient, n choose k
$\mathcal{B}(a, b)$	$\int_0^1 t^{a-1}(1-t)^{b-1} dt$ (Euler's beta function)
$\Gamma(x, a)$	$\int_a^\infty t^{x-1} e^{-t} dt$
$\Gamma(x)$	$\Gamma(x, 0)$
${}_2F_1(, ; ;)$	Gauss' hypergeometric function [5, (eq. 9.100)]
$f_X(\cdot)$	probability density function (PDF)
$F_X(\cdot)$	cumulative distribution function (CDF)
$\tilde{F}_X(\cdot)$	complimentary cumulative distribution function (CCDF)
$\mathcal{G}(\alpha, \lambda)$	Gamma distribution with $f_X(x) = \frac{\lambda^\alpha}{\Gamma(\alpha)} x^{\alpha-1} e^{-\lambda x}$, $x > 0$, with rate parameter $\lambda > 0$ and shape parameter $\alpha \geq 1$.
$k!$	factorial of k
$\mathcal{LN}(\mu, \sigma^2)$	log-normal distribution with $f_X(x) = \frac{1}{\sqrt{2\pi x \sigma}} \exp\left(-\frac{(\ln x - \mu)^2}{2\sigma^2}\right)$, $x > 0$.
$M_X(\cdot)$	moment generating function (MGF)
$\mathbb{E}_X[\cdot]$	expectation with respect to X
$\mathbb{P}(A)$	probability of event A
\mathbb{R}^2	two-dimensional real plane

~

Acronyms / List of Abbreviations

Acronym	Meaning
3GPP	Third Generation Partnership Project
BPSK	binary phase shift keying
CCDF	complementary cumulative distribution function
CDF	cumulative distribution function
DBPSK	differential binary phase shift keying
FSK	frequency shift keying
LOS	line-of-sight
LTE	Long Term Evolution
MGF	moment generating function
MIMO	multiple input multiple output
mmW	millimeter wave
MPSK	M-ary phase shift keying
M-QAM	M-ary quadrature amplitude modulation
NLOS	non-line-of-sight
NOMA	non-orthogonal multiple access
PDF	probability density function
PPP	Poisson point process
r.v.	random variable
SER	symbol error rate
SINR	signal to interference-plus-noise ratio
SNR	signal to noise ratio

~

Chapter 1

Introduction

The ubiquity of mobile communication brought about by decreasing device costs and increasing services is contributing significantly to the increased number of connections as well as the per-device data consumption. Specifically, current cellular networks have seen an unprecedented data growth due to proliferation of smartphones and bandwidth-intensive video and multimedia applications. Ericsson has predicted that the volume of mobile data traffic will increase five folds from 2018 to 2024, reaching 136 exabytes per month (Fig. 1.1), equivalent to a compound annual growth rate of 31% [1]. This ever growing trend is expected to continue mainly due to the services that require massive data, such as high definition video streaming, online gaming, and virtual reality applications [2]. For example, video streaming contributed 60% (~ 16 exabytes/month) of total mobile traffic in 2018, which is expected to reach 74% (~ 100 exabytes/month) by 2024 [1]. In addition, billions of new devices envisioned to be connected in the future generation of wireless networks to provide massive connectivity are also expected to contribute to the increase in data consumption [1], [6].

These incessant demand for improved services and data rates has led to the development of new generation of mobile communication standards every decade since the introduction of first generation (1G) in early 1980s, to the fourth generation (4G) in 2010 [7]. Right now, extensive efforts are being made by industries, regulators, and standardization bodies to develop fifth generation (5G) mobile communication with a target of commercial deployment starting from 2020 [2]. From the third generation (3G) onward, the development of each new generation started with a set of service quality requirements set out by International Telecommunications Union, a United Nations regulatory body; namely, IMT-2000

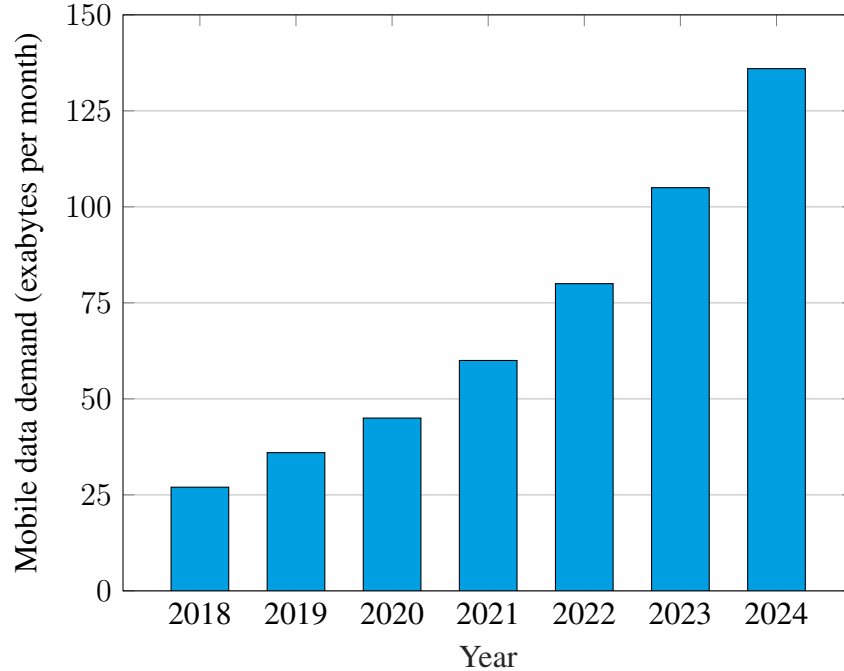


Figure 1.1: Expected worldwide mobile data demand [1].

for 3G, IMT-A for 4G, and IMT-2020 for 5G mobile cellular. This process is driven by the standardization body, Third Generation Partnership Project (3GPP), which was formed by major wireless industry players, and is continuing to release the standards up until now for 5G. For instance, the latest 3GPP standard is Release 15, which targets to meet IMT-2020 requirements for 5G cellular networks [8].

1.1 5G Cellular - Next Generation of Mobile Communication

Unlike the evolution from 1G to 4G, where the motivation was to improve a particular aspect of mobile communication (for example, 1G to 2G transition improved voice service and increased network capacity using digital communications, and 3G and 4G were developed to improve the data rates), the evolution of 5G features concurrent improvements in many areas. Specifically, they include high data rates (1 – 10 Gbps), low latency (less than 1 milliseconds), massive connectivity (\sim tens of billions new devices), and better quality of service [9]–[11].

1.1.1 5G Use Cases

The IMT-2020 requirements to be implemented by 5G networks are mainly classified into three use cases (Fig. 1.2): (i) enhanced mobile broadband (eMBB), (ii) massive ma-

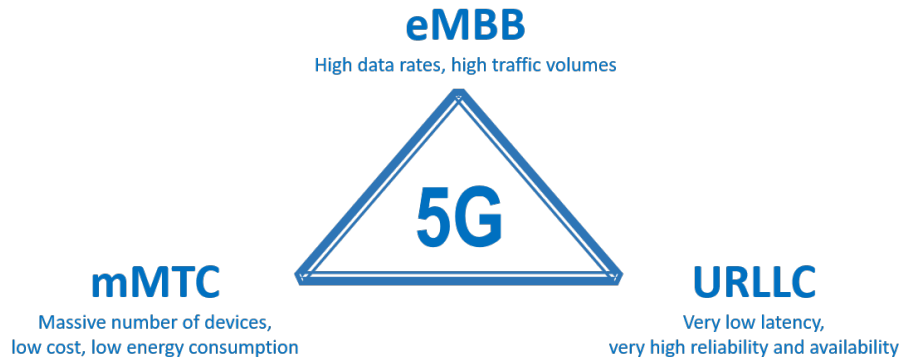


Figure 1.2: Three different use cases of 5G [2].

chine type communications (mMTC), and (iii) Ultra-reliable low latency communication (URLLC) [12], which are briefly summarized below. Note that, some services might fall in between these scenarios and some applications will require more than one of these use cases.

1. **Enhanced Mobile Broadband:** This refers to a straightforward improvement of the current mobile broadband technology (e.g., Long Term Evolution (LTE)) to achieve higher data rates with improved quality of service. Specifically, IMT-2020 requirements for 5G are: peak data rate of 20 Gbps in downlink, 10 Gbps in uplink, user perceived data rate of 100 Mbps in downlink and 50 Mbps in uplink, spectral efficiency of 30 bps/Hz in downlink and 15 bps/Hz in uplink [2], [12].
2. **Massive Machine Type Communications:** Billions of new devices will be connected to Internet of Things networks. These devices will require connectivity, low data rates and high energy efficiency to allow for very long battery life (~ 10 years), which are the major design goals of massive machine type communications. These connected devices might include a variety of consumer devices, sensors, and actuators that generate a huge amount of data collectively. The IMT-2020 requirements specify that 5G needs to have 1 million devices/km² and area traffic capacity in downlink is 10 Mbit/s/m² [2], [12].
3. **Ultra Reliable Low Latency Communications:** These connections require extremely low error rates and end-to-end delay. Applications are vehicular communication, remote surgery, factory automation, and more. The IMT-2020 requirements

specify the user plane latency (end-to-end packet transmission time) of 1 ms and the transmission failure probability of less than 1 in 10^5 [2], [12].

1.1.2 Enablers of High Data Rates in 5G

To achieve the high data rates (e.g., to meet the enhanced mobile broadband requirements), some key technologies are expected to be the integral parts of 5G, which are discussed below briefly [9], [13].

- **Network Densification:** This includes densification over space (e.g, dense deployment of small cells) and frequency (utilizing larger portions of radio spectrum in diverse bands). Large-scale cost-effective spatial densification depends on intercell interference management, and the realization of its full benefits needs backhaul densification and advanced interference cancellation methods [14]. Similar to 4G LTE, network densification is a highly effective solution for 5G networks as well [9] and essentially leads to heterogeneous deployments of nodes where macro, micro, pico and femto cells coexist to improve the overall network capacity [15].
- **Massive Multiple-Input-Multiple-Output (MIMO):** The base station uses a large number of antenna elements compared to the number of active users using the same time-frequency resources in the network [16]. This improves the spectral efficiency due to the averaging out of channel fading via the law of larger numbers, thereby significantly reducing small-scale channel fading effects [9]. In addition, massive MIMO can improve the network capacity significantly due to aggressive spatial multiplexing and can achieve high energy efficiency due to the ability to use low power antennas that can focus the transmitted energy into a small spatial region, which motivates its widespread use in 5G cellular networks [16].
- **Millimeter Wave (mmW):** Due to the congestion of sub-6 GHz bands used by current cellular networks, mmW bands (20-100 GHz and more) ¹ can offer large bandwidths of 1 GHz or more to achieve massive data rates [18], [19]. To illustrate, the total sub-6 GHz bandwidth allocated to current commercial wireless systems is a small fraction of the total available bandwidth in mmW spectrum (Fig. 1.3).

¹Although the formal definition of mmW is 30-300 GHz, this thesis confines to 20-100 GHz to include 28 GHz spectrum, a promising band for mmW cellular [17].

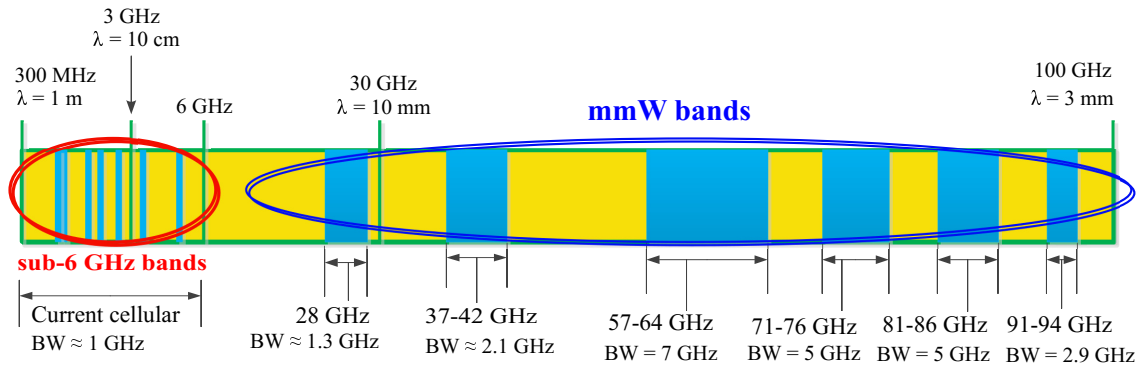


Figure 1.3: An overview of spectrum availability in sub-6 GHz and mmW frequency bands in the US.

1.2 Millimeter Wave Communication

Unlike sub 6-GHz bands, mmW bands suffer large signal attenuation with distance, cannot penetrate walls (specifically, brick, glass and metallic walls), and exhibit poor signal diffraction around the corners [17]. Therefore, mmW links are most reliable if a line of sight (LOS) path exists between the transmitter and receiver, and even a nearby receiver that falls in non line of sight (NLOS) condition may lack signal coverage [20].

The aforementioned losses can offset the link margins substantially, and the exploitation of vast mmW bandwidths becomes challenging. Thus, directional beamforming for mmW MIMO has been extensively developed [11], [18], [21]. This technique uses a large number (tens to hundreds) of antenna elements to form an antenna array which is capable of directing the large portion of signal power in the desired direction [11]. Antenna arrays are viable because of the continuous decrease in hardware costs and improved power efficiency [17]. Increased antenna element density (per unit area) is possible due to short mmW wavelengths (1 - 10 millimeters) [18]. Beamforming has an additional benefit of reducing co-channel interference at the receiver because the signal from any NLOS interferer is highly attenuated. Moreover, beamforming can enable, even if LOS link is not available, NLOS communications. The NLOS path can be formed by utilizing the reflectors and scatterers in the propagation environment [6]. The effect of blockage can be mitigated by using relays which can receive a signal from transmitter and forward to the intended receiver [20].

Although existing commercial wireless standards such as IEEE 802.15.3c and 802.11ad

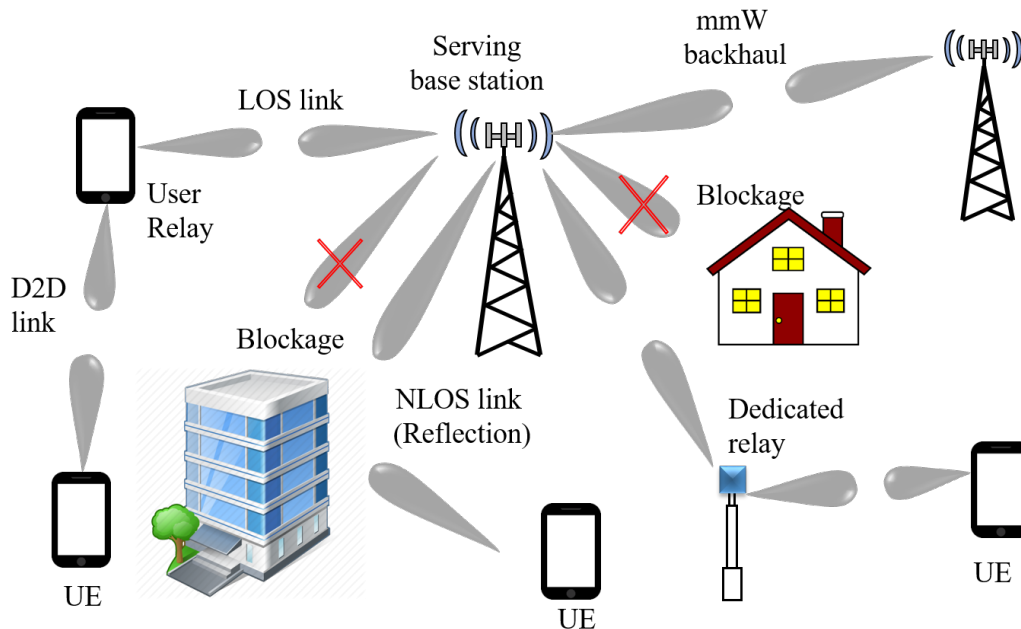


Figure 1.4: Millimeter wave cellular network with a base station, relays, blocking objects, and user equipments (UEs).

use mmW bands [17], mmW cellular communications was thought to be impractical due to their high path loss at larger distance. Specifically, when a base station must provide signal coverage over large cells of radius up to few kilometers, large mmW attenuation makes coverage infeasible. Another key challenge arises due to user mobility which makes it necessary to re-align the beams frequently [10]. However, to increase the network capacity in recent cellular networks, heterogeneous deployment with multiple tiers (macro, micro, pico, and femto) of base stations is used. While macro cells transmit at a higher power (≈ 40 W) to provide a coverage to a larger area, micro, pico and femto cells use the same frequency channels and time resources but transmit at a lower power each with decreasing coverage area. With pico and femto cells having typical coverage range of few hundred meters, mmW bands can be efficiently utilized to serve these cell users and are, in fact, more suitable than sub-6 GHz bands as the former result in less interference to co-channel cells due to higher signal attenuation in mmW bands. In addition, dense-urban and suburban propagation experiments have shown that mmW links work well within a cell radius of up to 200 meters [22], a size similar to that of the current pico cells deployed in sub-6 GHz bands. A mmW cellular network with access, backhaul, and relay links utilizing directional communication is shown in Fig. 1.4.

1.2.1 Standardization of mmW networks

This section provides a brief overview of existing and new wireless standards operating in mmW frequencies that are available for personal, local, and wide area networks.

IEEE 802.15.3c: This wireless personal area network (WPAN) standard for unlicensed 60 GHz band achieves a small coverage range (~ 10 m) [23]. The connections are ad-hoc based and its architecture defines two classes of devices, namely, a piconet coordinator (PNC), and remaining devices (DEVs). The PNC performs access control, synchronization, and quality of service (QoS) management for the DEVs. To suit a variety of QoS requirements, mmW capable physical layer (PHY) is specified for three different operating modes: (i) single carrier mode (SC), (ii) high speed interface mode (HSI), and (iii) audio/visual mode (AV), ranging the achievable data rates from a few Mbps up to a maximum of 5,775 Mbps [17]. A set of four channels each with a bandwidth of 2.16 GHz are used in the band 57.24-65.88 GHz to accommodate the different frequency bands allocated in different countries for 60 GHz communication. The standard uses binary phase shift keying (BPSK), quadrature phase shift keying (QPSK), and M-ary quadrature amplitude modulation (M-QAM) with $M = 16$ or 64. All the operating modes have directional beamforming capability where a set of predefined vectors (codebook) are used for beam training to establish and maintain communication.

IEEE 802.11ad: This local area network (LAN) standard operates in 60 GHz band with the core feature of directional multi-gigabit physical layer and uses multi-antenna beamforming [24]. Antenna training for beamforming is done in two steps: (i) sector sweeping, and (ii) beam refinement where in the first step, the best sector to communicate is selected and then the second step further refines the beams. Once the antenna arrays are configured for the best direction, beam tracking procedure defined in the standard will reconfigure the beams if the propagation environment changes. IEEE 802.11ad also features the use of sub-6 GHz bands for concurrent transmission with 60 GHz frequencies. To combat the link blockages, the standard defines relaying mechanisms where the relays can operate either in amplify-and-forward (AF) mode or decode-and-forward (DF) mode. Similar modulation schemes to IEEE 802.15.3c

are used: BPSK, QPSK, 16-QAM, and 64-QAM to achieve the PHY data rate capability of up to 6,756 Mbps [17].

5G New Radio (NR): It is a new radio access technology developed by 3GPP for 5G mobile communication in Release 14 and Release 15 of their standards. The major features of NR include the capability to use mmW bands to achieve high data rates, enhanced network energy performance, forward compatibility, low latency, and beam-centric design to allow for massive number of antennas. The use of mmW frequencies has been specified for two operating modes: (i) non-standalone (NSA) mode (Release 14), and (ii) standalone (SA) mode (Release 15). In NSA mode, NR devices are dependent on conventional LTE for control signals such as initial access and mobility, whereas in SA mode, NR devices are capable of handling mmW for both the control signal and data transfer without relying on sub-6 GHz LTE. In addition, to support the frequencies ranging from sub-1 GHz to mmW bands, NR features a flexible numerology where the orthogonal frequency division multiplexing (OFDM) subcarrier spacings from 15 KHz up to 240 KHz are used. Due to the propagation issues at mmW bands, joint use of lower bands (~ 2 GHz) and mmW bands is expected to be most effective to provide coverage and rate requirements in 5G networks [2].

1.3 Relays

Traditionally, cellular coverage has been improved by the deployment of more base stations. However, this approach has increasingly becomes infeasible due to high costs, energy and environmental constraints and other problems [14], [25]. To alleviate these problems, wireless relays may be deployed which can be ordinary user devices or dedicated nodes. Use of relays has been established as an effective method to increase the coverage, throughput and reliability in the sub-6 GHz wireless networks in which small scale fading is a major channel impairment [26]–[28]. On the other hand, in mmW networks, which are limited by blockage, relays can be deployed to establish a dominant LOS or NLOS path to the receiver and are vital to improve the coverage and rate [20]. In addition, with the increase in length of communication link, probability of the link being blocked is increased. By deploying the relays, longer links can be divided into shorter ones, thereby reducing the

blockage probability and improving overall received signal to noise ratio (SNR). Relays are already the part of LTE-A [29] and IEEE 802.11ad [24].

1.4 Non-orthogonal Multiple Access

Non-orthogonal multiple access (NOMA) refers to the use of same resource block, such as a subcarrier, a time-slot, or a spreading code, to serve multiple users within a network. For example, in power domain NOMA, a source transmits multiple signals to multiple receivers in the same time and frequency slot with distinct power levels. This enables each receiver to decode its own signal using successive interference cancellation (SIC). NOMA is particularly suitable when the users have distinct channel gains, and the users are ranked based on their channel condition: best user (strongest channel) to weakest user (poorest channel). Since the power is allocated to different users based on their data rate (or QoS) requirements, the time and frequency resources are more efficiently used to improve the system spectral efficiency compared to that of orthogonal transmission schemes where the entire time-frequency resources are dedicated to a single user regardless of its required QoS. Therefore, NOMA is included in the LTE-A standard [29], and is a strong candidate for 5G NR future releases [30]. Cooperative NOMA combines cooperative communication with NOMA where a user with strong channel condition, after decoding weaker users' messages, forwards the messages to the weaker users to improve their rates [31].

1.5 Motivation and Problem Statements

As mentioned before, the mmW bands offer potential opportunities to alleviate the spectrum crunch and to meet the wireless traffic growth in 5G and beyond networks. However, ubiquitous coverage is a major challenge for mmW links, which must be addressed before they can be widely deployed in outdoor and cellular networks. Early trials have achieved data rates of up to 4.5 Gbps over a 1.2 km distance [32], and mmW propagation measurements indicate achievable coverage over distances up to 200 meters even in dense city environments [19]. However, coverage over longer distances is essential, and wireless relaying has shown improvement in coverage, rate and diversity in sub-6 GHz wireless networks [26], [33]. Due to these benefits, relays are already a part of LTE-A system [29]. Compared to sub-6 GHz networks, mmW networks have more ability to deploy

relays because they are not limited by interference under less-dense deployment scenarios. Moreover, substantial coverage improvements have been reported [20]. Despite that initial work, mmW relays have not been studied extensively. Therefore, the major goal of this research is to analyze and evaluate the coverage and rate performance of several mmW relaying techniques in the context of 5G and beyond networks. The specific research problems investigated in this thesis are discussed below.

P1: *Decode-and-Forward (DF) Relaying in mmW Networks:* The mmW propagation is fundamentally different from that of sub-6 GHz bands due to directivity, path loss, blockages, and the disparity of LOS and NLOS parameters. Therefore, performance analyses [28], [33]–[41] and many similar sub-6 GHz contributions on relaying do not directly apply to mmW links. Moreover, these works do not consider random placement of relays (spatial randomness) and the distance-dependent path loss which is correlated with the node locations. Although works [42], [43] consider spatially random locations of the relays, mmW features are not treated. Performance evaluation of mmW AF spatial random relay nodes in [44] does not consider the effects of small-scale fading. In summary, a comprehensive analysis of mmW DF networks with various relay selection algorithms and considering the spatial randomness of relay nodes and small-scale fading has been lacking in the literature. Therefore, it is critical to investigate the coverage and rate improvements in mmW networks achieved by deploying DF relays.

P2: *Multi-hop DF Relaying in mmW Networks:* Multi-hop relays improve the outage and bit error performance in sub-6 GHz bands [45]–[47]. However, the study of multi-hop mmW relaying is not extensive, and although the existing works are limited to the upper layers (MAC and network layers) [48]–[54], they demonstrate the significantly improved connectivity, coverage, and rates. However, physical layer performance analysis of multi-hop mmW relays is limited to [55], which investigates a multi-hop AF relay network in terms of bit error probability (BEP). However, it does not include NLOS scenarios, which are common in mmW links [3], [22], and does not consider common performance measures such as coverage probability and ergodic capacity. More importantly, [55] is not applicable for DF relays. Therefore,

comprehensive performance analysis of DF multi-hop relaying considering mmW specific impairments is imperative.

P3: *Two-way Amplify-and-Forward (AF) Relaying in mmW Networks:* The problem with one-way relays is that two end users require four time slots to complete a bidirectional data exchange, which however is possible in just two time slots via a two-way relay; consequently, two-way relaying potentially doubles spectral efficiency. The performance of two-way relays has been analyzed extensively for conventional sub-6 GHz bands where small scale fading is the major channel impairment [28], [33]–[35]. However, as per **P1**, the existing works are not directly applicable to mmW links. The reason is that in mmW networks, even the nodes nearby the transmitter may not achieve sufficient SNR (coverage) if they are blocked by the obstacles and they do not have LOS links to the transmitter. Therefore, taking such effects into consideration, it is important to quantify the benefits of two-way relays in mmW networks.

P4: *Cooperative NOMA in mmW Networks:* Use of NOMA improves overall sub-6 GHz network capacity [56], [57]. However, mmW NOMA has received research attention only recently and is a promising research direction [58]. As mentioned before, one-way relays improve the coverage and rate in blockage prone mmW networks [59], [60], but at the expense of spectral efficiency. Therefore, relays can be combined with mmW NOMA, which is termed cooperative mmW NOMA, with the goal of reducing the number of time slots required in the relay channels. This cooperative NOMA will improve spectral efficiency and coverage simultaneously, and thus has been studied extensively for sub-6 GHz bands [61], [62]. However, cooperative NOMA for mmW bands has remained absent so far, thus the coverage and rate analysis is necessary.

1.6 Outline of the Thesis and Major Contributions

The rest of the thesis aims at addressing problems **P1**–**P4** stated in Section 1.5. The necessary theoretical background for the thesis are reviewed in Chapter 2. Chapters 3–6 present the comprehensive analysis of problems **P1**–**P4**, respectively. Finally, Chapter 7 provides a brief conclusion and future research problems. The major contributions of Chapters 3–6

are summarized below.

- In Chapter 3, **P1** is addressed where the coverage probability improvement due to the deployment of spatially random DF relays is analyzed using tools from stochastic geometry. To this end, all the fundamental features of mmW communication such as blockage, path loss, and directional gains are considered and the coverage for three cases: (i) direct link (without relay), (ii) best relay selection, and (iii) randomly picked relay are analyzed. First, the distribution of the decoding set of relays is derived and from this set a relay with the minimum path loss to the destination is selected as the best relay. The analysis is extended to study the effect of beam alignment errors, power splitting at source and relay, rate coverage probability, and spectral efficiency. The relay selection significantly improves the statistics of the destination SNR compared to that achieved with a direct link and a randomly picked relay.
- To address **P2**, Chapter 4 analyzes the coverage probability, symbol error rate (SER), and ergodic capacity of a mmW multi-hop DF relay network. To this end, both the LOS and NLOS link states are incorporated in the analysis and two scenarios are considered: (i) sparse deployment of nodes where the relays and destination are limited by additive noise, and (ii) dense deployment of nodes where the relays and destination are limited by co-channel interference. In case (i), closed form expression of the SNR distribution is derived and it is used to obtain the coverage probability, ergodic capacity, and SER for three classes of digital modulation schemes, namely, BPSK, differential BPSK (DBPSK), and square M-QAM. In case (ii), signal-to-interference-ratio (SIR) distributions are derived for two cases: (a) interference powers are independent and identically distributed (i.i.d.) and (b) they are independent but not identically distributed (i.n.i.d.). While the per-hop SNR in (a) follows beta-prime distribution, the closed-form analysis is highly complicated in (b). So the *Welch-Satterthwaite Approximation* for the sum of Gamma variables is used to derive the distribution of the total interference. Then the performance metrics same as in case (i) are derived. The derived results show that multi-hop relaying provides significant coverage improvement in blockage-prone mmW networks. The effect of the block-

age object density on coverage probability is also investigated and shown that it can be compensated by increasing the number of hops.

- In Chapter 5, **P3** is addressed where the potential benefits of deploying two-way AF relays to assist bidirectional data exchange between two end users in a mmW network is studied. The presented analysis accounts for the random locations of the potential relays which exchange the data for two fixed users. A relay that maximizes the minimum of two users' end-to-end SNR is selected for which coverage probability is derived. The results show that the selected relay provides significantly higher coverage probability and spectral efficiency compared to a randomly picked relay. Coverage is also shown to improve with the increase in density of the relay deployment.
- Chapter 6 addresses **P4** where a cooperative NOMA in mmW network is investigated in terms of achievable coverage and rate via stochastic geometry tools. The network consists of a source, a set of randomly located active users which act as potential relays, and a destination which lacks direct coverage from the source. While the transmission from source to relay uses NOMA scheme, selected relay to destination transmission occurs in orthogonal mode. To this end, the decoding set consists of a set of relays that meet certain rate threshold, and a relay is selected from this set based on (i) closest to source and (ii) closest to destination criteria. Compared to orthogonal multiple access (OMA) relaying, NOMA relay selection schemes show higher coverage. Random relay selection was also analyzed but it performed worse off compared to OMA, which signifies the importance of appropriate relay selection.

~

Chapter 2

Background

This chapter presents the relevant mathematical backgrounds and concepts. Since the wireless channel model is critical to the analysis, in Section 2.1, mmW channel models are discussed first. Then, brief discussions of mmW directional beamforming, beam alignment error modeling, and blockage modeling are provided. Section 2.2 presents wireless relay types, their signal models and SNR models. Section 2.3 discusses stochastic modeling of node locations in wireless networks. Finally, in Section 2.4, principle of NOMA is discussed using a two-user case as an example.

2.1 Key Aspects of Millimeter Communications

In the following, some key features and impairments of mmW channels and their common modeling techniques for performance analysis are outlined.

2.1.1 MmW Channel Modeling

Channel measurements at mmW frequencies in outdoor environments show that received signal is the sum of a small number of dominant multipaths [22]. Assuming N_T and N_R be the number of antennas at transmitter and receiver, respectively, equivalent channel matrix \mathbf{H} can be written as [63]

$$\mathbf{H} = \sqrt{\frac{N_T N_R}{L_l}} \sum_{k=1}^K h_k \mathbf{a}_T(\theta_{T,k}) \mathbf{a}_R^H(\theta_{R,k}), \quad (2.1)$$

where L_l is the path loss between the transmitter and the receiver (2.4), K is the total number of multipath components, h_k is the small-scale fading of the k -th path, $\theta_{T,k}$ and

$\theta_{R,k}$ denote the angle of departure (AoD) at the transmitter and angle of arrival (AoA) at the receiver, respectively, for the k -th path. The vectors $\mathbf{a}_T(\theta_{T,k})$ and $\mathbf{a}_R(\theta_{R,k})$ are the array response vectors at the transmitter and receiver, respectively, and the superscript H in \mathbf{a}_R^H denotes the conjugate transpose operation. When a uniform linear array with N number of antennas and an inter-antenna spacing of q is used, where $N \in \{N_T, N_R\}$, the array response in the direction $\theta \in \{\theta_{T,k}, \theta_{R,k}\}$ can be written as

$$\mathbf{a}(\theta) = \frac{1}{\sqrt{N}} [1, e^{j(2\pi/\lambda)q \sin(\theta)}, e^{j2(2\pi/\lambda)q \sin(\theta)}, \dots, e^{j(N-1)(2\pi/\lambda)q \sin(\theta)}]^T. \quad (2.2)$$

where λ is the wavelength and T denotes transpose. The channel model in (2.1) can be simplified to a single path model where, instead of adding multiple paths, only one dominant path is assumed to exist. This approximation is widely used in mmW works that analyze the network performance using stochastic geometry [3], [64], [65]. In [65], simulations show that similar key insights can be obtained on achievable rates using single path approximations and using three paths. The single path approximation can be written as

$$\mathbf{H} = \sqrt{\frac{N_T N_R}{L_l}} h \mathbf{a}_T(\theta_T) \mathbf{a}_R^H(\theta_R), \quad (2.3)$$

where h is the small scaling fading coefficient in the dominant path. The modeling for L_l , h , and the array response are provided in the subsequent sections.

2.1.2 Path Loss Modeling

Path loss refers to the attenuation of signal power when it travels along a distance from the transmitter [66]. It consists of a combined effect of (i) distance dependent loss which is monotonically decreasing function of distance, and (ii) the signal variation that occurs in a relatively shorter distance of few tens of wavelengths (known as shadow fading or shadowing). While the distance dependent loss is due to the decreasing density of electromagnetic field strength when it propagates away in the three dimensional space, shadowing loss is caused by the blocking obstacles in the environment which absorb the transmitted power. The combined effect is also known as large scale propagation loss or local mean attenuation [66].

The large-scale propagation loss or path loss is generally modeled by applying a linear

fit to the path loss data from propagation measurements. The variation due to the shadowing component follows a log-normal distribution (normal distribution on a log or dB scale). This thesis uses the model in [67], which incorporates log-normal shadowing and free-space path loss. Consequently, the total path loss (in dB) between two points $a, b \in \mathbb{R}^2$ is given by

$$L_l(a, b) = \beta + 10\alpha_l \log_{10} \|a - b\| + \mathcal{X}_l, \quad (2.4)$$

where $\|a - b\|$ denotes the distance between points a and b , $\mathcal{X}_l \sim \mathcal{N}(0, \sigma_l^2)$ is the shadowing component and models the deviation in fitting the measured data, and $l \in \{L, N\}$ indicates the LOS and NLOS link states that dictate the choice of path loss exponent α_l and shadowing variance σ_l^2 , and $\beta = 20 \log_{10} \left(\frac{4\pi f}{c} \right)$ represents path loss at a reference distance of 1 meter where f and c are frequency and speed of light.

2.1.3 Small-scale Fading

Small-scale fading refers to the rapid variation in the received signal power when the transmitter and/or receiver moves a small distance (in the order of signal wavelength). Thus, constructive or destructive interference occurs among multipath signals with different phases impinging on the receiver. Therefore, small-scale fading is dictated by the signal propagation mechanisms and the paths taken by the signal while traveling from the transmitter to the receiver. In mmW communication, these mechanisms are distinct in LOS and NLOS cases making significant differences in received signal power. For example, in an LOS link, the total received power is dominated by the signal from direct path, and reflection and scattering component is a negligible contribution to the received power. This is due to the losses associated with these propagation mechanisms in NLOS paths. Therefore, the degree of small-scale fading is small in LOS links. However, in NLOS links, the total received power is due to distinct multiple NLOS paths with different phases. Thus, large variations of total received power are possible. As a result, the degree or severity of fading is different in LOS and NLOS cases [22]. Therefore, any small scale fading model for mmW channels must include these variations.

To this end, small-scale fading effects are modeled by the Nakagami- m distribution and this thesis considers different fading parameters $m_l \in [\frac{1}{2}, \infty)$ where $l = \{L, N\}$ is used to denote LOS and NLOS links, respectively [3], [68]. If the small-scale fading coefficient

is $h_l, l \in \{L, N\}$, then its probability density function (PDF) is given by

$$f_{h_l}(x) = \frac{2m_l^{m_l}}{\Omega^{m_l}\Gamma(m_l)} x^{2m_l-1} \exp\left(\frac{-m_l x^2}{\Omega}\right), \quad x > 0 \quad (2.5)$$

where Ω is the mean square value of h_l , and $\Gamma(z) = \int_0^\infty x^{z-1} e^{-x} dx$ is the gamma function. Then, the fading power gain $|h_l|^2$ follows a Gamma distribution, which for the normalized power is given by

$$f_{|h_l|^2}(x) = \frac{m_l^{m_l}}{\Gamma(m_l)} x^{m_l-1} \exp(-m_l x), \quad x > 0. \quad (2.6)$$

For further analysis, $m_L, m_N \in \{1, 2, 3, \dots\}$ and larger m_L values model LOS links where the fading variation is low, and smaller m_N values are used to realize bigger variability in NLOS links [3].

2.1.4 Directional Beamforming Modeling

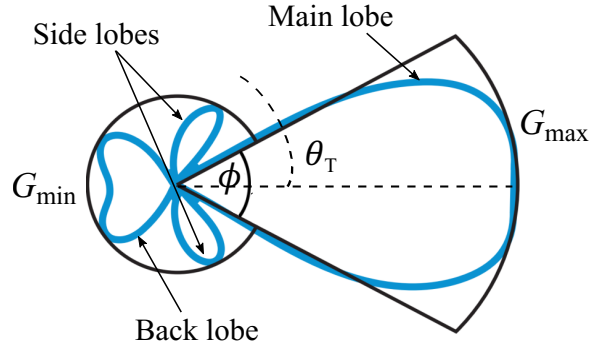


Figure 2.1: A sectoral antenna model [3].

Electronically steerable directional antenna arrays are assumed for the transmitter and receiver. Since these arrays form beamforming patterns to compensate for the high path loss [11], beamforming parameters must be included in the performance analysis. While the true directional gain function (2.2) of an antenna array consists of a main lobe, multiple side lobes and back lobes, use of the exact pattern will incur high analytical complexity. Therefore, the directional gain is approximated using a simple sectored antenna model (Fig. 2.1). In this model, the gain is a function of azimuth angle θ_T and is constant G_{\max} when θ_T is within the half power beamwidth (ϕ), and otherwise is constant G_{\min} in all other directions [64]. For an AoD of θ_T at the transmitter, assuming corresponding beamforming

vector \mathbf{w}_n is used for signal transmission, the effective beamforming gain at the transmitter can be written as follows:

$$G_T(\theta_T) = |\mathbf{a}_T^*(\theta_T)\mathbf{w}_n|^2 = \begin{cases} G_{\max} & \text{if } |\theta_T| \leq \frac{\phi}{2} \\ G_{\min} & \text{otherwise.} \end{cases} \quad (2.7)$$

where $\mathbf{a}_T^*(\theta_T)$ is written from (2.2) and the subscripts T are used to denote the transmitter and * denotes the complex conjugate operation. The gain at the receiver can be written similarly using $G_R(\theta_R) = |\mathbf{a}_R^*(\theta_R)\mathbf{v}_n|^2$, where \mathbf{v}_n is the receive combining vector. The beamforming and combining vectors \mathbf{w}_n and \mathbf{v}_n are assumed to be known at the transmitter and receiver [65].

The effective antenna gain G_{eq} of a link will be the product of gains of transmit and receive antennas, i.e., for perfect beam alignment $G_{\text{eq}} = G_{\max}^2$, assuming identical main lobe gains (G_{\max}) at the transmitter and receiver. The typical values for G_{\max} and G_{\min} can be 18 dBi and -10 dBi, respectively [4].

Beam Alignment Error Modeling

In sub-6 GHz bands, due to the use of omni-directional antennas, beamforming is generally not essential. The reason is that the link gain is independent of the directional orientation of the transmitter and receiver. On the other hand, in mmW bands, transmitter and receiver beams must be aligned; that is, the main lobes must accurately point to each other. However, perfect beam alignment may not be possible due to channel estimation errors and node mobility. This means, the overall end-to-end antenna gain G_{eq} can be G_{\max}^2 , $G_{\max}G_{\min}$, or G_{\min}^2 .

In this thesis, first a perfect beam alignment is considered between the communicating nodes with $G_{\text{eq}} = G_{\max}^2$ in the desired link. Then, to study the effect of beam misalignment, analytical method in [68] is utilized. According to this method, the beam alignment error of a link is a zero-mean Gaussian random variable (r.v.) $\varepsilon \sim \mathcal{N}(0, \sigma_E^2)$ with variance σ_E^2 . Then the absolute value $|\varepsilon|$ follows a half normal distribution, and the cumulative distribution function (CDF) is $F_{|\varepsilon|}(x) = \text{erf}\left(\frac{x}{\sqrt{2}\sigma_E}\right)$ where $\text{erf}(z) = \frac{2}{\sqrt{\pi}} \int_0^z e^{-t^2} dt$ is the Gauss

error function. With this, the PDF of the effective antenna gain G_{eq} becomes

$$f_{G_{\text{eq}}}(g) = F_{|\varepsilon|} \left(\frac{\phi}{2} \right)^2 \delta_{(g-G_{\text{max}}^2)} + 2F_{|\varepsilon|} \left(\frac{\phi}{2} \right) \left(1 - F_{|\varepsilon|} \left(\frac{\phi}{2} \right) \right) \delta_{(g-G_{\text{max}}G_{\text{min}})} + \left(1 - F_{|\varepsilon|} \left(\frac{\phi}{2} \right) \right)^2 \delta_{(g-G_{\text{min}}^2)}, \quad (2.8)$$

where $\delta_{(\cdot)}$ is the Kronecker delta function defined as $\delta_{(i-j)} = 1$ for $i = j$, and *zero* otherwise. With this PDF (2.8), coverage performance with beam alignment error can be evaluated by averaging the conditional coverage probability.

2.1.5 Blockage Modeling

Blockage is defined as a condition where a mmW link between two communicating nodes is obstructed by some objects, such as buildings and vehicles, which are present in the propagation environment. While it is not a severe problem in sub-6 GHz communication, mmW links exhibit a very high path loss when blocked. This is because, in mmW links, path loss is significantly higher for NLOS path compared to an LOS case [67]. Therefore, including a blockage parameter that distinguishes LOS and NLOS cases in the performance analysis is crucial [69].

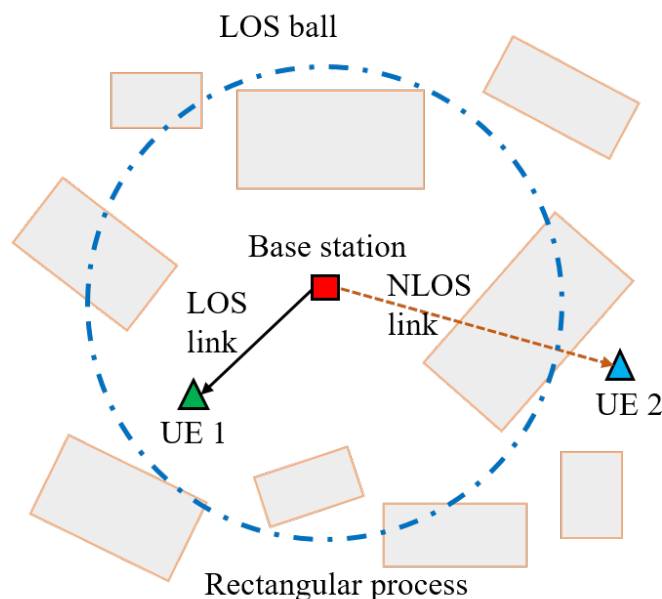


Figure 2.2: Random shape theory model for blockages where the irregular LOS region to a typical user is approximated by a ball in the fixed LOS ball model [4].

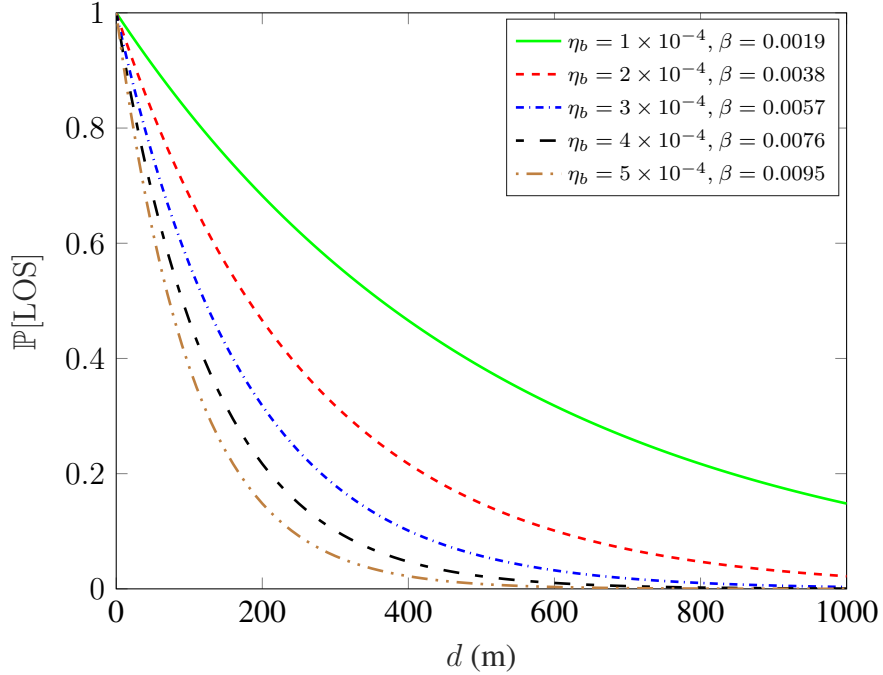


Figure 2.3: LOS probability (2.9) for different blockage densities with $\mathbb{E}[L] = \mathbb{E}[W] = 15$ m.

Since the obstacles in propagation environment (buildings, vehicles, humans, trees, utility poles and other objects) do not follow a fixed geometry either due to their orientation or due to their mobility, probabilistic modeling of these objects becomes necessary. Therefore, the authors in [69] have proposed a geometry based stochastic model using the concept of random shape theory to model the objects and corresponding blockage probability. Specifically, they assume blockage objects to be rectangles with the centers distributed as a homogeneous Poisson point process (PPP) and their size (length and width) are selected from certain probability distribution and their orientation angles are uniformly distributed in $(0, 2\pi]$. With this, it has been shown that a link of length d has the following LOS and NLOS probabilities:

$$\mathbb{P}[\text{LOS}] = p_L(d) = e^{-\beta d} \quad (2.9)$$

$$\mathbb{P}[\text{NLOS}] = p_N(d) = 1 - e^{-\beta d}, \quad (2.10)$$

where $\beta = \frac{2\eta_b (\mathbb{E}[L] + \mathbb{E}[W])}{\pi}$ is the blockage parameter in which η_b is the blockage density (i.e., the number of blockage obstacles or buildings per unit area), and $\mathbb{E}[L]$ and $\mathbb{E}[W]$ respectively, are the average length and width of the objects [69]. Their model provides

an accurate approximation to the real deployment scenario if the blockage parameter β is chosen to match the size and density of blockage obstacles in the environment. Since the exponential decay model above leads to rather intractable analysis of received signal to interference plus noise ratio (SINR) statistics, some approximations are proposed in [3], [68] using a fixed LOS ball (FLB) model, where a node in an area within a fixed radius from the transmitter is in LOS state with a fixed probability (Fig. 2.2). In this thesis, both the FLB and the exponential decay models are utilized to meet the suitability of analytical complexity.

2.2 Relays

The two most common modes of relay operation are: i) Amplify and forward (AF) and ii) Decode and forward (DF) modes. In AF mode, a relay simply amplifies the signal from the source and retransmits it to the destination. In contrast, a DF relay decodes the source signal completely, makes the decision on the received bits, and re-encodes the bits before retransmitting to the receiver. The signal model for AF and DF relay operation is summarized below. In the first time slot, the source transmits its signal x_s , with power P_s . Letting $d_{s,r}$ and $h_{s,r}$ be the distance and fading amplitude, respectively, of source to relay link, received signal at a relay (AF or DF) can be written as

$$y_r = \sqrt{P_s} d_{s,r}^{-\alpha/2} h_{s,r} x_s + n_r, \quad (2.11)$$

where α is the path loss exponent and n_r is the additive noise at the relay. In the next time slot, AF relay retransmits the amplified version of y_r and DF relay decodes x_s from y_r and retransmits the decoded signal \hat{x}_s . Then, the received signals at the destination (d) through AF and DF relaying can be written as

$$\begin{aligned} y_d^{\text{AF}} &= \mathcal{A} d_{r,d}^{-\alpha/2} h_{r,d} y_r + n_d \\ y_d^{\text{DF}} &= \sqrt{P_r} d_{r,d}^{-\alpha/2} h_{r,d} \hat{x}_s + n_d, \end{aligned} \quad (2.12)$$

where $\mathcal{A} = \sqrt{\frac{P_r}{P_s d_{s,r}^{-\alpha} |h_{s,r}|^2 + N_0}}$ is the amplification gain of AF relay, P_r is the transmit power at the relay, N_0 is the power of n_r , and n_d is the additive noise at the receiver.

It is clear from expression of \mathcal{A} that an AF relay reverts the effects of path loss, fading and additive noise on received signal. Considering equal power of N_0 for n_r and n_d , and substituting $\frac{P_s|h_{s,r}|^2}{d_{s,r}^\alpha N_0} = \gamma_1$ and $\frac{P_r|h_{r,d}|^2}{d_{r,d}^\alpha N_0} = \gamma_2$, equivalent end-to-end SNR due to AF and DF relaying are given by [26], [70]

$$\begin{aligned}\gamma_{\text{eq}}^{\text{AF}} &= \frac{\gamma_1 \gamma_2}{\gamma_1 + \gamma_2 + 1} \\ \gamma_{\text{eq}}^{\text{DF}} &= \min\{\gamma_1, \gamma_2\},\end{aligned}\tag{2.13}$$

where γ_1 and γ_2 are defined as the SNRs in the source-relay and relay-receiver links, respectively. From the equivalent SNRs in (2.13), outage probability, which is the event that end-to-end SNR drops below a predefined threshold, can be easily computed. It is found that outage probability due to AF relaying is lower bounded by the outage probability of DF relaying [70].

Relays can be further classified based on the number of time-slots required to complete an end-to-end bidirectional data exchange as: i) One-way relaying and ii) Two-way relaying, which are discussed below.

2.2.1 One-way Relaying

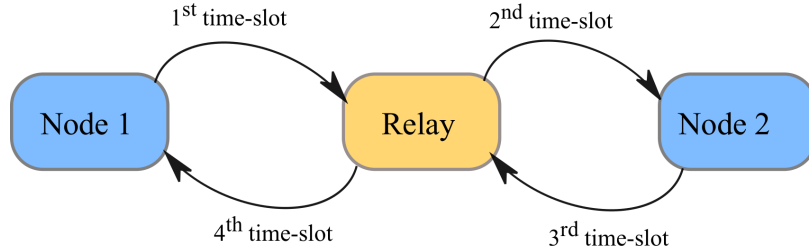


Figure 2.4: A basic one way relay operation.

An one-way relay is unidirectional and operates in half duplex mode. That is, use of this relay requires a total of four time-slots to complete a data exchange between two nodes, i.e., it requires 4 orthogonal time-slots each for link (Node1-Relay, Relay-Node2, Node2-Relay, and Relay-Node1, see Fig. 2.4). The same data exchange would require two orthogonal time-slots if done without using relays and, as a result, the spectral efficiency is halved due to relaying. This efficiency loss can be prevented completely if two-way relays are used.

2.2.2 Two-way Relaying

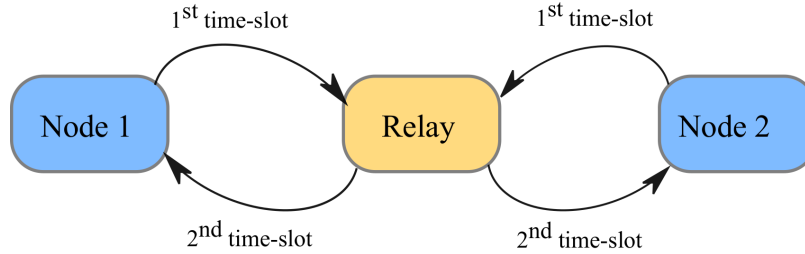


Figure 2.5: A basic two way relay operation.

In two-way relaying, bi-directional data exchange between two nodes (Node 1 and Node 2) requires only two orthogonal time-slots. This is because both the nodes can transmit their signals (say x_1 and x_2) to the relay in the first time-slot, and the relay broadcasts $x_1 + x_2$ the second time-slot (Fig. 2.5). Therefore, it potentially doubles the spectral efficiency compared to the one-way relaying, or maintains the same spectral efficiency as that of a direct link [71]. The equivalent end-to-end SNRs at Node 1 and Node 2 for a two-way AF relaying system are given by [33, eq.2]

$$\begin{aligned}\gamma_{\text{eq}}^{\text{Node 1}} &= \frac{P Q |h_1 h_2|^2}{1 + (P + Q)|h_1|^2 + P|h_2|^2} \\ \gamma_{\text{eq}}^{\text{Node 2}} &= \frac{P Q |h_1 h_2|^2}{1 + P|h_1|^2 + (P + Q)|h_2|^2},\end{aligned}\tag{2.14}$$

where P and Q denote the transmit power of end nodes and relay, respectively, and h_1 and h_2 are the fading coefficients of Node 1 to Relay and Relay to Node 2 links, respectively.

2.2.3 Multi-hop Relaying

Multi-hop relaying uses one or more intermediate nodes to forward the data from transmitter to the receiver. The idea is to break the direct long link into shorter links, thereby reducing the blockage probability in each hop. With a dense deployment of relays, most nodes can be fairly close to one or more relays. This proximity will reduce path loss and blockages, the major challenges in mmW networks, thereby providing higher data rates, coverage and reliability [52]. Multi-hop relays also operate in either AF or DF modes and their outage probability is defined as the probability that end-to-end SNR (γ_{eq}) is below a

predefined threshold γ_{th} . Mathematically, [37]

$$P_{\text{out}} = \mathbb{P}[\gamma_{\text{eq}} \leq \gamma_{\text{th}}] = \int_0^{\gamma_{\text{th}}} f_{\gamma_{\text{eq}}}(\gamma) d\gamma = F_{\gamma_{\text{eq}}}(\gamma_{\text{th}}), \quad (2.15)$$

where $f_{\gamma_{\text{eq}}}(x)$ and $F_{\gamma_{\text{eq}}}(x)$ respectively are the PDF and CDF of γ_{eq} . For AF mode, the expression of P_{out} for a N -hop system can be further simplified as follows [72]

$$\begin{aligned} P_{\text{out}}^{\text{AF}} &= \mathbb{P}[\gamma_{\text{eq}} < \gamma_{\text{th}}] \\ &= \mathbb{P}\left[\left[\prod_{n=1}^N \left(1 + \frac{1}{\gamma_n}\right) - 1\right]^{-1} < \gamma_{\text{th}}\right] \\ &= \mathbb{P}\left[\left[\prod_{n=1}^N \left(1 + \frac{1}{\gamma_n}\right) - 1\right] > \frac{1}{\gamma_{\text{th}}}\right] \\ &= \mathbb{P}\left[\left[\prod_{n=1}^N \left(1 + \frac{1}{\gamma_n}\right)\right] > \frac{1}{\gamma_{\text{th}}} + 1\right] \\ &= \mathbb{P}\left[\bar{\gamma} > \frac{1}{\gamma_{\text{th}}} + 1\right], \end{aligned} \quad (2.16)$$

where $\bar{\gamma} = \prod_{n=1}^N \left(1 + \frac{1}{\gamma_n}\right)$ and γ_n is the per-hop SNR. For DF mode, the outage decisions are made on a per hop basis, and the overall system outage is dominated by the weakest link. Consequently, the outage probability of N -hop DF relaying is given by [46]

$$P_{\text{out}}^{\text{DF}} = \mathbb{P}[\min(\gamma_1, \gamma_2, \dots, \gamma_N) < \gamma_{\text{th}}]. \quad (2.17)$$

2.3 Stochastic Geometry in Wireless Networks

In conventional networks with well planned cellular layouts, such as grid-based or hexagonal cells, signal-to-interference plus noise ratio (SINR) can be analyzed for a fixed user with small number of interfering stations by considering worst-case user location, such as cell edge. However, if shadowing and/or fading are considered, then SINR becomes random and the statistics of SINR are required to compute average rate and outage probability. Monte Carlo simulations could be performed in such cases but these are site specific and do not provide the flexibility in the network analysis [73]. This complication is increased further in modern networks, where network capacity is increased by deploying a

variety of small cells such as micro, pico and femto cells, and locations of the base stations no longer follow a fixed pattern due to deployment constraints and site acquisition issues. User locations are also not fixed due to mobility. Therefore, highly idealized grid-based models are highly inaccurate in these heterogeneous deployments with varying heights and transmission powers of base stations and varying user density [73].

In such networks, stochastic geometry can be used effectively to study the average network behavior over many spatial realizations where the nodes (base stations and users) are placed according to some probability distribution [74]. Stochastic geometry is a branch of applied probability theory which allows the study of random phenomena on the plane or in higher dimensions by using the theory of point processes which deals with a random collection of points in space [75]. A brief overview of points processes that are commonly used in modeling cellular and wireless networks is given below.

1. Binomial point process (BPP): BPP is a basic process where a fixed number of nodes n are identically and independently distributed on a bounded set $W \subset \mathbb{R}^d$ [76]. More formally, it is defined as a point process $\Phi = \{z_1, \dots, z_n\}$ in a bounded set $W \subset \mathbb{R}^d$ with the total number of nodes in $B \subset W$ being a binomial random variable, i.e.,

$$P(\Phi(B) = k) = \binom{n}{k} p^k (1-p)^{n-k}, \quad k = 0, \dots, n \quad (2.18)$$

where n is the total number of nodes in W , and $p = \frac{v_d(B)}{v_d(W)}$ with $v_d(\cdot)$ being a volume measure (e.g., $d = 1$ means length, and $d = 2$ means area). BPP is also obtained by conditioning a homogeneous PPP on the number of nodes, i.e., for $\Phi(W) = n$.

2. Poisson point process (PPP): A point process $\Phi = \{z_1, z_2, z_3, \dots\} \in \mathbb{R}^d$ is a PPP of intensity measure $\lambda(z)$ if it follows the following two fundamental properties [75]:

- (a) Poisson distribution of point counts: the number of points $\Phi(B)$ in a bounded set B is a Poisson random variable with mean $\Lambda(B) = \int_B \lambda(z) dz$, i.e.,

$$\mathbb{P}(\Phi(B) = k) = \frac{(\Lambda(B))^k}{k!} e^{-\Lambda(B)}, \quad k = 0, 1, 2, \dots$$

- (b) Independence of point counts: the number of points in any disjoint sets are

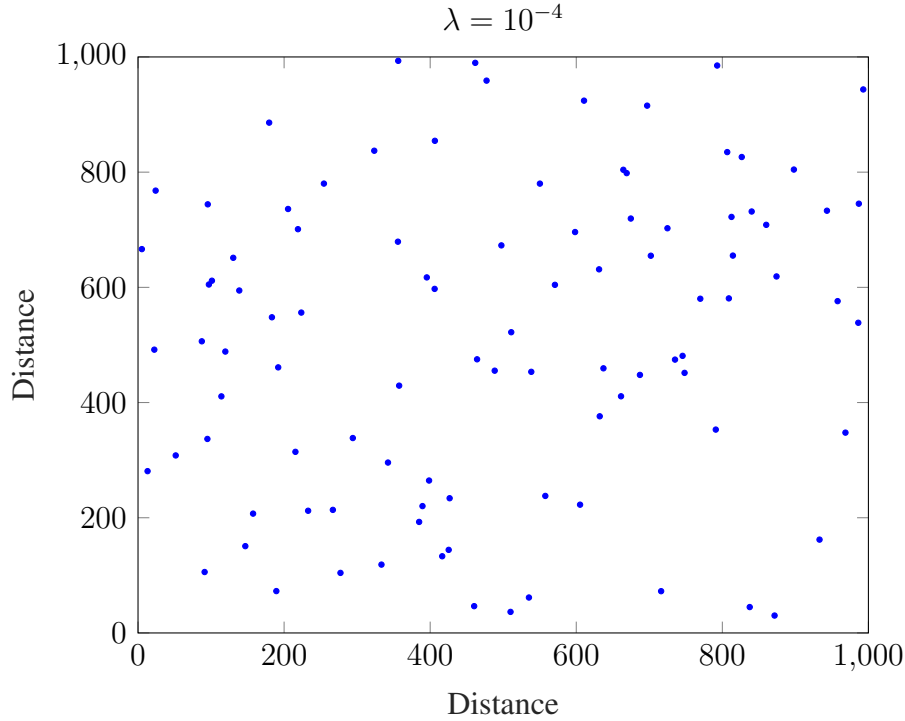


Figure 2.6: A realization of a homogeneous PPP with $\lambda = 10^{-4}$ on $[0, 1000]^2$ area.

independent random variables.

A homogeneous PPP has a constant intensity measure $\lambda(z)$, i.e., $\lambda(z) = \lambda$. This means the density of the point process is independent of the spatial location (Fig. 2.6). Otherwise, in an inhomogeneous PPP, the intensity of the points is location dependent (Fig. 2.7). PPP has been widely used to model the location of base stations and users because it enables tractable computation of coverage probability and rate [3], [73]. The tractability of the PPP is because of the independence of base station locations, allowing substantial tools to be used from stochastic geometry [74]. Although base stations are not independently deployed in practice, the results from PPP analysis can be generalized to more practical deployments where base stations are placed after a minimum distance to reduce interference to/from neighboring base station. The user locations can be modeled similarly using a PPP with a different density.

3. Cluster Process: A cluster process consists of a parent point process and around each point in the parent process are the daughter point processes. The union of daughter point processes forms the cluster process [76]. Let $\Phi_p = \{z_1, z_2, \dots, z_n\}$

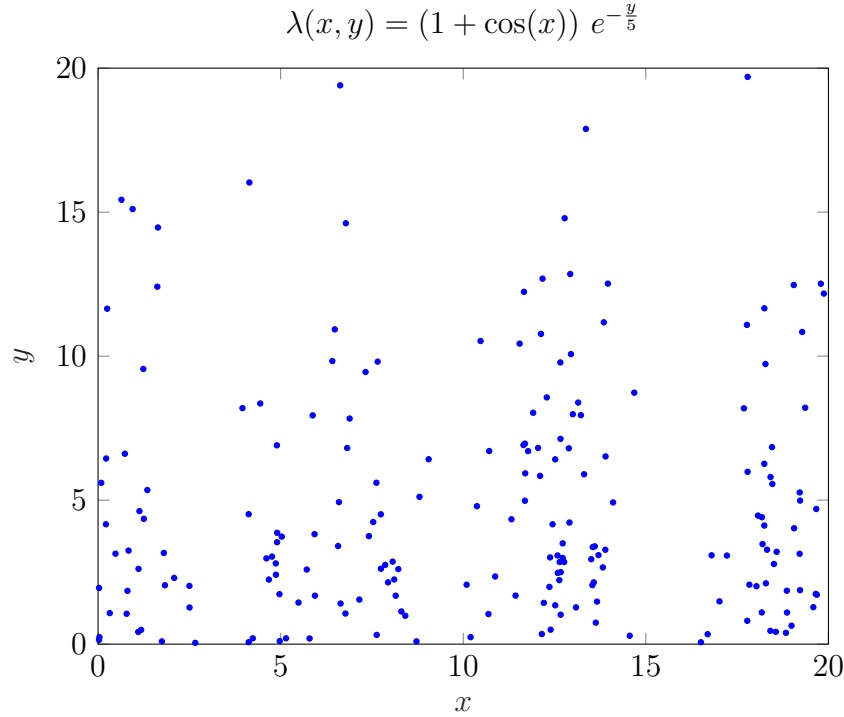


Figure 2.7: A realization of an inhomogeneous PPP with a density function $\lambda(x, y) = (1 + \cos(x)) e^{-\frac{y}{5}}$ on $[0, 20]^2$. As the function indicates, the point density is periodic along x and decreases along y .

be a parent point process with $n \in \mathbb{N}$ number of points in it. Each parent point $z_i, i \in n$, has a corresponding daughter process (Φ_i) . The cluster process Φ can then be written as $\Phi \triangleq \bigcup_{i=1}^n \Phi_i + z_i$. If the parents form a uniform PPP of intensity λ_p and the daughter points in each cluster are random in number, independent of each other and identically distributed, then the point process is known as Neyman-Scott process [76]. This process can be further divided in two types: (i) Thomas cluster process (TCP) and (ii) Matern cluster process (MCP). In TCP, the daughter points are normally scattered with variance σ^2 around each parent point and its intensity is $\lambda = \lambda_p \bar{c}$ where \bar{c} is the mean number of daughter points. In MCP, the daughter points are uniformly scattered on the ball of radius r centered at each point and its intensity is also $\lambda = \lambda_p \bar{c}$ where \bar{c} is the mean number of daughter points. Both the TCP and MCP are doubly Poisson point processes, i.e., their parent and daughter processes both follow the PPP.

4. Hard core point process (HCPP) [76]: In a hard core point process, points are dependent and are required to maintain at least a predefined minimum distance between

them. Based on their generation method, HCPP can be of two types: (i) Matern hard-core process of type I (MHCPP-I) and (ii) Matern hard-core process of type II (MHCPP-II). While MHCPP-I can be generated from a homogeneous PPP Φ with intensity λ by removing all the points that have a neighbor within a predefined distance r , MHCPP-II is formed by assigning each point in Φ an independent random variable, uniformly distributed on $[0, 1]$ and then removing all points that have a neighbor within a distance r that has a smaller mark. HCPP is suitable to model the base station locations, since in practice, two base stations are not placed very close to each other.

2.3.1 Properties of the PPP

PPP possesses a number of special properties which allow mathematical tractability to analyze the network performance. The major properties of the PPP are briefly discussed below [75]–[77], and some of these are used in this thesis.

1. **Superposition Theorem:** Given a countable collection of independent PPPs $\Phi_1, \Phi_2, \dots, \Phi_N$ in \mathbb{R}^d with intensity measures $\lambda_1, \lambda_2, \dots, \lambda_N$, respectively, their superposition is another PPP $\Phi = \bigcup_{n=1}^N \Phi_n$ with a mean measure $\lambda = \sum_{n=1}^N \lambda_n$.
2. **Independent Thinning:** Thinning is an operation of removing certain points from a point process based on a certain probabilistic rule. When the points are removed independent of all other points, the process is called the independent thinning. This property can be stated formally as: *Let Φ be a PPP on \mathbb{R}^d with intensity function $\lambda(z)$ and $f : \mathbb{R}^d \rightarrow [0, 1]$ be a thinning function. If f is applied to Φ such that it deletes each point z with probability $1 - f(z)$, independently of all other points, it generates an inhomogeneous PPP $\hat{\Phi}$ with intensity function $\hat{\lambda}(z) = \lambda(z)f(z)$.*
3. **Mapping Theorem:** It states that if a PPP Φ in one state space \mathbb{R}^d is mapped into another space \mathbb{R}^s , the transformed random points again form a PPP with a different intensity measure. It can be formally defined as: *Let Φ be a PPP with a mean measure Λ on \mathbb{R}^d , and let $f : \mathbb{R}^d \rightarrow \mathbb{R}^s$ be a measurable function such that $\Lambda(f^{-1}\{z\}) = 0, \forall z \in \mathbb{R}^s$. Assume that $\mu(B) = \Lambda(f^{-1}\{B\})$ satisfies $\mu(B) < \infty$*

for all bounded B . Then, $f(\Phi) \triangleq \bigcup_{x \in \Phi} \{f(x)\}$ is a PPP with intensity measure $\mu = \int_{f^{-1}(B)} \lambda(x) dx$ for all bounded $B \subset \mathbb{R}^s$.

4. Slivnyak's Theorem: The basic concept of Slivnyak's theorem (or Slivnyak-Mecke theorem) is that conditioning on a point at z of a PPP Φ does not change the properties of Φ . That is, for a PPP Φ , any new point can be added or removed from it without affecting the distributions or properties of Φ . Mathematically, it is given by

$$\mathbb{P}_z^! \equiv \mathbb{P} \quad (2.19)$$

where $\mathbb{P}_z^!$ is the reduced palm distribution of Φ at z (conditional distribution defined by excluding z from Φ) and \mathbb{P} is the Palm distribution at z (conditional distribution of Φ given that a point z belongs to Φ).

5. Campbell's Theorem: This theorem is useful to obtain the expectation of a sum over a point process. Let Φ be a PPP on \mathbb{R}^d with intensity function $\lambda(z)$ and $f : \mathbb{R} \rightarrow \mathbb{R}$ be a measurable function. The sum $S = \sum_{z \in \Phi} f(z)$ is a random variable having a mean

$$\mathbb{E}[S] = \int_{\mathbb{R}^d} f(z) \lambda(z) dz. \quad (2.20)$$

6. Probability Generating Functional (PGFL): PGFL is used to compute the expectation of a product over a PPP. Let Φ be a PPP on \mathbb{R}^d with intensity function $\lambda(z)$ and $f : \mathbb{R}^d \rightarrow [0, 1]$ be a measurable function. Then the product $G(f) = \prod_{z \in \Phi} f(z)$ is a random variable with a mean

$$\mathbb{E}[G(f)] = \exp \left(\int_{\mathbb{R}^d} (1 - f(z)) \lambda(z) dz \right). \quad (2.21)$$

2.4 Non-Orthogonal Multiple Access (NOMA)

The key concept of power domain NOMA is to assign more power to the user with poorer channel condition. For simplicity, the case of two user NOMA is described here (Fig. 2.8). Let s_1 and s_2 be the transmit symbols intended for user 1 and user 2, respectively. Also, let $h_i, i \in \{1, 2\}$ be the two user channels and assume $|h_1| > |h_2|$. Then the base station

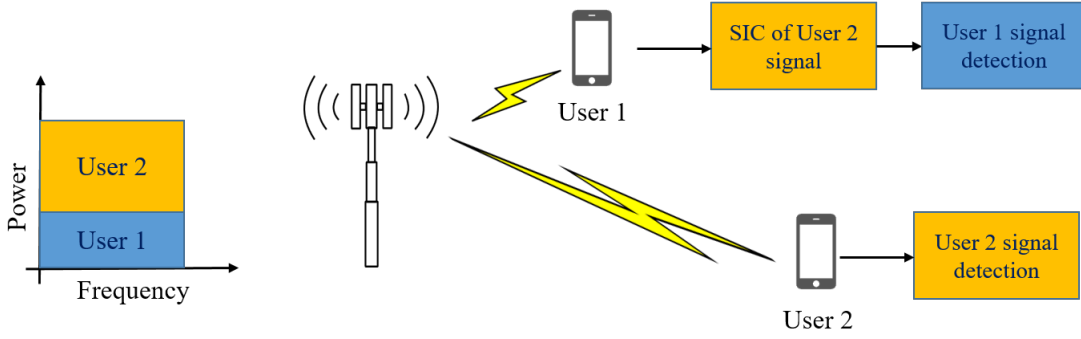


Figure 2.8: Two user downlink NOMA using power domain multiplexing.

transmits the superimposed message signal $x = \alpha_1 s_1 + \alpha_2 s_2$ for user 1 and user 2 using the power coefficients of $\alpha_i, i \in \{1, 2\}$. As mentioned before, since $|h_1| > |h_2|$, let $\alpha_2 > \alpha_1$ where $\alpha_1^2 + \alpha_2^2 = 1$. Now the received signals y_1 and y_2 at user 1 and user 2, respectively, are given by

$$y_1 = (\alpha_1 s_1 + \alpha_2 s_2) h_1 + w_1 \quad (2.22)$$

$$y_2 = (\alpha_1 s_1 + \alpha_2 s_2) h_2 + w_2 \quad (2.23)$$

where w_1 and w_2 are the additive white Gaussian noises at user 1 and user 2, respectively. Now, user 2 can decode s_2 directly by treating s_1 component as interference, with the SINR of $\frac{\alpha_2^2 |h_2|^2}{\alpha_1^2 |h_2|^2 + \frac{1}{\gamma}}$, where γ is the transmit SNR (ratio of the transmit power and receiver noise). This will result in an achievable rate of $\log_2 \left(1 + \frac{\alpha_2^2 |h_2|^2}{\alpha_1^2 |h_2|^2 + \frac{1}{\gamma}} \right)$ bps/Hz at user 2. However, user 1 cannot decode its signal directly and needs to decode user 2's message s_2 first and then perform SIC to remove s_2 and then decode its own message s_1 . In this case, the SINR at user 1 to decode s_2 is equal to $\frac{\alpha_2^2 |h_1|^2}{\alpha_1^2 |h_1|^2 + \frac{1}{\gamma}}$. After successfully decoding s_2 , user 1 removes it from y_1 and decodes its own message with the SNR of $\gamma \alpha_1^2 |h_1|^2$ and the resulting data rate at user 1 becomes $\log_2 (1 + \gamma \alpha_1^2 |h_1|^2)$.

~

Chapter 3

Coverage Analysis of Millimeter Wave Decode-and-Forward Networks With Best Relay Selection

This chapter¹ analyzes and quantifies the performance improvements of a mmW link due to the deployment of spatially random DF relays. All potential relay nodes are distributed as a two dimensional (2D) homogeneous PPP. The set of potential relay nodes whose received SNRs are above a minimum SNR threshold is called the decoding set. This set forms an inhomogeneous PPP and the spatial density of it is derived. From the decoding set, a relay is selected that provides maximum average received power at the destination and the achievable coverage is derived due to this selection. The analysis is developed using tools from stochastic geometry and is verified using Monte-Carlo simulation. The effects of beam misalignment and different power allocations at the source and relay on coverage probability are also analyzed. Finally, a direct link without relaying, a randomly chosen relay link, and a link with proposed relay selection are compared in terms of coverage probability, rate coverage and spectral efficiency. Impressive performance gains achievable with relay selection are demonstrated.

3.1 Introduction and Motivation

As mentioned in Chapter 2, the use of mmW bands is constrained by several propagation challenges, but the payback is the abundance of spectrum with potential 5G applications.

¹Chapter 3 has been published in the IEEE Access as [59] and also in part in the Proceedings of IEEE Conference on Communications [78].

For these reason, the performance of mmW networks has been investigated extensively [3], [4], [64], [68], [79], [80]. For example, the work in [3] develops a general framework to analyze coverage and data rate. It considers blockages, directional antenna gains, mmW channel models, random locations of base stations and users, and their association probabilities to LOS or NLOS base stations. A tractable fixed ball LOS model which considers mmW links for user access in lognormal shadowed channels is derived in [64]. Using empirical path loss models, this model derives both coverage and rate distribution. By exploiting the coverage analysis in [3], the work in [4] develops a comprehensive analysis of mmW cellular networks. Further, the work in [68] analyzes heterogeneous downlink coverage with multiple tiers of mmW cells, and also includes sub-6 GHz macro cells. In [79], signal-to-interference distribution is derived to study the rate performance of one-way and two-way ad-hoc networks by considering directional antennas, random blockages, and random channel access; surprisingly, the significant ability of NLOS links to mitigate outages is demonstrated.

Previous work on sub-6 GHz relays

Relay deployment improves coverage, throughput and reliability [28]. Performance analyses of relay networks have been extensive, and a few is briefly mentioned here. Based on analysis of outage probability and channel capacity, it is demonstrated that maximum SNR relay selection provides a full diversity order [37]. Reference [38] provides a unified analysis of two-hop AF relaying, with an exact CDF, a PDF and a moment generating function (MGF) of the received SNR. The work in [39] considers one source, one destination, and multiple relays. The relays whose end-to-end SNR are above a threshold are selected to help, to exploit the diversity. In [41], a cognitive multi-hop DF relay network with channel estimation errors is analyzed. Reference [40] considers multiple source-destination pairs, and each pair is assigned a fixed relay. Joint optimal bandwidth and power allocation are developed, with a target at sum rate maximization.

Previous work on mmW relays

Relaying may provide seamless coverage to NLOS regions such as the areas blocked by buildings and may also extend indoor coverage to outdoors [20]. Reference [81] provides the first multi-hop medium access control protocol for 60 GHz mmW relaying by utiliz-

ing the diffracted signals to overcome outages when the direct source-destination link is blocked. Optimal placement of dual-hop relays to overcome blockages and rain attenuation is proposed in [82]. Highly dense mmW AF relays have been investigated to improve coverage [44]. The coverage probability is derived by considering spatially random relays, effect of blockage, and log-normal shadowing. Coverage of device-to-device mmW relaying is analyzed in [83]. Two-way relay selection also provides substantial coverage improvements [60].

Previous work on spatial randomness of relays in mmW and sub-6 GHz bands

A great deal of previous research on relays going back to several decades has focused on fixed network topologies, where the locations of users and relay nodes are fixed. However, this focus has shifted to random configurations in recent years [76]. The reason is that due to the massive growth of mobile networks, deployment constraints, and user mobility, it is clear that the locations of most nodes are not fixed, but random. Thus, for added realism, the locations of relay nodes can be modeled via one of the point processes described in Section 2.3. However, the wireless literature has widely used the homogeneous PPP because of its analytical tractability [73]. That is also the choice made in this thesis.

For sub-6 GHz relay networks, the locations of nodes as PPPs have been widely modeled [42], [43], [84]–[87]. For instance, in [42], using tools from stochastic geometry, outage performance is analyzed for a DF relay network. This work has been extended to DF cognitive relay networks in [84]. In [85], coverage probability is analyzed for AF relays, where the locations of the relays form a homogeneous PPP. The achievable transmission capacity of relay-assisted device-to-device links has been analyzed in [86]. Simulation results for DF relaying in a cellular network are presented in [87], where the base stations, relays, and user nodes are distributed as PPPs. For mmW bands, on the other hand, the effect of spatial randomness of relays has also been studied, albeit not so widely. For example, AF relays for one-way [44], [83] and two-way [60] relaying significantly improve coverage probability and spectral efficiency. However, the effect of small-scale fading is not considered in the analysis [44], [60], [83].

3.1.1 Problem Statement and Contributions

A comprehensive analysis of mmW DF networks with best relay selection² and taking into consideration the spatial randomness of relay nodes and small-scale fading is useful. Specifically, the following engineering questions are of interest. What is the impact of small-scale fading? What role does the spatial randomness of relay nodes play? What are the coverage and rate improvements possible with relay selection? What is the impact of beam-alignment errors? Both analysis and computational results will be explored to answer these questions.

The major contributions of this chapter are as follows:

- To model mmW small-scale fading, Nakagami- m fading with different m values are used represent LOS and NLOS cases [3]. Blockages from obstacles such as buildings in urban areas are also incorporated. The blockage model derived in [69] is adopted, which uses random shape theory and randomly drawn blockage parameters. The locations of the mmW DF relays are modeled as a homogeneous PPP in the \mathbb{R}^2 plane with the constant spatial density of $\lambda > 0$ nodes per unit area.
- To analyze the best relay selection, the spatial distribution of the decoding set of relays that meet the decoding SNR threshold is derived first. The locations of the relays in the decoding set form an inhomogeneous PPP whose spatial density $\hat{\lambda}(x)$ is non-uniform over $x \in \mathbb{R}^2$. This set is then partitioned into LOS and NLOS subsets and the distributions of the distance from destination to the nearest relay in these subsets are derived. By using these distributions, the association probabilities of the destination to the LOS and NLOS sets are derived.
- To quantify the performance of best relay selection, coverage probability is derived and compared against that of the direct link (no relaying). Significant gains are demonstrated. The coverage probability with random relay selection is also derived. Again, the best relay selection significantly outperforms random selection.
- Finally, to study the impact of various deployment constraints, the impact of beam alignment errors and the effect of power allocation at source and relay is analyzed.

²In this chapter, best relay selection refers to selecting the relay that provides maximum average SNR at the destination. Thus, this scheme may also be termed as “maximum average SNR based relay selection”.

The rate coverage probability and the spectral efficiency are derived. All the theoretical derivations are validated by comparing them with extensive Monte Carlo simulations.

It is further emphasized that previous works, including [3], [4], [64], [68], [79], [80], have not considered relay deployments. Other works on mmW relaying [44], [60], [83] do not consider the effect of small-scale (multi-path) fading as they only include distance-dependent path loss or lognormal shadowing. They also do not consider DF relays. Note that, multi-path components are not insignificant in NLOS scenarios [22], [79]. Therefore, different m factors for LOS and NLOS cases will paint a more realistic picture [3].

The rest of the chapter is organized as follows. Section 3.2 presents the system model including SNR and network models. Section 3.3 provides the main analytical results, including coverage probability, the spatial density of the decoding set, and coverage of the direct link. Section 3.4 investigates the effect of beam misalignment errors, different power allocation at the source and the relay, rate coverage and spectral efficiency. Section 3.5 discusses the analytical and simulation results. Section 3.6 summarizes the contribution of this chapter and provides the conclusion.

3.2 System Model

This section introduces the system model including the network model and the SNR model.

3.2.1 Network Modeling

Consider a mmW wireless network with a source (S), a destination (D) and a set of relays which are distributed in \mathbb{R}^2 -plane according to a homogeneous PPP of density λ (Fig. 3.1). The fixed distance between S and D is denoted by W . S can communicate with D either directly or via a relay selected from the available set of relays. A typical relay is denoted by R . S transmits with power P_S , and for simplicity, all potential relay nodes are assumed to have equal transmit power of P_R . The extension to unequal transmit powers of relays is straightforward and omitted. Without loss of generality, the destination (D) is assumed to be located at the origin for the tractability of the analysis. In fact, any other location for the destination provides the same performance in a homogeneous PPP due to Slivnyak theorem [75].

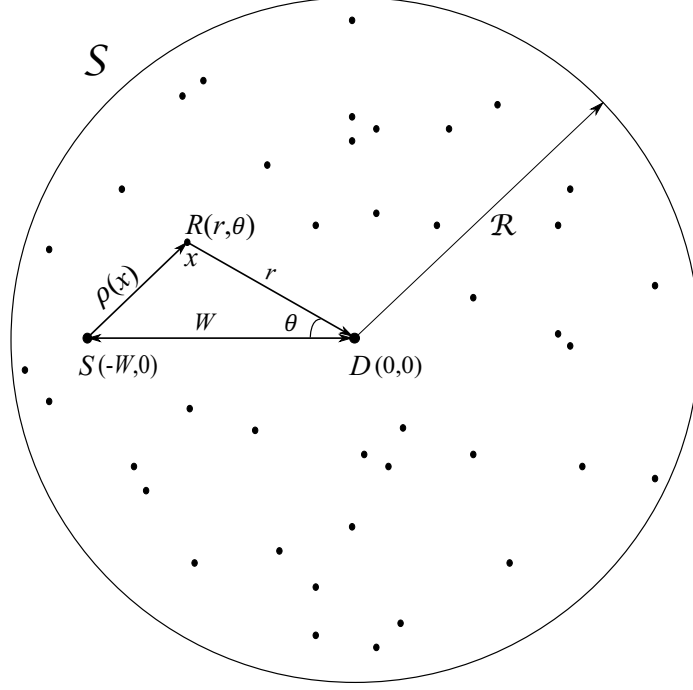


Figure 3.1: Geometrical locations of S , D and a typical relay (R).

The PPP is denoted by $\Phi = \{x_1, x_2, x_3, \dots\}$, where $x_j \in \mathbb{R}^2$ is the location of the j -th relay, $j \in \{1, 2, \dots, N\}$, and N is a Poisson random variable with mean $\lambda\pi\mathcal{R}^2$. Without loss of accuracy, only the relay nodes inside the circular disc \mathcal{S} of radius \mathcal{R} are considered. The nodes outside \mathcal{S} are ignored because of very high path loss and increased blockage probability associated with large distances. Therefore, \mathcal{S} is essentially equivalent to entire \mathbb{R}^2 [60]. For notational convenience, x rather than x_j denotes the location of a typical relay node (R), and x is interchangeably used as a polar coordinate (r, θ) . In this chapter, the exponential decay blockage model in Section 2.1.5, the directional beamforming model in (2.7), and the small scale fading discussed in Section 2.1.3 are used.

3.2.2 SNR Model

With the system model above, the instantaneous received SNR for a link of length d is given by

$$\text{SNR} = \frac{P\Psi|h_l|^2}{d^{\alpha_l}N_0}, \quad (3.1)$$

where $l \in \{L, N\}$ denote the LOS and NLOS conditions, respectively, $P \in \{P_S, P_R\}$ is the transmit power, $\Psi \triangleq G_{\text{eq}} \left(\frac{c}{4\pi f} \right)^2$ is a constant that includes the directional gain and reference path gain at a 1 m distance with c being the speed of light and f being the

operating frequency, $|h_l|^2$ is the gamma distributed fading power, α_L and α_N are the path loss exponents for LOS and NLOS links, respectively, and N_0 is the noise power.

3.3 Performance Analysis

In this section, the coverage probability is analyzed for three modes: (1) direct mode (i.e. no relaying), (2) best relay-selection mode and (3) random relay-selection mode. Beam misalignment errors, effect of source and relay power allocation factor, rate coverage and spectral efficiency will be analyzed in Section 3.4. To aid the analysis, the following two standard assumptions are made.

1. Only additive noise is considered at the relay and destination and co-channel interference is ignored. The noise-limited analysis is realistic for sparse deployment of nodes and high path loss with distance and the narrow mmW beams [19]. However, with dense deployment of nodes, this assumption no longer holds. The system in that case will be limited co-channel interference. An interference-limited case is treated in Chapter 4.
2. Channel state information is assumed to be available at S , D and R so the beam alignment to the desired direction is possible without the need for further beam training. For example, methods in [28] can be used to obtain fading information, and the methods in [63], [80], [88] can be used to acquire information on direction. Impacts of imperfect channel state information and timing overhead associated with initial beam training can be potential future research topics. Moreover, to reduce the overhead in practical systems, the search for potential relays can be restricted to few sectors aligned with the direction of the destination.

3.3.1 Direct Mode

When there is no blockage in the $S - D$ link, transmission can occur even without the help of a relay. The direct link can achieve the required SNR or data rate when the $S - D$ distance is short or when the $S - D$ link is not blocked. Using the direct link has the additional benefit of needing only one time slot, compared to the two time slots required in a relay link. Therefore, the analysis of the coverage probability of a direct link is also of great significance.

Coverage Probability of Direct Link

This is defined as the probability that the received SNR exceeds a predefined threshold γ_{th} .

Lemma 1. *The coverage probability of the direct link ($S - D$) is given by*

$$P_{\text{cov},SD} = p_L(W)P_{SD,L}(\gamma_{\text{th}}) + p_N(W)P_{SD,N}(\gamma_{\text{th}}), \quad (3.2)$$

where $p_L(W)$ and $p_N(W)$, respectively, are the LOS and NLOS probabilities of the $S - D$ link given in (2.9) and (2.10), $P_{SD,L}(\gamma_{\text{th}})$ and $P_{SD,N}(\gamma_{\text{th}})$ are the conditional coverage probabilities given that the links are in LOS and NLOS conditions, respectively, and are expressed as

$$P_{SD,L}(\gamma_{\text{th}}) = \sum_{n=1}^{m_L} (-1)^{n+1} \binom{m_L}{n} \exp\left(-na_L W^{\alpha_L}\right) \quad (3.3)$$

and

$$P_{SD,N}(\gamma_{\text{th}}) = \sum_{n=1}^{m_N} (-1)^{n+1} \binom{m_N}{n} \exp\left(-na_N W^{\alpha_N}\right), \quad (3.4)$$

where $a_L = \frac{\eta_L \gamma_{\text{th}} N_0}{P_S \Psi}$, $a_N = \frac{\eta_N \gamma_{\text{th}} N_0}{P_S \Psi}$, $\eta_L = m_L (m_L!)^{-\frac{1}{m_L}}$, and $\eta_N = m_N (m_N!)^{-\frac{1}{m_N}}$.

Proof. Equation (3.2) is obtained using the law of total probability, where $p_L(W)$ and $p_N(W)$ represent the LOS and NLOS probabilities for a link of distance W . Next the conditional coverage probability $P_{SD,L}(\gamma_{\text{th}})$ is derived, which is the probability that $\text{SNR}_{SD,L}$ (SNR of the $S - D$ link when it is in LOS condition) is above the predefined threshold γ_{th} , as follows.

$$\begin{aligned} P_{SD,L}(\gamma_{\text{th}}) &= \mathbb{P}(\text{SNR}_{SD,L} > \gamma_{\text{th}}) \\ &= \mathbb{P}\left(\frac{P_S \Psi |h_L|^2 W^{-\alpha_L}}{N_0} > \gamma_{\text{th}}\right) \\ &= 1 - \mathbb{P}\left(|h_L|^2 < \frac{\gamma_{\text{th}} N_0 W^{\alpha_L}}{P_S \Psi}\right) \\ &\stackrel{(a)}{\approx} 1 - \left(1 - \exp\left(-\frac{\eta_L \gamma_{\text{th}} N_0 W^{\alpha_L}}{P_S \Psi}\right)\right)^{m_L} \\ &= \sum_{n=1}^{m_L} (-1)^{n+1} \binom{m_L}{n} \exp(-na_L W^{\alpha_L}), \end{aligned} \quad (3.5)$$

where the approximation (a) is used similar to that in [3] for the normalized gamma random

variable and the final step follows from the binomial expansion. Similarly, $P_{SD,N}(\gamma_{\text{th}})$ can be derived as shown in (3.4). ■

Remark 1. *Lemma 1 provides the coverage probability in terms of LOS and NLOS link coverages using the law of total probability.*

3.3.2 Relay Selection

When a direct link is not possible due to excessive path loss or blockage, transmission must occur via a relay link. The DF relaying protocol is used and no decoding error is assumed to occur if the received SNR is greater than the threshold γ_{th} . A half duplex relaying operation is adopted, i.e., two time slots are used. During the first time slot, the source sends to the relays. For a candidate relay, it can successfully decode the source's message if its received SNR is above the threshold γ_{th} .

In fixed topology AF or DF networks, the optimal relay selection criterion is the maximization of end-to-end SNR [28] or the maximization of the minimum SNR of $S - R$ and $R - D$ links [37]. However, when the relay locations form a PPP, closed-form analysis of these criteria is intractable. Therefore, a tractable selection strategy is used with the following two stages:

- A set of relays is selected that can successfully decode the source's message. This is referred as the decoding set and denoted by $\hat{\Phi}$. This set is a subset of Φ , i.e., the set of relays that can meet the required SNR threshold for decoding. Any node in $\hat{\Phi}$ can retransmit the successfully decoded message to the destination D . Since the relay's SNR in $S - R$ link highly depends on its distance from S and whether the link is in the LOS or NLOS condition, the decoding set is not uniform in \mathbb{R}^2 . The spatial distribution of the decoding set is critical to derive coverage probability. This distribution is derived below.
- Next, a relay is selected from the decoding set that has the best link to the destination, i.e., provides the maximum average received power at D in $R - D$ link. Mathematically, the selected relay \hat{R} can be written as

$$\hat{R} = \underset{j}{\text{arg max}} \bar{P}_{R,D}(x_j, D) \quad (3.6)$$

where $\bar{P}_{R,D}(x_j, D) = P_R \Psi r^{-\alpha_l}$, $l \in \{L, N\}$ is the average received power at D due to an arbitrary relay located at x_j . Note that this does not mean selecting the point in $\hat{\Phi}$ closest to D due to the LOS and NLOS path loss differences. However, once the relays are divided according to LOS and NLOS sets in reference to D , only then the selected relay will be the nearest node in either LOS or NLOS set. The closest distance of the selected relay from D is a random variable and its probability density will be derived using Lemma 2.

The major reason for using the above-mentioned two-stage relay selection scheme is to facilitate the tractability of the analysis. This is because the analysis of existing relay selection strategies, such as presented in [27] and references therein, which maximize the instantaneous received SNR at D require the path loss or distance information for each relay from S and D when randomly located relays are considered. The scheme used in this chapter avoids such necessity and still provides the average network performance by utilizing stochastic geometry tools for randomly located relay nodes. Moreover, this scheme decreases the signaling overhead needed for relay selection because the channel estimation in the $R - D$ link is required only for the decoding set of relays instead of the entire set.

Distribution of Decoding Set of Relays

Mathematically, the decoding set can be defined as

$$\hat{\Phi} = \{x \in \Phi, \text{SNR}_{s,x} \geq \gamma_{\text{th}}\} \quad (3.7)$$

where s is the location of S , and $\text{SNR}_{s,x}$ is the received SNR of the relay at point $x \in \Phi$. With this rule, a relay located at x in the original point process Φ is included in $\hat{\Phi}$ if the received SNR at x from S is above the predefined threshold γ_{th} . Since $\text{SNR}_{s,x}$ is a function of the distance from x to S , the probability of inclusion in $\hat{\Phi}$ is also a function of x . Specifically, the nodes that are close to S have higher probability of being in the decoding set. Also since $\text{SNR}_{s,x}$ and $\text{SNR}_{s,x'}$ are independent for $x \neq x'$, this selection process is an independent thinning of the original process Φ . However, the thinning probability is not a constant but a function of x . Thus, $\hat{\Phi}$ is an inhomogeneous PPP for which the spatial density of nodes is location dependent. As such, the density of the resultant point process

can be written as [75]:

$$\hat{\lambda}(x) = \lambda \mathbb{P}(\text{SNR}_{s,x} \geq \gamma_{\text{th}}), \quad (3.8)$$

where $\mathbb{P}(\cdot)$ means probability. The final expression for $\hat{\lambda}(x)$ is given by

$$\hat{\lambda}(x) = \lambda \left\{ p_L(\rho(x)) \sum_{n=1}^{m_L} (-1)^{n+1} \binom{m_L}{n} \exp\left(-na_L(\rho(x))^{\alpha_L}\right) + (1 - p_L(\rho(x))) \sum_{n=1}^{m_N} (-1)^{n+1} \binom{m_N}{n} \exp\left(-na_N(\rho(x))^{\alpha_N}\right) \right\} \quad (3.9)$$

where $\rho(x)$ is the distance from S to an arbitrary relay R located at x and $p_L(\rho(x))$ is the LOS probability of $S - R$ link. Since the relays are considered to be distributed in a disc \mathcal{S} of radius \mathcal{R} centered at D (origin), the average number of decoding relays can be obtained as

$$\hat{\Lambda}(\mathcal{S}) = \int_{\mathcal{S}} \hat{\lambda}(x) dx = \int_0^{\mathcal{R}} \int_0^{2\pi} \hat{\lambda}(r, \theta) r d\theta dr, \quad (3.10)$$

where (r, θ) represents the location x in polar coordinate and in the rest of the chapter, $\hat{\lambda}(x)$ and $\hat{\lambda}(r, \theta)$ are used interchangeably. The analysis of coverage requires the distributions of the Euclidean distances from the relays to S and D . Since the path loss is dependent on the distance, use of a polar coordinate to represent the location of a relay is the most convenient for analysis. Thus, the coordinate axis is set to be oriented along the line joining source and destination so that $\rho(x) = \|x - s\| = \sqrt{r^2 - 2rW \cos \theta + W^2} = \rho(r, \theta)$. The final expression for $\hat{\Lambda}(\mathcal{S})$ is given by

$$\hat{\Lambda}(\mathcal{S}) = \lambda \left\{ \sum_{n=1}^{m_L} (-1)^{n+1} \binom{m_L}{n} \int_{r=0}^{\mathcal{R}} \int_{\theta=0}^{2\pi} p_L(\rho(r, \theta)) \exp\left(-na_L(\rho(r, \theta))^{\alpha_L}\right) r d\theta dr + \sum_{n=1}^{m_N} (-1)^{n+1} \binom{m_N}{n} \int_{r=0}^{\mathcal{R}} \int_{\theta=0}^{2\pi} (1 - p_L(\rho(r, \theta))) \exp\left(-na_N(\rho(r, \theta))^{\alpha_N}\right) r d\theta dr \right\}. \quad (3.11)$$

A realization of all nodes, the decoding set, and the selected relay are depicted in Fig. 3.2. Since $\hat{\Phi}$ is an inhomogeneous PPP of density $\hat{\lambda}(x)$, it can be divided into two independent processes of densities $p_L(r)\hat{\lambda}(x)$ and $(1 - p_L(r))\hat{\lambda}(x)$ to represent the LOS and NLOS sets, respectively from D . The LOS and NLOS sets are denoted by $\hat{\Phi}_L$ and $\hat{\Phi}_N$,

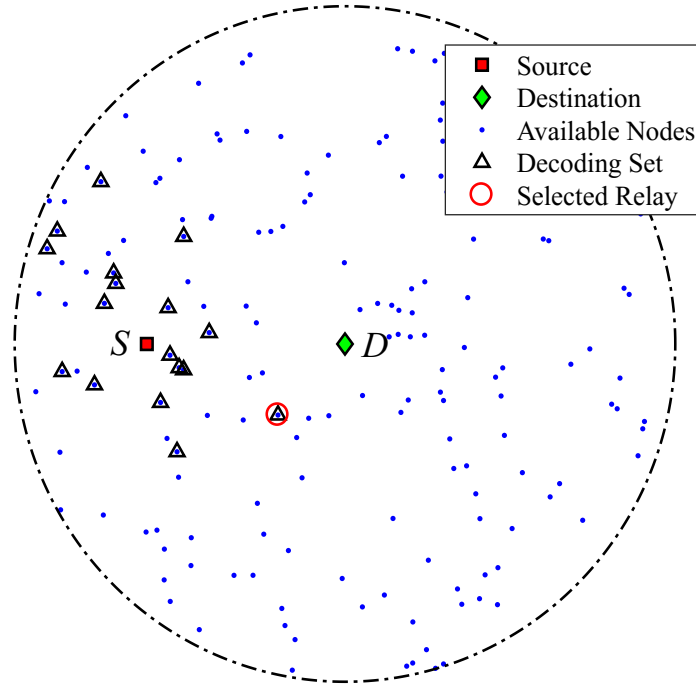


Figure 3.2: One snapshot of relay locations with S and D as shown. The potential relays (dots) form a PPP. The decoding set is clustered around S . Its nodes form an inhomogeneous PPP. In the decoding set, the node with minimum path loss to D is selected as the relay.

respectively.

Coverage Probability With Relay Selection

Coverage is the probability that the received SNR at the destination D from the selected relay is above the predefined threshold γ_{th} . Note that the same threshold γ_{th} is used to determine the relays in the decoding set $\hat{\Phi}$ shown in eq. (3.7). The reason for this is that the equivalent end-to-end SNR of a DF relay is the minimum of two-hop SNRs [26], and setting the same threshold for both links ensures that this condition is satisfied. To derive the coverage probability with relay selection, selected relay needs to be determined first. It is the one with the smallest path loss at the destination in an $R - D$ link. This means the selected relay can only be either the nearest node in $\hat{\Phi}_L$ or the nearest one in $\hat{\Phi}_N$. To derive the coverage probability, the knowledge of whether a relay from $\hat{\Phi}_L$ or $\hat{\Phi}_N$ is selected is needed, and for that, the distribution of distance of the nearest relays in $\hat{\Phi}_L$ and $\hat{\Phi}_N$ from destination are required.

Lemma 2. *The complimentary cumulative distribution function (CCDF) of r_L , which is*

the distance from the destination to the nearest LOS relay, is given by

$$\bar{F}_{r_L}(z) = \exp\left(-\int_{r=0}^z \int_{\theta=0}^{2\pi} p_L(r) \hat{\lambda}(x) r d\theta dr\right), \quad z > 0. \quad (3.12)$$

Proof. The distribution of the distance between the nearest LOS relay from the destination D (at origin) can be derived by utilizing the probability that no LOS relays are in $\mathcal{B}(0, z)$, where $\mathcal{B}(0, z)$ is the ball centered at D and with radius z . This is called the void probability for a PPP, and can be written as [75]

$$\begin{aligned} \bar{F}_{r_L}(z) &= \mathbb{P}(r_L > z) \\ &= \mathbb{P}\{\text{no LOS relays in } \mathcal{B}(0, z)\} \\ &= \exp(-\Lambda_L([0, z])), \end{aligned} \quad (3.13)$$

where $\Lambda_L([0, z])$ is the mean number of LOS relays in $\mathcal{B}(0, z)$, which can be derived as

$$\Lambda_L([0, z]) = \int_{r=0}^z \int_{\theta=0}^{2\pi} p_L(r) \hat{\lambda}(x) r d\theta dr. \quad (3.14)$$

Substituting (3.14) in (3.13), the distribution in (3.12) is obtained. ■

Remark 2. Lemma 2 provides an intermediate result to derive the probability density function (PDF) of the distance of the nearest LOS relay from the destination.

Now, because PDF is the negative derivative of the CCDF, $f_{r_L}(z)$ is given by

$$f_{r_L}(z) = z p_L(z) \hat{\lambda}(z, \theta) e^{-\int_{r=0}^z \int_{\theta=0}^{2\pi} p_L(r) \hat{\lambda}(x) r d\theta dr}. \quad (3.15)$$

Similarly, the CCDF of r_N , which is the distance from the destination to the nearest NLOS relay, can be derived as

$$\bar{F}_{r_N}(z) = \exp\left(-\int_{r=0}^z \int_{\theta=0}^{2\pi} (1 - p_L(r)) \hat{\lambda}(x) r d\theta dr\right), \quad (3.16)$$

and the corresponding PDF as

$$f_{r_N}(z) = z(1 - p_L(z)) \hat{\lambda}(z, \theta) e^{-\int_{r=0}^z \int_{\theta=0}^{2\pi} (1 - p_L(r)) \hat{\lambda}(x) r d\theta dr}. \quad (3.17)$$

By using these distributions of the distance from the destination to the nearest LOS and NLOS relays, the probability A_L that an LOS relay will be selected to serve is derived next. The selection is based on maximizing the average received power from the candidate relay node or equivalently minimizing the path loss of $R - D$ link.

Lemma 3. *The probability that an LOS relay is selected is given by*

$$A_L = \int_0^\infty \bar{F}_{r_N}(z^{\frac{\alpha_L}{\alpha_N}}) f_{r_L}(z) dz \quad (3.18)$$

where $\bar{F}_{r_N}(z)$ is given in (3.16).

Proof. The nearest LOS relay is selected if it provides higher average received power than that from the nearest NLOS relay, i.e.,

$$\begin{aligned} A_L &\triangleq \mathbb{P}(P_R \Psi r_L^{-\alpha_L} > P_R \Psi r_N^{-\alpha_N}) \\ &= \mathbb{P}\left(r_N > r_L^{\left(\frac{\alpha_L}{\alpha_N}\right)}\right) \\ &= \int_0^\infty \mathbb{P}\left(r_N > r_L^{\left(\frac{\alpha_L}{\alpha_N}\right)} \mid r_L = z\right) f_{r_L}(z) dz \\ &= \int_0^\infty \bar{F}_{r_N}\left(z^{\left(\frac{\alpha_L}{\alpha_N}\right)}\right) f_{r_L}(z) dz, \end{aligned} \quad (3.19)$$

where $\bar{F}_{r_N}(z)$ is given in (3.16). ■

Remark 3. *Lemma 3 gives the probability that the destination is associated to an LOS or NLOS relay, and is also used to derive the distribution of the distance of a selected relay from the destination in Lemma 4. This probability is similar to the base station association probabilities in multi-tier and heterogeneous cellular networks [68], but with inhomogeneous PPP distributed base stations. The integral can be computed numerically using mathematical software such as MATLAB.*

The probability that an NLOS relay will be used to serve, A_N , is given by

$$A_N = 1 - A_L. \quad (3.20)$$

Lemma 4. *Given that an LOS relay is selected to serve, the PDF of its distance from the destination is*

$$g_{r_L}(z) = \frac{f_{r_L}(z)}{A_L} \exp \left(- \int_{r=0}^{z^{\frac{\alpha_L}{\alpha_N}}} \int_{\theta=0}^{2\pi} (1 - p_L(r)) \hat{\lambda}(x) r d\theta dr \right). \quad (3.21)$$

Given that an NLOS relay is selected to serve, the PDF of its distance from the destination is

$$g_{r_N}(z) = \frac{f_{r_N}(z)}{A_N} \exp \left(- \int_{r=0}^{z^{\frac{\alpha_N}{\alpha_L}}} \int_{\theta=0}^{2\pi} p_L(r) \hat{\lambda}(x) r d\theta dr \right). \quad (3.22)$$

Proof. The proof is given in Appendix A.1. ■

Lemma 4 enables the computation of coverage probability in the following theorem.

Theorem 1. *The overall coverage probability at the destination using the selected relay is given by*

$$P_{\text{cov},SRD} = A_L P_{R,L}(\gamma_{\text{th}}) + A_N P_{R,N}(\gamma_{\text{th}}), \quad (3.23)$$

where $P_{R,l}(\gamma_{\text{th}})$, $l \in \{L, N\}$ is the conditional coverage probability given that a relay from $\hat{\Phi}_l$, $l \in \{L, N\}$ is selected, which is given by

$$P_{R,L}(\gamma_{\text{th}}) \approx \sum_{k=1}^{m_L} (-1)^{k+1} \binom{m_L}{k} \int_{\theta=0}^{2\pi} \int_{z=0}^{\infty} e^{-kb_L z^{\alpha_L}} g_{r_L}(z) z dz d\theta, \quad (3.24)$$

and

$$P_{R,N}(\gamma_{\text{th}}) \approx \sum_{k=1}^{m_N} (-1)^{k+1} \binom{m_N}{k} \int_{\theta=0}^{2\pi} \int_{z=0}^{\infty} e^{-kb_N z^{\alpha_N}} g_{r_N}(z) z dz d\theta, \quad (3.25)$$

where $b_L = \frac{\eta_L \gamma_{\text{th}} N_0}{P_R \Psi}$, and $b_N = \frac{\eta_N \gamma_{\text{th}} N_0}{P_R \Psi}$.

Proof. Here, the conditional coverage probability is derived when a relay from LOS relays is selected, i.e., the relay from $\hat{\Phi}_L$ closest to the destination is selected. Thus, coverage can

be written as

$$\begin{aligned} P_{R,L}(\gamma_{\text{th}}) &= \mathbb{P} \left(\frac{P_R \Psi |h_L|^2 r_L^{-\alpha_L}}{N_0} > \gamma_{\text{th}} \right) \\ &= 1 - \mathbb{P} \left(|h_L|^2 < \frac{\gamma_{\text{th}} N_0 r_L^{\alpha_L}}{P_R \Psi} \right). \end{aligned}$$

Now, using a similar approximation to that in (3.5), the following can be obtained:

$$\begin{aligned} P_{R,L}(\gamma_{\text{th}}) &\approx \mathbb{E}_{\hat{\Phi}_L} \left[\sum_{k=1}^{m_L} (-1)^{k+1} \binom{m_L}{k} e^{-k b_L r_L^{\alpha_L}} \right] \\ &= \sum_{k=1}^{m_L} (-1)^{k+1} \binom{m_L}{k} \int_{\theta=0}^{2\pi} \int_{z=0}^{\infty} e^{-k b_L z^{\alpha_L}} g_{r_L}(z) z dz d\theta \end{aligned} \quad (3.26)$$

where $\mathbb{E}_{\hat{\Phi}_L}[\cdot]$ means expectation over $\hat{\Phi}_L$. Following same steps, the expression for $P_{R,N}(\gamma_{\text{th}})$ in (3.25) can be derived. ■

The integrals in (3.24) and (3.25) can be numerically evaluated using mathematical software such as MATLAB.

3.3.3 Coverage Probability With Random Relay Selection

The aforementioned best relay selection strategy requires the directional and channel state information either at an end-node or at a central controller to perform the relay selection. Moreover, accurate directional estimation and channel estimation needs multiple time-slots and pilot signals, and the signaling and time overhead increase with an increasing number of nodes [28], [63], [80], [88]. For example, in sub-6 GHz networks, an optimal relay selection strategy that maximizes the minimum end-to-end received SNR for a single source-destination pair with multiple relays has a complexity that is quadratic in the number of relays [89]. Similarly, a suboptimal relay selection scheme in [28] for a single source-destination pair has a linear complexity in the number of users. However, the complexity of relay selection scheme used in this chapter depends both on the number of relays as well as on the initial access scheme used to establish directional links [80]. For instance, when a codebook consisting of a predefined or adaptive directional vectors is used to find the best path for a given link, extensive channel training requiring multiple time slots can be avoided [63], [88]. Therefore, these overheads required for initial access can significantly

impact the performance and should be taken into account in evaluating the complexity of relay selection in mmW networks.

Therefore, it may be worthwhile to consider lower-complexity alternatives. Perhaps the simplest option is to randomly pick relay in the proximity to both S and D . To do this, only the position information of the nodes is required, which can be readily obtained [90], and pick a relay at random from available nodes that reside in between S and D . This offers a trade-off between complexity and performance, because such a relay might perform poorly as it can be in NLOS from S or D with high probability. Intuitively, picking a relay in between S and D makes $S - R$ and $R - D$ links shorter and results in smaller path loss in each link. Of course, it is not possible to locate a node exactly on the straight line joining S and D . Therefore, a relay is selected from within a circle centered at the midpoint of S and D and having radius \mathcal{L} . Note that this circle is smaller than entire \mathcal{S} (Fig. 3.1) and the coverage is zero if there is no nodes inside the circle. Now, the coverage probability at the destination with such a selection can be written as

$$P_{\text{cov,rand}} = P_{\text{rand,SR}} \times P_{\text{rand,RD}}, \quad (3.27)$$

where $P_{\text{rand,SR}} = \mathbb{P}(\text{SNR}_{SR} \geq \gamma_{\text{th}})$ and $P_{\text{rand,RD}} = \mathbb{P}(\text{SNR}_{RD} \geq \gamma_{\text{th}})$ respectively are the CCDFs of individual link SNRs (i.e., coverage probabilities in $S - R$ and $R - D$ links).

The expression for $P_{\text{rand,SR}}$ is given by

$$\begin{aligned} P_{\text{rand,SR}} &= \sum_{n=1}^{m_L} (-1)^{n+1} \binom{m_L}{n} \frac{1}{2\pi} \int_{\theta=0}^{2\pi} \int_{\zeta=0}^{\mathcal{L}} \zeta e^{-\beta\rho_1} e^{-na_L\rho_1^{\alpha_L}} f_{\zeta}(\zeta) d\zeta d\omega, \\ &+ \sum_{n=1}^{m_N} (-1)^{n+1} \binom{m_N}{n} \frac{1}{2\pi} \int_{\theta=0}^{2\pi} \int_{\zeta=0}^{\mathcal{L}} \zeta (1 - e^{-\beta\rho_1}) e^{-na_N\rho_1^{\alpha_N}} f_{\zeta}(\zeta) d\zeta d\omega, \end{aligned} \quad (3.28)$$

where $\rho_1 = \sqrt{\zeta^2 + (W/2)^2 - \zeta W \cos\omega}$ is the distance of a randomly selected relay from S , in which ζ is the distance of this relay from the midpoint of S and D and ω is its angular location with reference to the midpoint of S and D . The expressions of a_L and a_N are given in Lemma 1, and $f_{\zeta}(\zeta)$ is the PDF of the distance of a randomly picked relay from

the midpoint of the $S - D$ link and is given by

$$f_{\zeta}(\zeta) = \frac{2\zeta}{\mathcal{L}^2}, \quad 0 < \zeta < \mathcal{L}. \quad (3.29)$$

The derivation of (3.28) follows that of (3.3) and is omitted. The coverage probability of the $R - D$ link, $P_{\text{rand},RD}$ can be written similar to (3.28), with ρ_1 replaced by ρ_2 , where $\rho_2 = \sqrt{\zeta^2 + (W/2)^2} + \zeta W \cos \omega$ is the distance of the randomly picked relay from the destination, and a_L and a_N replaced by b_L and b_N , respectively, which are given in Theorem 1. In the simulations, unless otherwise stated, $\mathcal{L} = W/2$ is used, i.e., a relay is picked from inside a circle centered at midpoint of S and D with diameter W .

3.4 Some Extensions

3.4.1 Coverage Probability With Beam Alignment Errors

Up until now, perfect beam alignment is assumed, and thus coverage probabilities (3.2) and (3.23) are derived without considering beam alignment errors. Next, the effect of beam alignment errors on coverage probability is investigated.

The analytical method discussed in Section 2.1.4 is used here. For an $S - D$, $S - R$, or $R - D$ link, let ε denote the beam alignment error, which follows a Gaussian distribution with zero mean and variance σ^2 . Thus, CDF of $|\varepsilon|$ (absolute value of the error) is expressed as $F_{|\varepsilon|}(x) = \text{erf}(x/(\sqrt{2}\sigma))$, where $\text{erf}(\cdot)$ is the Gaussian error function. Denote PDF of the effective antenna gain $G_{\text{eq},SD}$, $G_{\text{eq},SR}$ and $G_{\text{eq},RD}$ for the $S - D$, $S - R$ and $R - D$ links as $f_{G_{\text{eq},SD}}(y)$, $f_{G_{\text{eq},SR}}(y)$ and $f_{G_{\text{eq},RD}}(y)$, respectively. Thus, $f_{G_{\text{eq},SD}}(y)$, $f_{G_{\text{eq},SR}}(y)$ and $f_{G_{\text{eq},RD}}(y)$ all have the expression same as (2.8).

Error in direct link

Since the coverage probability (3.2) depends on the effective antenna gain $G_{\text{eq},SD}$ of the $S - D$ link, total $P_{\text{cov},SD}$ can be computed by averaging over $f_{G_{\text{eq},SD}}(y)$ as follows [68]:

$$\begin{aligned} P_{\text{cov},SD} &= \int_0^{\infty} P_{\text{cov},SD}(y) f_{G_{\text{eq},SD}}(y) dy \\ &= F_{|\varepsilon|}(\phi/2)^2 P_{\text{cov},SD}(G_{\text{max}}^2) + 2F_{|\varepsilon|}(\phi/2) \bar{F}_{|\varepsilon|}(\phi/2) P_{\text{cov},SD}(G_{\text{max}} G_{\text{min}}) \\ &\quad + \bar{F}_{|\varepsilon|}(\phi/2)^2 P_{\text{cov},SD}(G_{\text{min}}^2) \end{aligned} \quad (3.30)$$

where $P_{\text{cov},SD}(y)$ refers to the coverage probability (3.2) as a function of effective antenna gain y of $S - D$ link gain, and $\bar{F}_{|\varepsilon|}(\cdot) \triangleq 1 - F_{|\varepsilon|}(\cdot)$.

Error using relays

It is reasonable to assume that the beam alignment errors in the $S - R$ and $R - D$ links are independent. Thus, the overall coverage probability $P_{\text{cov},SRD}$ by using the selected relay is given by [60]

$$\begin{aligned}
P_{\text{cov},SRD} &= \int_0^\infty \int_0^\infty P_{\text{cov},SRD}(y_1, y_2) f_{G_{\text{eq},SR}}(y_1) f_{G_{\text{eq},RD}}(y_2) dy_1 dy_2 \\
&= F_{|\varepsilon|}(\phi/2)^4 P_{\text{cov},SRD}(G_{\text{max}}^2, G_{\text{max}}^2) \\
&\quad + 2F_{|\varepsilon|}(\phi/2)^3 \bar{F}_{|\varepsilon|}(\phi/2) P_{\text{cov},SRD}(G_{\text{max}}^2, G_{\text{max}}G_{\text{min}}) \\
&\quad + F_{|\varepsilon|}(\phi/2)^2 \bar{F}_{|\varepsilon|}(\phi/2)^2 P_{\text{cov},SRD}(G_{\text{max}}^2, G_{\text{min}}^2) \\
&\quad + 2F_{|\varepsilon|}(\phi/2)^3 \bar{F}_{|\varepsilon|}(\phi/2) P_{\text{cov},SRD}(G_{\text{max}}G_{\text{min}}, G_{\text{max}}^2) \\
&\quad + 4F_{|\varepsilon|}(\phi/2)^2 \bar{F}_{|\varepsilon|}(\phi/2)^2 P_{\text{cov},SRD}(G_{\text{max}}G_{\text{min}}, G_{\text{max}}G_{\text{min}}) \\
&\quad + 2F_{|\varepsilon|}(\phi/2) \bar{F}_{|\varepsilon|}(\phi/2)^3 P_{\text{cov},SRD}(G_{\text{max}}G_{\text{min}}, G_{\text{min}}^2) \\
&\quad + F_{|\varepsilon|}(\phi/2)^2 \bar{F}_{|\varepsilon|}(\phi/2)^2 P_{\text{cov},SRD}(G_{\text{min}}^2, G_{\text{max}}^2) \\
&\quad + 2F_{|\varepsilon|}(\phi/2) \bar{F}_{|\varepsilon|}(\phi/2)^3 P_{\text{cov},SRD}(G_{\text{min}}^2, G_{\text{max}}G_{\text{min}}) \\
&\quad + \bar{F}_{|\varepsilon|}(\phi/2)^4 P_{\text{cov},SRD}(G_{\text{min}}^2, G_{\text{min}}^2), \tag{3.31}
\end{aligned}$$

where $P_{\text{cov},SRD}(y_1, y_2)$ means the coverage probability (3.23) as a function of y_1 (the effective antenna gain of the $S - R$ link) and y_2 (the effective antenna gain of the $R - D$ link).

3.4.2 Effect of power allocation factor

Let the total transmit power of the system be P_T . To study the effect of dividing up P_T between the source and the relay, a power factor $\xi = \frac{P_S}{P_S + P_R}$ is defined first. With this, the power of $P_S = \xi P_T$ is allocated to the source and $P_R = (1 - \xi) P_T$ to the selected relay.

3.4.3 Rate Coverage Probability

Rate coverage is the probability that the link achieves a rate greater than or equal to the rate threshold $\Gamma_{\text{th}} > 0$. Since the rate gives a true measure of data bits received per second at the

receiver, it is a critical performance metric, indicating the capacity of the link. Moreover, this measure is specially relevant for mmW links, which are fundamentally motivated by achieving higher rates. The achievable rate using the relay can be written as

$$\Gamma = \frac{1}{2}B \log_2(1 + \text{SNR}), \quad (3.32)$$

where the factor of $1/2$ is used because two time slots are required for a complete transmission using a relay and B is the signal bandwidth.

Lemma 5. *The rate coverage probability of a relay transmission is given by*

$$P_{\text{cov,Rate}} = \mathbb{P}(\Gamma > \Gamma_{\text{th}}) = P_{\text{cov}}\left(2^{\frac{2\Gamma_{\text{th}}}{B}} - 1\right) \quad (3.33)$$

where $P_{\text{cov}}(\cdot)$ is the coverage probability in (3.23) or (3.27), which is a function of SNR threshold, γ_{th} .

Proof. The expression (3.33) is obtained straightforwardly by manipulating (3.32) and is omitted here. ■

Remark 4. *The rate coverage for the direct link is given by $P_{\text{cov,Rate}} = P_{\text{cov}}\left(2^{\frac{\Gamma_{\text{th}}}{B}} - 1\right)$ due to the use of single time slot for S to D transmission, and $P_{\text{cov}}(\cdot)$ is the coverage probability in (3.2) which is written as a function of SNR threshold γ_{th} .*

3.4.4 Average Throughput

This is the throughput of a given link per hertz of bandwidth. For two-hop transmission it can be expressed as,

$$\text{SE} = \frac{1}{2}P_{\text{cov}}(\gamma_{\text{th}}) \log_2(1 + \gamma_{\text{th}}), \quad (3.34)$$

where the factor of $1/2$ is due to the use of two time slots when relaying is used. For a fair comparison, this factor is not included in the spectral efficiency of the direct link.

3.5 Simulation and Analytical Results

In this section, the analytical results are validated by Monte Carlo simulations. Each simulation point is averaged over 10^5 independent realizations. Table 4.1 shows the simulation parameters unless otherwise specified. In the figures, the curves represent the analytical

Table 3.1: Simulation Parameters

Notation	Parameter	Value
P_S	Source transmit power	30 dBm
P_R	Relay transmit power	30 dBm
\mathcal{R}	Radius of the simulation area	1000 m
f	Operating frequency	28 GHz
B	System bandwidth	1 GHz
α_L, α_N	LOS and NLOS path loss exponents	2, 3.3 [67]
m_L, m_N	Nakagami-m parameters for LOS and NLOS cases	3, 2 [3]
G_{\max}, G_{\min}	Main lobe and side lobe gains	18 dBi, -10 dBi
ϕ	Half power beamwidth	30°
σ	Beam alignment error	0°, 5°, 8°, 10°
β	Blockage parameter	0.0095 [69]
N_0	Noise power	-174 dBm/Hz + 10 log ₁₀ (B) + 10 dB

results and the markers denote simulations. Overall, the analytical results closely match the simulations, thereby verifying the correctness of the presented analysis.

It is important to get a sense of how big the decoding set is. After all, if it is nearly empty, the relay selection may fail. To show the size of the decoding set, Fig. 3.3 plots the average number of relays (3.11) in the decoding set which meet the required SNR threshold for different relay densities. As a result, these relays are capable of decoding the source's message. The locations of these relays form an inhomogeneous PPP with density (3.9). As expected, when the required SNR threshold increases, the decoding relay number decreases. This is because only the relays which are closer to S and fall in LOS region from S may achieve the required SNR threshold. For example, for a moderate relay density of 100 relays per km², seven nodes can act as decoding relays at an SNR threshold of 20 dB. The coverage at the destination is contributed by a relay from this decoding set, and the bigger the size of the decoding set, the better is the probability of coverage.

Fig. 3.4 plots the association probabilities (3.18), (3.20) versus SNR thresholds for two sets of relay densities. This is the probability whether a relay is selected from $\hat{\Phi}_L$ or from $\hat{\Phi}_N$ in the second link. This figure shows that association to an LOS relay decreases with an

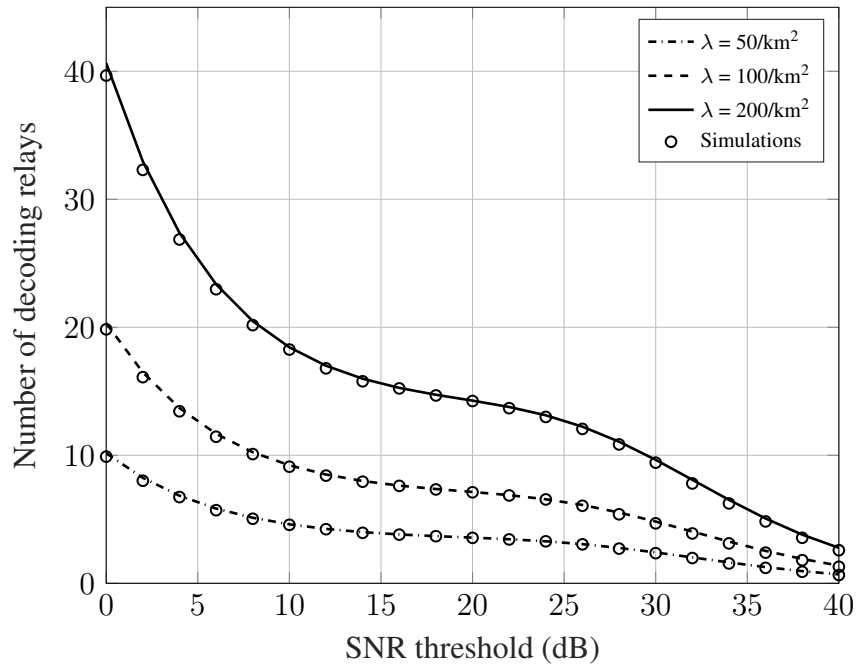


Figure 3.3: Size of the decoding set versus SNR threshold for different relay densities, $W = 300$ m.

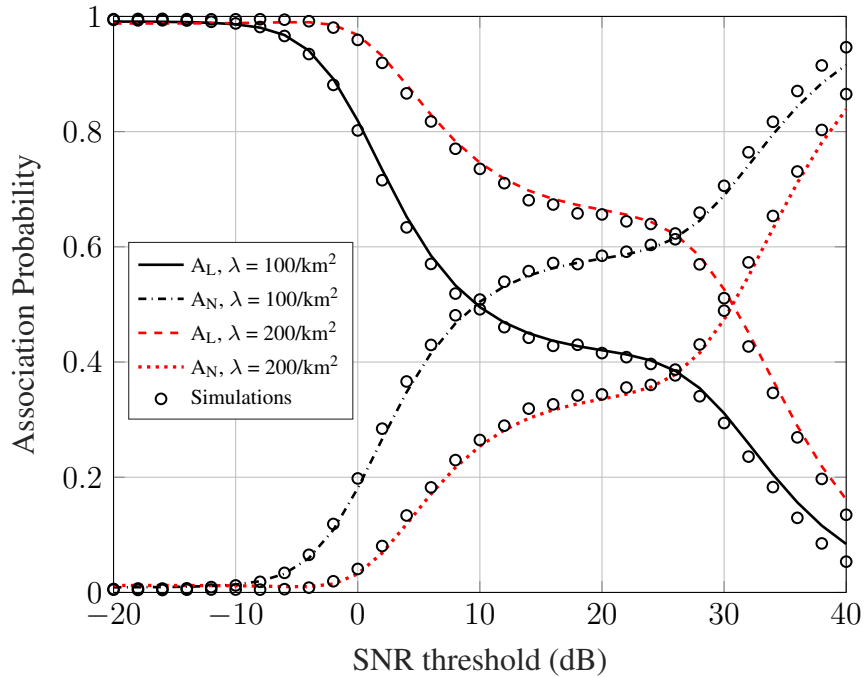


Figure 3.4: Association probability of destination (D) with LOS and NLOS relays for different relay densities for $W = 300$ m.

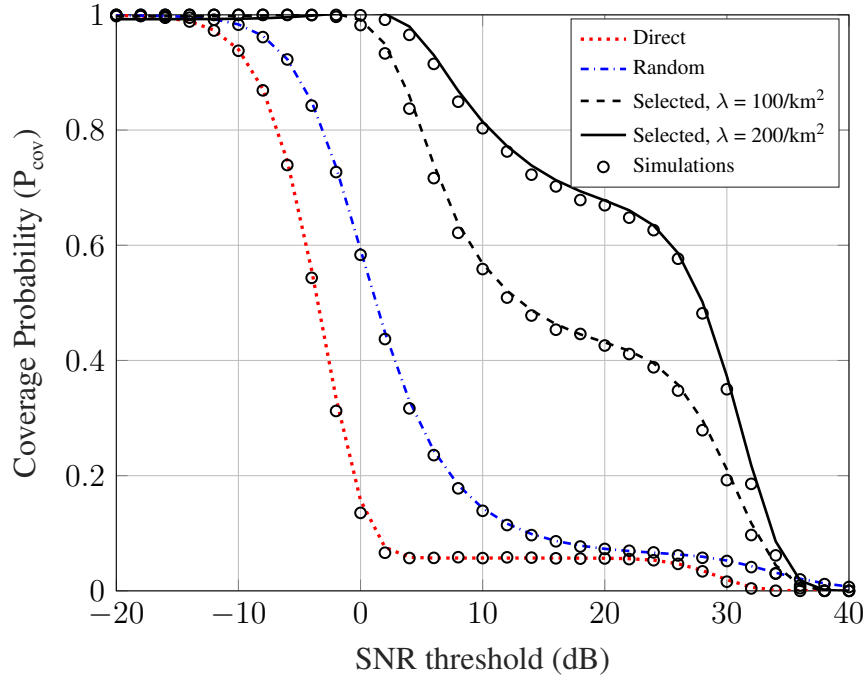


Figure 3.5: Coverage probability vs. SNR thresholds with direct link, relay selection and random relay for different relay densities when $W = 300$ m.

increase in SNR threshold (γ_{th}) and the trend is opposite for the NLOS relays. The reason is as follows: for a high SNR threshold, the decoding set will consist of the nodes which are very close to S , which are most likely to fall in NLOS range from D according to the negative exponential blockage model in (2.10). It is also observed that LOS association probability is higher for higher relay densities, as the chance of more LOS relays improves with an increased total number of relays.

Fig. 3.5 plots and compares the coverage for a direct link (3.2), randomly selected relay in (3.27), and best relay in (3.23) when $S - D$ distance W is set to 300 meters. While the likelihood of destination exceeding the threshold improves slightly with random relay compared to the direct link, relay selection confers dramatic improvements. Since at this distance the direct link is unlikely to be LOS, its coverage probability remains close to 5% for the practical range of SNR thresholds (2 – 26 dB). With relay selection, it improves drastically; for example, the destination SNR exceeds 10 dB for 57% of the time with 100 relays/km² and 80% with 200 relays/km². Also significant coverage improvement is observed with increasing relay density. For example, when the node density doubles from 100 to 200 relays/km², the percentage that destination SNR exceeds 20 dB increases

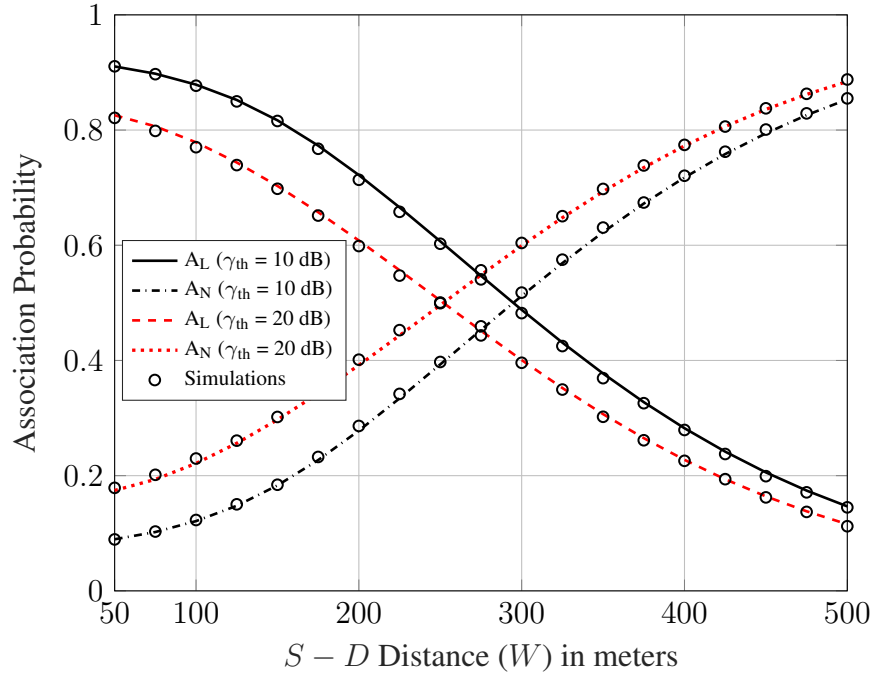


Figure 3.6: Association probability of the destination (D) with LOS and NLOS relays versus the $S - D$ distance W ($\lambda = 100/\text{km}^2$).

from 43% to more than 68%. The coverage for the randomly picked relay appears equal for $\lambda = 100/\text{km}^2$ and $200/\text{km}^2$ due to the fact that both densities lead to a negligible probability that the number of relay nodes inside the selection region is zero, which is the void probability for a PPP (given by $e^{-\lambda\pi\mathcal{L}^2}$) [75]. Once a relay is present inside the selection region, coverage due to random selection is independent of density of relays due to the node locations being independent and uniformly distributed in the region [60].

Fig. 3.6 plots the association probability of LOS and NLOS relays versus $S-D$ distance for two sets of SNR thresholds. As shown in the figure, LOS association probability is slightly decreases when γ_{th} changes from 10 dB to 20 dB. This is because there is a larger number of decoding relays available at lower SNR thresholds, and this provides better coverage. In both cases, as the destination moves farther from the source, LOS association probability decreases. This is expected since for a fixed SNR threshold, the average number of decoding relays is fixed and those relays are located near S . This means the distance between decoding relays and the destination increases with increasing W , consequently decreasing the probability that the $R - D$ link is in LOS. From this, it can be concluded that when the separation starts to increase, NLOS relays in the $R - D$ link play a major

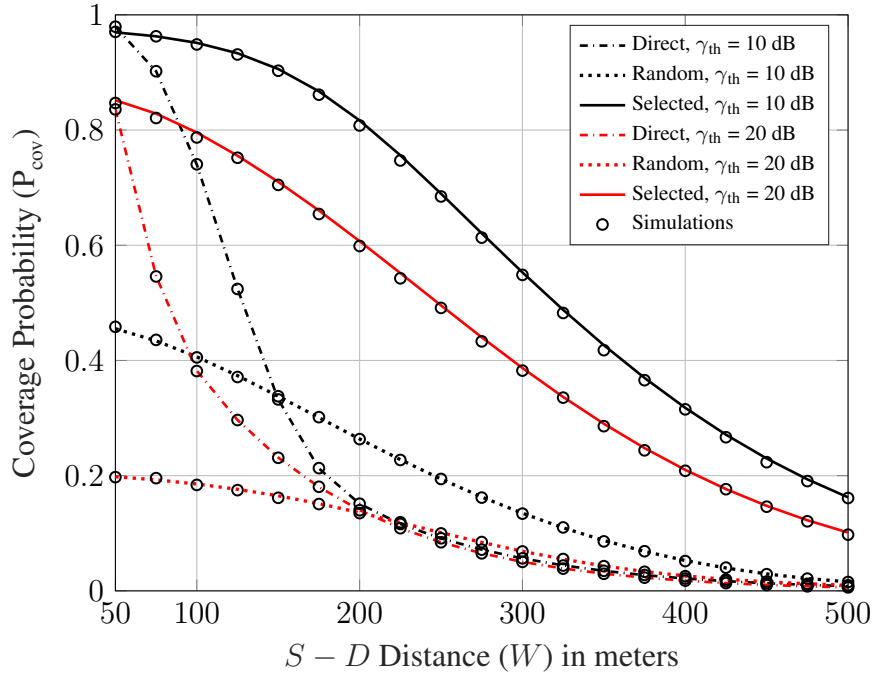


Figure 3.7: Coverage probability versus W for different SNR thresholds, $\lambda = 100/\text{km}^2$.

role in providing coverage to the destination.

Fig. 3.7 plots and compares the coverage probability of the direct link, a randomly chosen relay and the selected relay versus the $S - D$ separation distance W . Note that the coverage probabilities decrease with increasing distance, and this is mainly due to blockage and path losses which increase with increasing distance. Also, it is observed that, compared to direct link, the coverage is significantly improved when relay selection is used. For example, when $S - D$ distance is 200 meters, the coverage probability increases from 15% to more than 60% and 80% for 20 dB and 10 dB SNR thresholds, respectively. As can be seen, direct link coverage probability converges to that of relay selection only when W is 50 meters. This is because, for the shorter links, the chance of blockage in $S - D$ link is small and there is a high probability that the $S - D$ link is in the LOS condition and has very small path loss. The random relay was picked from a disc centered at the midpoint of S and D and with radius 150 meters³. This relay offers a lower coverage compared to the direct link up to a distance of 150 meters when $\gamma_{th} = 10$ dB, and it only provides a small coverage gain for $W > 150$ meters. For a higher SNR threshold of $\gamma_{th} = 20$ dB, the coverage remains less than 20% for the entire range of W . Therefore, simple random relay

³The purpose of this setting is to have a higher chance that there is at least one relay in the selection region.

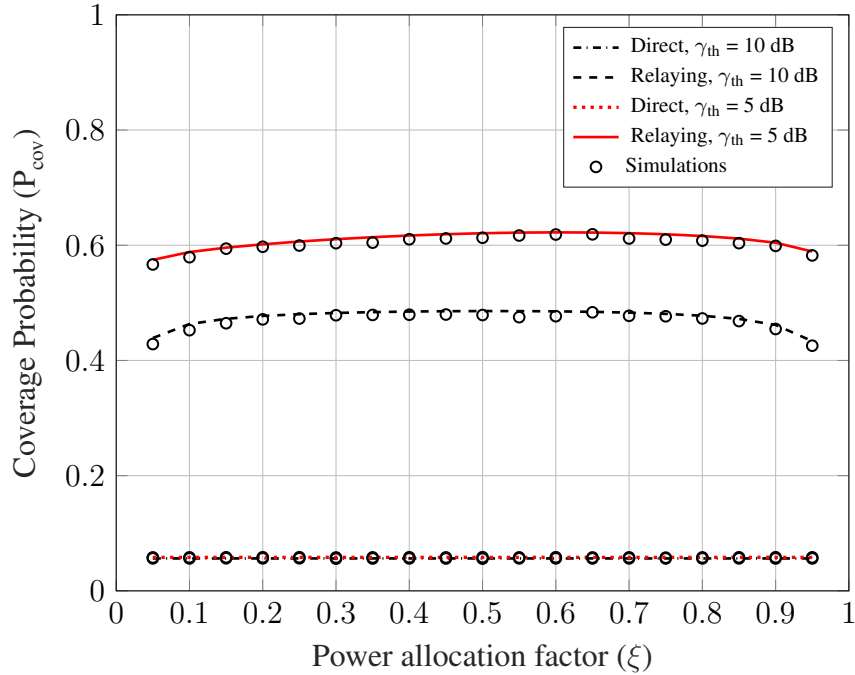


Figure 3.8: Coverage probability versus ξ for different SNR thresholds ($W = 300$ m, $\lambda = 100/\text{km}^2$).

selection does not improve the coverage, which further signifies the role of relay selection.

In Fig. 3.8, the effect of the power allocation factor $\xi = \frac{P_S}{P_T}$ on the coverage probability of the direct link and selected relay is plotted when W is set to 300 meters for different SNR thresholds. The total power P_T is divided between source and relay as $P_S = \xi P_T$ and $P_R = (1 - \xi)P_T$, where ξ varies from 0.05 up to 0.95. As expected, higher coverage is observed for lower SNR thresholds when relays are deployed. The coverage probability for a direct link has a negligible difference for different γ_{th} and remains unchanged for the entire range of ξ . This is because of the fact that at an $S - D$ distance of 300 meters, the LOS probability of the link is very small and fixed but dominates the overall coverage. Using relays, the optimal coverage for both SNR thresholds is observed close to $\xi = 0.5$, i.e., when the power is equally divided between the source and the relay.

To study the effect of beam alignment errors on overall coverage probability, the coverage probabilities for different values of beam alignment errors are plotted in Fig. 3.9. When λ is $200/\text{km}^2$, $W = 300$ meters and $\phi = 30^\circ$, a negligible change is observed in coverage when σ is up to 5 degrees. However, when σ reaches 8° and above, the likelihood of the destination SNR exceeding the threshold begins to drop for both the direct link and the

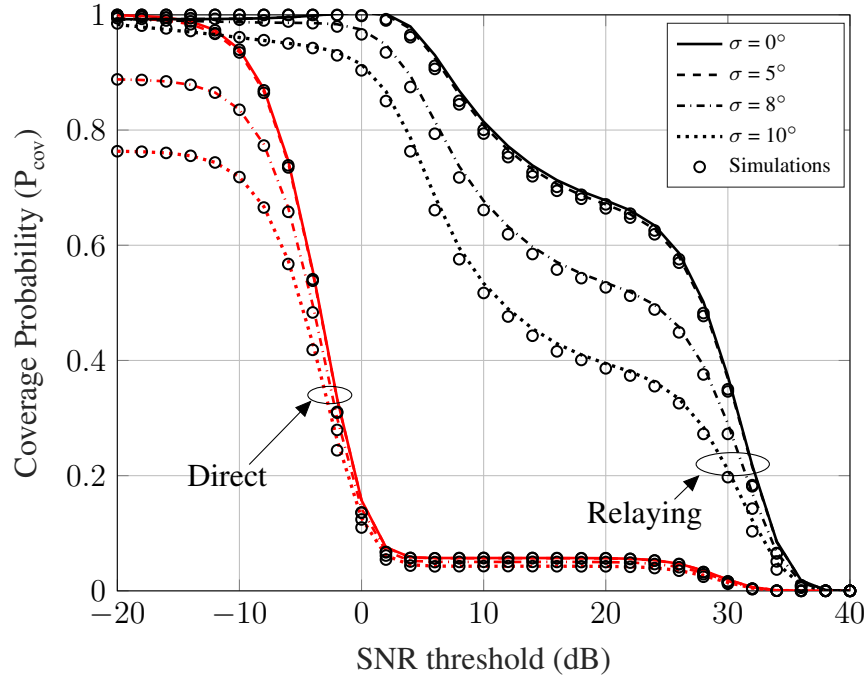


Figure 3.9: Coverage Probability versus SNR threshold for different beamforming errors when $\lambda = 200/\text{km}^2$ and $W = 300$ m.

relay aided link.

In Fig. 3.10, the rate coverage probability is plotted, which gives the measure of achievable rate of the considered system. The rate coverages are plotted for two densities of $100/\text{km}^2$ and $200/\text{km}^2$ versus the rate threshold in Gbps and observe that the selected relay provides a higher rate coverage for rate regions up to 5.8 and 6 Gbps, respectively. Despite the need for two time slots when using relay link, which halves the achievable rate, relay selection achieves better rate coverage. However, for a very high rate threshold in the range of 6 – 12 Gbps (although plotted only up to 7 Gbps in Fig. 3.10), the direct link provides better coverage and eventually drops close to zero at 12 Gbps threshold. The randomly picked relay provides slightly higher rate coverage in the rate regions between 2 and 4 Gbps compared to the direct link but the coverage is significantly smaller than that with relay selection.

Fig. 3.11 plots the system spectral efficiency shown in (3.34). As can be seen, the spectral efficiency is significantly higher with relay selection when compared to the direct link and randomly picked relay. In addition, the spectral efficiency improves notably when increasing the relay density. Specifically, at a 20 dB SNR threshold, it improves from 1.5

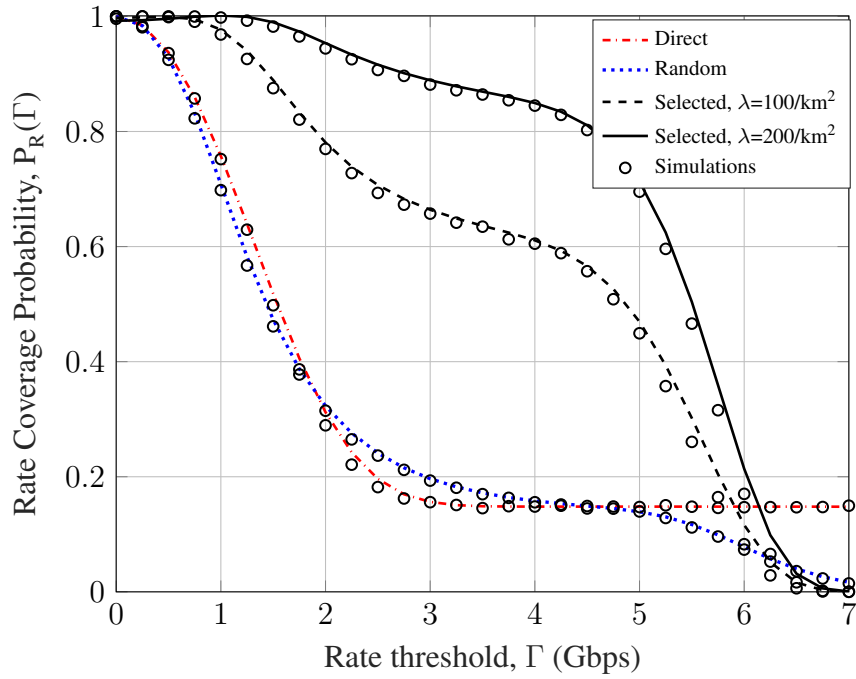


Figure 3.10: Rate Coverage versus rate threshold for different relay densities when $W = 200$ m.

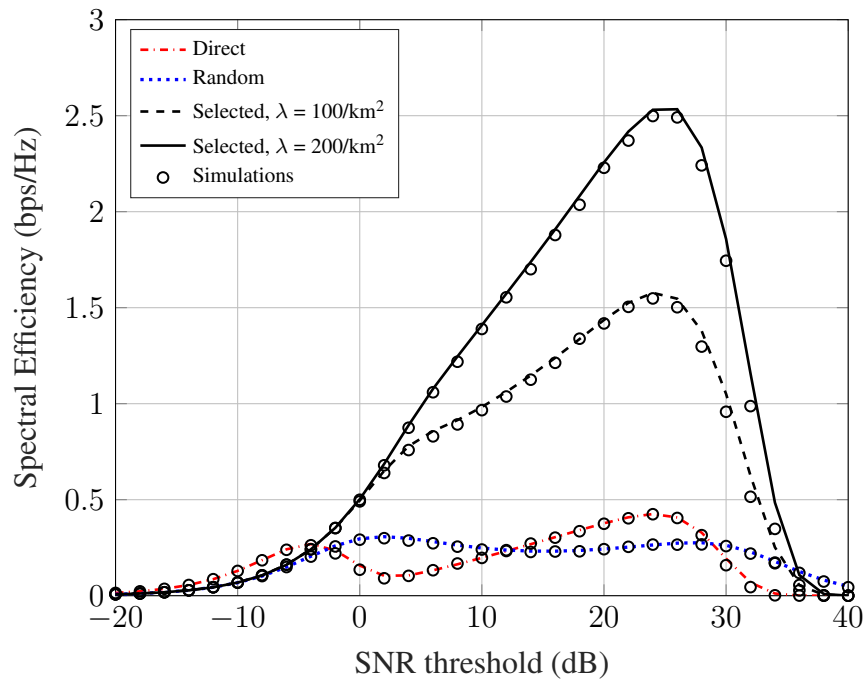


Figure 3.11: Spectrum Efficiency versus SNR threshold for different relay densities when $W = 300$ m.

bps/Hz to 2.25 bps/Hz (50% improvement) when increasing relay density from $100/\text{km}^2$ to $200/\text{km}^2$. The peaks occur close to 24 dB SNR threshold in most cases which suggests that setting this optimal SNR threshold provides the best spectral efficiency.

3.6 Summary

DF mmW relays may provide enhanced coverage and capacity improvements. This chapter, therefore analyzed their coverage probability using tools and models from stochastic geometry. Specifically, the relay locations were modeled as a PPP. All the fundamental mmW features including blockage, path loss, and directional gain were considered. The coverage for the direct link, best relay selection and random relay selection are analyzed. The analysis of best relay selection is the most demanding. To this end, first the decoding set is represented as an inhomogeneous PPP, and the distribution of the distance of the relay which provides the minimum path loss to the destination is derived. Coverage probability is also derived for random relay selection. The analysis is extended to study the effect of beam-alignment errors, the effect of power splitting, rate coverage probability, and spectral efficiency. Some of the observations are as follows:

1. Relay deployment provides significant coverage improvements. For example, at an SNR threshold of 10 dB, coverage improves from 5% without relays to 57% with relay selection for a node deployment density of $100/\text{km}^2$.
2. Random relay selection achieves a marginal improvement in coverage compared to direct link. However, it performs much worse than best relay selection, signifying the importance of an appropriate relay selection method.
3. In addition, mmW DF relay deployment is shown to provide significant rate coverage and spectral efficiency gains compared to the direct link.

~

Chapter 4

Coverage, Capacity, and Error Rate Analysis of Multi-Hop Millimeter-Wave Decode and Forward Relaying

This chapter¹ analyzes the performance of a mmW multi-hop DF relay network. The path loss and blockages are incorporated by allowing each link to be in either LOS or NLOS state. Small-scale fading is modeled by the Nakagami-m distributions with different m-parameters for LOS and NLOS states. Both sparse and dense deployments are considered. In the former, the relays and the destination are limited by additive noise only. Closed-form expressions are derived for the distribution of the destination SNR, coverage probability, ergodic capacity, and SER for three class of digital modulation schemes, namely, BPSK, DBPSK, and square M-QAM. In the latter, the relays and the destination are limited by interference only. Here two situations are considered: (a) interference powers are i.i.d and (b) they are i.n.i.d. For (b), closed-form analysis is exceedingly difficult. Therefore, the *Welch-Satterthwaite Approximation* for the sum of Gamma variables is used to derive the distribution of the total interference. For both situations, the distribution of SIR, coverage probability, ergodic capacity, and SERs for DBPSK and BPSK are derived. The effect of the number of hops on these measures are studied and the accuracy of the analytical results is verified via Monte-Carlo simulation. It is shown that multi-hop relaying provides significant coverage improvement in blockage-prone mmW networks.

¹Chapter 4 has been submitted to the IEEE Access as [91].

4.1 Introduction and Motivation

As mentioned in Section 1.2, mmW links are impaired by high path losses, blockages by obstacles (human bodies, buildings, vehicles and others) are common, and the signals diffract poorly around the corners [22]. For example, at 28 GHz, 28 dB and 40 dB attenuation occur due to a 185 cm brick wall and 3.8 cm tinted glass, respectively [17]. Such high attenuations yield poor coverage in indoor areas, in outdoor areas blocked by buildings and in the NLOS regions even for short communication distances [20].

These problems can be mitigated by the use of wireless relays. In mmW networks, they extend the cellular radio range, improve the cell-edge user experience, combat shadowing and reduce infrastructure deployment costs [17]. For example, in lognormal shadowing environments, coverage and spectral efficiency can be improved by deploying randomly located AF relays [44], and similar performance gains have been demonstrated for two-way AF relay networks [60]. In [59], coverage improvement by mmW DF relay is demonstrated by selecting a relay that provides minimum path loss to the destination. Optimal placement of a relay using unmanned autonomous vehicles can overcome the blockages and enable faster connectivity in mmW networks [92]. Both the ground reflected signal and LOS signals can be used for relaying, and beamwidth and self interference affect the achievable rate [93]. These works demonstrate the ability of relaying to overcome blockages and improve the rate and coverage of mmW networks.

In a multi-hop link, one or more relays are placed between the source and destination, which breaks the link into two or more short links (hops), overcoming coverage holes and the low data rates due to heavy path losses. The intermediate relays receive and forward data to the next hop until the data reaches the destination. LOS conditions can be ensured by carefully planning the relay positions, thus improving the data rates. If relay nodes are fairly densely deployed, then the source and destination nodes can be fairly close to one or more relays. Moreover, the major limitation of mmW is not necessarily the high path loss per se, rather the attenuation due to the blockages because of high penetration loss and poor signal diffraction at mmW frequencies [94]. Fortunately, the use of multiple hops may mitigate them as these impairments decrease with the reduction of transmission distance. Therefore, seamless coverage in blocked and indoor areas is possible [20].

4.1.1 Performance analysis of sub-6 GHz multi-hop relays

Multi-hop relaying alleviates outage in conventional networks in sub-6 GHz bands [45], [46]. For example, reference [45] analyzes outage probability of a multi-hop network. The work in [46] presents a multi-hop network analysis with co-channel interference at relays and destination. In [47], the authors analyze outage probability and SERs in a multi-hop network perturbed by Poisson distributed co-channel interferer, considering distance dependent path losses in signal and interference power. Many multi-hop studies demonstrate the improved performance [95]–[99].

4.1.2 Performance analysis of mmW multi-hop networks

Although multi-hop mmW relaying has been studied [48]–[55], all of them except [55] focus on the upper layers (medium access control and network layers). For example, in [48], a directional medium access control protocol is provided to select a relay for data forwarding using multi-hop path. Routing protocols for device-to-device multi-hop systems are proposed in [49] for transmitting video. In [50], dynamic traffic is scheduled for self backhaul networks. Reference [51] proposes a dynamic duplex resource allocation for uplink and downlink transmissions given concurrent co-channel transmissions. All these works show that multi-hop links improve coverage and rate significantly in mmW networks. For instance, the work in [53] optimizes the performance of large-scale mmW backhaul networks for multiple mobile network operators. A self-organizing mmW backhaul link can be established with existing LTE dual connectivity techniques [54]. Moreover, multi-hop relaying also significantly improves connectivity in mmW networks affected by random blockages [52].

Among all the above works, only the work in [55] investigates the physical layer performance of a multi-hop relay network in terms of bit error probability for AF relay network. Exact analysis is developed for M-ary QAM and M-ary PSK in terms of multivariate Meijer's G-function. A tight lower bound is also derived using a novel Mellin-approach along with diversity and the coding gains. In addition, the power allocation is optimized to minimize the bit error probability. In contrast, this work reported in this chapter focuses on DF relays and thus takes a radically different analytical approach. This chapter does not attempt the power optimization and investigates both sparse and dense mmW scenarios

whereas the work [55] focuses on the dense scenario only. Also, the comprehensive performance measures, namely, coverage probability, ergodic capacity, and SER are derived. In addition, all the previous works omit NLOS scenarios in their study, which are common for mmW links [3], [22]. This work considers NLOS scenarios as well.

4.1.3 Problem Statement and Contributions

Hence, the works in [48]–[53] and other previous mmW multi-hop contributions have not provided a general, comprehensive analysis of system performance and QoS parameters from the end user perspective. Such an analysis is important for both design and innovation purposes of mmW networks and for the advancement of wireless research. To fill this missing link, the performance of the multi-hop mmW network (Fig. 4.1) is analyzed by fully considering mmW specific impairments such as blockages and path losses and small-scale fading. Blockages are considered by allowing each link to be in either LOS or NLOS state with a certain probability that depends on the density and size of the blocking objects and the length of the link. The specific contributions are as follows:

1. First a sparse deployment scenario is considered. The mmW multi-hop network is then noise limited and each hop can be in either LOS or NLOS state. The closed-form distribution of destination SNR is derived given the DF relays. This is a general result that is applicable to any combination of link states, and special cases such as all links being LOS can be easily evaluated.
2. The destination coverage probability is also derived via CCDF. Moreover, rate coverage probability, ergodic capacity and SER for three class of digital modulation schemes, namely, BPSK, DBPSK, and square M-QAM are derived. These modulations are widely used in existing 60 GHz systems, such as 802.11ad, IEEE 802.15.3c and ECMA-387, and are expected to be used in future mmW standards [17].
3. Next, for dense relay deployment scenarios (interference-limited case), the distribution of SIRs at the relays and destination is derived. The SIR of each relay has beta prime distribution when interference signals are independent and identically Gamma distributed. However, when they are i.n.i.d., the distribution of sum of interference powers is extremely complicated. To overcome this challenge, a classical Welch-

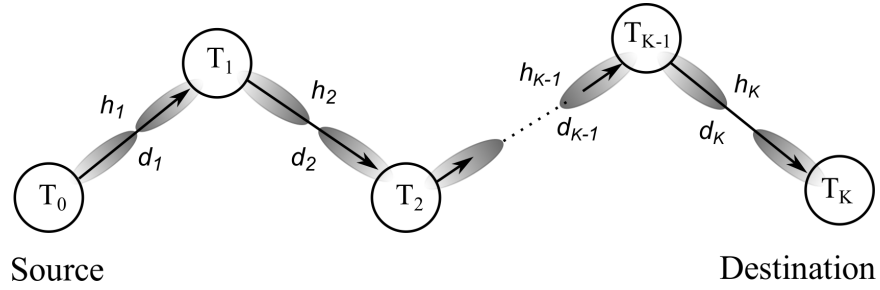


Figure 4.1: A multi-hop wireless relay network.

Satterthwaite approximation is used for the sum of Gamma variables [100], [101]. Then the CCDFs of the SIRs at the relays and destination are derived.

4. However, the analysis of ergodic capacity and SER when relay SIRs are i.n.i.d. is not tractable. Therefore, considering identical SIRs at all relays, the closed-form expressions for ergodic capacity and SER are derived. Due to the high complexity of exact ergodic capacity expressions, high SNR approximate capacity expressions are also derived.
5. Extensive simulation results are provided to verify the derivations and to draw broad conclusions on the performance of mmW multi-hop links.

The chapter is organized as follows. Section 4.2 presents the system model. In Section 4.3, the probability that the destination SNR exceeds the threshold is derived for the noise limited multi-hop system; this requires the distribution of the destination SNR. The ergodic capacity and SER are derived in Section 4.3. Section 4.4 derives the coverage probabilities in interference limited scenario together with ergodic capacity and SER.² Section 4.5 presents the numerical results and Section 4.6 presents the conclusion.

4.2 System Model

4.2.1 Network Modeling

This chapter considers a multi-hop mmW wireless network with source (T_0), destination (T_K), and $K - 1$ intermediate relays so that the total number of hops in the system is K (Fig. 4.1). All nodes operate at a mmW band and are capable of directional beamforming

²Noise limited scenario and interference limited scenario are typical scenarios in mmW analysis. Further details on when these scenarios arise and the transitional behavior of mmW network from noise-limited to interference-limited regime can be found in [102]

(Section 2.1.4) [11], which can be analog, digital, and hybrid methods [17]. Node T_k ($k = 0, \dots, K - 1$) transmits with power \mathcal{P}_k , the distance between T_{k-1} and T_k ($k = 1, \dots, K$) is d_k , and G_k is the beamforming gain of T_k . The channel coefficient of the k -th link is denoted by h_k .

Here, DF relays are considered where each relay decodes the received message, re-encodes it and retransmits it to the next relay until the message reaches the destination. Due to this decoding/regeneration process, additive noise is not accumulated over the hops, which improves the performance compared to that of AF relaying. However, if there are decoding errors, error propagation can be a problem [103].

4.2.2 Path Loss Modeling

In this chapter, a simple but common path loss $d^{-\nu_l}$ is assumed where d is the transmitter-receiver distance and $\nu_l \geq 2$ is path loss exponent for $l \in \{L, N\}$ denoting LOS and NLOS conditions. The typical values of $\nu_L = 2$ and $\nu_N = 3.3$ are used [22]. Due to larger ν_N , the NLOS link output SNR tends to be less than that of a LOS link; however, it can be sufficient for communication purposes because reflected and scattered components in a NLOS link provide significant energies [22]. Therefore, this chapter allows each link to be in either LOS or NLOS state. In practice, nodes can be placed to increase the likelihood of LOS links by minimizing blockages.

The small scale fading model (Section 2.1.3), the simplified two sector model (Section 2.1.4), and the exponential decay blockage model (Section 2.1.5) are adopted here. Perfect beam alignment between transmit and receive nodes (T_{k-1} and T_k) is assumed, so that the link gain is $G_{\text{eq}} \triangleq G_{\text{max}}^2$. Nevertheless, beam misalignment errors can be a topic of future research.

4.2.3 Received Signal Model

With the above system model and mmW specific propagation assumptions, average received signal power at T_k is given by

$$Q_{k,l} = \frac{\mathcal{P}_{k-1} \Psi_k \mathbb{E}[|h_{k,l}|^2]}{d_k^{\nu_l}} \quad (4.1)$$

where \mathcal{P}_{k-1} is the transmit power of T_{k-1} , $\Psi_k = G_{k-1}G_k \left(\frac{c}{4\pi f}\right)^2$ is a constant where G_k and G_{k-1} are the beamforming gains at T_{k-1} and T_k respectively, c is the speed of light in free space and f is the operating frequency, $h_{k,l}$, $l \in \{L, N\}$ is the normalized small-scale fading amplitude of the k -th ($k = 1, \dots, K$) link which follows Nakagami- m distribution with parameter m_l , $\mathbb{E}[|h_{k,l}|^2]$, $l \in \{L, N\}$ is the average fading power, d_k is the distance between T_{k-1} and T_k , and ν_l , $l \in \{L, N\}$ is the path loss exponent, where L and N denote LOS and NLOS link conditions, respectively.

4.3 Performance of Noise Limited Network

Noise limited case applies to a sparse mmW network. Thus, SNR coverage probability, rate coverage, ergodic capacity, and symbol error rate (when the noise power is dominant and interference is negligible) are derived. In this case, the received signal at T_k can be written as

$$y_{k,l} = \sqrt{Q_{k,l}} h_{k,l} x_{k-1} + w_k, \quad (4.2)$$

where x_{k-1} is the symbol the transmitted from T_{k-1} , w_k is the zero mean Gaussian noise with power N_0 at the input of T_k . Considering all these factors, the received SNR at node k ($k = 1, 2, \dots, K$) can be written as

$$\gamma_k = \bar{\gamma} X_k, \quad (4.3)$$

where $\bar{\gamma}$ is an average SNR constant applicable to each hop and X_k is a gamma r.v. whose parameters depend on LOS or NLOS state of the hop. With this model, the output SNR of the multi-hop network is derived. However, before that, two necessary lemmas are presented, which will subsequently help in deriving the distribution of this SNR.

Lemma 6. *The CCDF of $X_{\min} = \min\{X_1, X_2, \dots, X_K\}$ where $X_k \sim \mathcal{G}(1, \lambda_k)$, $k = 1, \dots, K$, are independently distributed is given by*

$$\tilde{F}_{X_{\min}}(x) = e^{-(\lambda_1 + \dots + \lambda_K)x}, \quad 0 \leq x < \infty. \quad (4.4)$$

Proof. All the X_k 's are independent exponential r.v.s with the $\tilde{F}_{X_k}(x) = e^{-\lambda_k x}$. Since $\tilde{F}_{X_{\min}}(x) = \prod_k \tilde{F}_{X_k}(x)$, the lemma follows immediately. \blacksquare

Lemma 6 is sufficient to describe independent Rayleigh-fading hops only. More generally, Lemma 7 applies for independent Nakagami-fading hops.

Lemma 7. *The CCDF of $X_{\min} = \min\{X_1, X_2, \dots, X_K\}$ where $X_k \sim \mathcal{G}(\alpha_k, \lambda_k)$, $k = 1, \dots, K$, are independently distributed is given by*

$$\tilde{F}_{X_{\min}}(x) = e^{-(\lambda_1 + \dots + \lambda_K)x} \sum_{m=0}^{\hat{k}} \mu_m x^m \quad 0 \leq x < \infty \quad (4.5)$$

where $\hat{k} = \sum_k \alpha_k - K$ and $\mu_m = \prod_{\sum n_k = m} \frac{(\lambda_k)^{n_k}}{n_k!}$, $m = 0, 1, \dots, \hat{k}$.

Proof. See Appendix B.1. ■

Next, Lemmas 6 and 7 will be used to derive the distribution of SNRs.

4.3.1 Distribution of the destination SNR

In a DF multi-hop relaying, independent outages occur in each hop, and the destination outage is dominated by the weakest link [45]. Therefore, the CCDF of equivalent SNR, denoted by γ_{eq} , can be written as

$$\begin{aligned} \tilde{F}_{\gamma_{\text{eq}}}(x) &= \mathbb{P}(\min(\bar{\gamma}X_1, \dots, \bar{\gamma}X_K) > x) \\ &= \mathbb{P}(\bar{\gamma} \min(X_1, \dots, X_K) > x), \end{aligned} \quad (4.6)$$

where each X_k , $k = 1, \dots, K$ can have one of the two statistical distributions due to the k -th link being in LOS or NLOS condition. In the following, for convenience, it is assumed that the probability of each hop being in LOS or NLOS state is identical for all hops. This describes spatially homogeneous blockage distribution. Accordingly, for each hop, the probability of LOS state is denoted as p and the probability of NLOS state is denoted as q with $p + q = 1$.

Theorem 2. *The CCDF of destination SNR in a multi-hop network when the k -th hop SNRs ($k = 1, \dots, K$) are independently distributed as $\mathcal{G}(1, \lambda_k^{s_k})$ is given by*

$$\tilde{F}_{\gamma_{\text{eq}}}(x) = \sum_s p^{w(s)} q^{K-w(s)} e^{-\frac{\Lambda_s x}{\bar{\gamma}}}, \quad 0 \leq x < \infty. \quad (4.7)$$

where $w(s)$ is the Hamming weight of state $s = [s_1, \dots, s_K]$ where $s_k \in \{0, 1\}$ denotes if k -th hop is LOS ($s_k = 1$) or NLOS ($s_k = 0$). State s will take 2^K distinct values, and $\Lambda_s = \lambda_1^{s_1} + \dots + \lambda_K^{s_K}$.

Proof. Consider (4.6) in order to illustrate the proof by an example. For example, if $K = 3$, then $s \in [000, 001, 010, \dots]$. If $s = 010$, the first and third hops are NLOS and the second hop is LOS. The probability of this state is pq^2 . In this state, the three hop SNRs will be exponential with parameters λ_1^0, λ_2^1 and λ_3^0 , respectively. By applying Lemma 1, the CCDF of the minimum SNR is $e^{-(\lambda_1^0 + \lambda_2^1 + \lambda_3^0)x/\bar{\gamma}}$. The same process applies to all the other states. Finally, these CCDFs are weighted by their probabilities and sum up over all possible link states s , and then (4.7) is obtained. ■

Theorem 2 provides the coverage probability for independent Rayleigh fading hops, i.e., all hop SNRs are exponentially distributed. Incidentally, this is the most common fading model used for sub-6 GHz multi-hop networks.

Theorem 3. *The CCDF of equivalent SNR in a multi-hop network when k -th hop SNR are independently distributed as $\mathcal{G}(\alpha_k^{s_k}, \lambda_k^{s_k})$ is given by*

$$\tilde{F}_{\gamma_{\text{eq}}}(x) = \sum_s p^{w(s)} q^{K-w(s)} e^{-\frac{\Lambda_s x}{\bar{\gamma}}} \sum_{m=0}^{\hat{k}} \mu_m^s \left(\frac{x}{\bar{\gamma}} \right)^m. \quad (4.8)$$

where μ_m^s are obtained from Lemma 7, in which the superscript s denotes one of the states of the K -hop system.

Proof. The proof follows similar to that of Theorem 2 and is omitted. Note that, in this case k -th hop parameters $\alpha_k^{s_k}$ and $\lambda_k^{s_k}$ are chosen according to LOS or NLOS condition. ■

Theorem 3 provides the distribution of destination SNR for independent Nakagami- m hops and helps us to analyze coverage, capacity and error rates of the network (Fig. 4.1). Before proceeding to these analysis, Theorem 3 is used to derive the PDF of destination SNR in Proposition 1.

Proposition 1. *The PDF of the equivalent SNR can be written as*

$$f_{\gamma_{\text{eq}}}(x) = \sum_s p^{w(s)} q^{K-w(s)} \left(\frac{1}{\bar{\gamma}}\right) e^{-\frac{\Lambda_s x}{\bar{\gamma}}} \left(\Lambda_s \sum_{m=0}^{\hat{k}} \mu_m^s \left(\frac{x}{\bar{\gamma}}\right)^m - \sum_{m=1}^{\hat{k}} m \mu_m^s \left(\frac{x}{\bar{\gamma}}\right)^{m-1} \right). \quad (4.9)$$

Proof. The PDF in (9) follows by differentiating $\tilde{F}_{\gamma_{\text{eq}}}(x)$ given in (4.8). ■

With the closed-form PDF in Proposition 1, the performance measures such as ergodic capacity and SER are derived below.

4.3.2 SNR Coverage Probability

SNR coverage is the probability that the destination SNR exceeds a predefined threshold, γ_{th} .

Proposition 2. *The SNR coverage probability of the noise-limited mmW multi-hop DF link is given by*

$$P_{\text{cov}} = \sum_s p^{w(s)} q^{K-w(s)} e^{-\frac{\Lambda_s \gamma_{\text{th}}}{\bar{\gamma}}} \sum_{m=0}^{\hat{k}} \mu_m^s \left(\frac{\gamma_{\text{th}}}{\bar{\gamma}}\right)^m. \quad (4.10)$$

Proof. By definition, coverage probability is the CCDF of the destination SNR at γ_{th} , which is obtained from (4.8) with $x = \gamma_{\text{th}}$. ■

P_{cov} in Proposition (2) provides a quantitative measure on the quality of service and may help network designs. For example, if $P_{\text{cov}} = 0.8$ at $\gamma_{\text{th}} = 10$ dB, SNR of at least 10 dB is achieved for 80% of the time. Thus, link parameters may be fine tuned based on the service quality requirements.

4.3.3 Rate Coverage Probability

Rate coverage is the probability that the achievable transmission rate exceeds a predefined threshold $R_{\text{th}} > 0$. Clearly, the number of data bits received per second is a critical performance metric to gauge the quality of the link. Moreover, since the use of mmW bands is fundamentally motivated to achieve higher rates, rate coverage is a highly relevant performance measure for mmW communications.

In mmW networks, large path losses make signal propagation beyond the nearest node highly difficult. With this condition, alternately located relays can co-transmit to their

corresponding receiving nodes during the same time slot without causing any significant interference to other nodes [48]. Therefore, $K/2$ simultaneous transmissions can occur when the number of hops K is even or alternatively $(K + 1)/2$ and $(K - 1)/2$ simultaneous transmissions can occur when K is odd. To this end, the achievable rate for the multi-hop relay network can be written as

$$R = \frac{B}{2} \log_2(1 + \gamma_{\text{eq}}) \text{ bits per second} \quad (4.11)$$

where B is the bandwidth assigned to the typical user and the factor of $1/2$ is used because the network can equivalently transmit one symbol per two time slots.

Corollary 1. *The rate coverage probability of a multi-hop relay transmission is given by*

$$P_{\text{cov}}^{\text{Rate}} = \sum_s p^{w(s)} q^{K-w(s)} e^{-\frac{\Lambda_s C}{\bar{\gamma}}} \sum_{m=0}^{\hat{k}} \mu_m^s \left(\frac{C}{\bar{\gamma}} \right)^m \quad (4.12)$$

where $C = 2^{\frac{2R_{\text{th}}}{B}} - 1$.

Proof. By manipulating (4.11), it can be found that $\mathbb{P}(R > R_{\text{th}}) = \mathbb{P}(\gamma_{\text{eq}} \geq C)$. ■

Using (4.12), the probability of achieving a given minimum data rate at the destination can be computed, which justifies the use of mmW in multi-hop relaying as the major motive is to achieve higher data rate. In addition, system parameters such as transmit power, beamforming gain, and number of hops can be adjusted to achieve a required rate via (4.12).

4.3.4 Ergodic Capacity

To compute the ergodic capacity, similar to Section 4.3.3, it is assumed that alternate relays (T_k and T_{k+2}) can co-transmit in the same time-frequency slot without causing significant mutual interference [48]. With this setup, a multiplexing gain of $1/2$ can be achieved irrespective of the number of hops. The subsequent capacity expressions are stated accordingly.

Theorem 4. *For a multi-hop mmW DF relay network, ergodic capacity (bps/Hz) is given*

by

$$\begin{aligned} \tilde{C} = & \frac{1}{2 \ln 2} \sum_s p^{w(s)} q^{K-w(s)} e^{\frac{\Lambda_s}{\bar{\gamma}}} \left[\mu_0^s \Gamma \left(0, \frac{\Lambda_s}{\bar{\gamma}} \right) \right. \\ & \left. + \sum_{m=1}^{\hat{k}} \frac{\mu_m^s}{\bar{\gamma}^m} \left((-1)^m \Gamma \left(0, \frac{\Lambda_s}{\bar{\gamma}} \right) + \sum_{n=1}^m \binom{m}{n} (-1)^{m-n} \left(\frac{\bar{\gamma}}{\Lambda_s} \right)^n \Gamma \left(n, \frac{\Lambda_s}{\bar{\gamma}} \right) \right) \right], \end{aligned} \quad (4.13)$$

where $\Gamma(x, a) = \int_a^\infty t^{x-1} e^{-t} dt$ is the upper incomplete gamma function.

Proof. With the CDF expression of the e2e SNR at hand, ergodic capacity can be computed as

$$\begin{aligned} \tilde{C} &= \frac{1}{2 \ln 2} \int_0^\infty \ln(1+x) f_{\gamma_{\text{eq}}}(x) dx \\ &= -\frac{1}{2 \ln 2} \int_0^\infty \ln(1+x) d\tilde{F}_{\gamma_{\text{eq}}}(x) \\ &= \frac{1}{2 \ln 2} \int_0^\infty \frac{\tilde{F}_{\gamma_{\text{eq}}}(x)}{(1+x)} dx \end{aligned} \quad (4.14)$$

where $\tilde{F}_{\gamma_{\text{eq}}}(x)$ is the CCDF of equivalent e2e SNR given in (4.8). Now, solving the integral in (4.14), (4.13) is obtained. ■

The expression (4.13) provides the capacity versus average per hop SNR of the multi-hop network and can be easily evaluated using mathematical software such as MATLAB. Note that $\Gamma(0, z)$ is equivalent to exponential integral function $E_1(z)$ [5].

High SNR Capacity Approximation

Simplification of the exact capacity expression (4.13) is desirable; for example, simpler high-SNR expressions can be extremely accurate and they allow the study of limiting performances. Therefore, the asymptotic capacity expression is derived next.

Corollary 2. *At high SNR, i.e., $\bar{\gamma} \rightarrow \infty$, the ergodic channel capacity is given by*

$$\tilde{C}_{\text{high SNR}} = \frac{1}{2 \ln 2} \left[\ln(\bar{\gamma}) + \sum_s p^{w(s)} q^{K-w(s)} \left(\sum_{m=0}^{\hat{k}} \frac{\mu_m^s m!}{\Lambda_s^m} (\Psi(m+1) - \ln(\Lambda_s)) \right) \right]$$

$$- \sum_{m=1}^{\hat{k}} \frac{\mu_m^s m!}{\Lambda_s^m} \left(\Psi(m) - \ln(\Lambda_s) \right) \Bigg] \quad (4.15)$$

where $\Psi(z) = \frac{d(\ln \Gamma(z))}{dz}$ is a Digamma function [104, 6.3.1].

Proof. When $\bar{\gamma} \rightarrow \infty$, the following approximation can be used:

$$\mathbb{E} [\ln(1 + \bar{\gamma}X)] \approx \ln(\bar{\gamma}) + \mathbb{E}[\ln X]. \quad (4.16)$$

For a r.v. $X > 0$, $\mathbb{E}[\ln X]$ is equal to the first derivative of the Mellin transform of X evaluated at $t = 1$. The Mellin transform of X is defined as

$$M_X(t) = \mathbb{E} [X^{t-1}] \quad (4.17)$$

where $X = \min\{X_1, \dots, X_K\}$. Theorem 3 yields the PDF of X as

$$f_X(x) = \sum_s p^{w(s)} q^{K-w(s)} e^{-\Lambda_s x} \left(\Lambda_s \sum_{m=0}^{\hat{k}} \mu_m^s x^m - \sum_{m=1}^{\hat{k}} m \mu_m^s x^{m-1} \right). \quad (4.18)$$

Now, using the PDF (4.18) to compute the expectation in (4.17) results in

$$M_X(t) = \sum_s p^{w(s)} q^{K-w(s)} \left(\sum_{m=0}^{\hat{k}} \frac{\mu_m^s \Gamma(m+t)}{\Lambda_s^{(m+t-1)}} - \sum_{m=1}^{\hat{k}} \frac{m \mu_m^s \Gamma(m+t-1)}{\Lambda_s^{(m+t-1)}} \right). \quad (4.19)$$

By differentiating (4.19) over t , substituting $t = 1$, and again substituting the resulting expression in (4.16), (4.15) can be obtained. ■

The asymptotic capacity in (4.15) is a function of $\bar{\gamma}$ and represents a straight line with slope $(2 \ln(2))^{-1}$ and y -intercept that depends on the summation term in s .

4.3.5 SER Analysis

Symbol error occurs if the received symbol at destination differs from the transmitted symbol from the source. Thus, SER is the ratio of the number of erroneous symbols received to the total number of transmitted symbols. In a multi-hop network, error in any intermediate hop can cause the error at destination. Hence, the exact computation of SER in DF network

needs to consider all possible errors of symbol being erroneously mapped to a different symbol in the given constellation and in each hop. This means that, for higher constellation size such as M-QAM, SER computation is cumbersome and complicated due to the large number of possible mapping permutations and the increased number of hops. Therefore, SER in a multi-hop networks is generally computed assuming that symbol error in any hop will contribute to the overall SER and without forward error correction at intermediate nodes [103], [105]. However, this approach can only provide an upper bound on the SER which is computed using per hop SER as follows

$$P_{\text{ub}} \leq \sum_s p^{w(s)} q^{K-w(s)} \left(1 - \prod_{k=1}^K (1 - P_k^{s_k}) \right) \quad (4.20)$$

where $P_k^{s_k}$ is the SER in k -th hop having state s and (4.20) simply means that symbol error will occur if error occurs in any of the hops. In the following three propositions, the k -th hop SER are provided for three classes of modulation schemes, namely *noncoherent binary signaling*, *coherent binary signaling*, and *M-QAM*. For the notational simplicity, the superscript s_k is omitted and k -th hop SER is simply written as P_k and the Nakagami-m fading parameters as α_k and λ_k .

Proposition 3. *For a class of noncoherent binary signaling, such as DBPSK and frequency shift keying (FSK), k -th hop SER is given by*

$$P_k = a \left(\frac{\lambda_k}{\lambda_k + b\bar{\gamma}} \right)^{\alpha_k} \quad (4.21)$$

where α_k and λ_k are the fading parameters of k -th hop, and a and b are modulation specific constants, see [106, Table I]. For example, for DBPSK, $a = 0.5$ and $b = 1$.

Proof. In this case, SER conditioned on link SNR x can be written as $P_k(x) = a \exp(-bx)$. Now P_k can be computed by averaging $P_k(x)$ over the SNR PDF using

$$P_k = \int_0^{\infty} P_k(x) f_{\gamma_k}(x) dx, \quad (4.22)$$

where $f_{\gamma_k}(x) = \frac{1}{\Gamma(\alpha_k)} \left(\frac{\lambda_k}{\bar{\gamma}} \right)^{\alpha_k} x^{\alpha_k-1} e^{-\frac{\lambda_k}{\bar{\gamma}}x}$. The integral can be simplified to (4.21) using [5, eq. 3.351.3]. ■

Since the noncoherent signaling schemes do not require the phase information for demodulation, implementation complexity decreases. This is highly desired in low complexity mmW terminals. Next, the SER for coherent binary signaling schemes is provided in the following proposition.

Proposition 4. *For a class of coherent binary signaling, such as BPSK and FSK, k -th hop SER is given by*

$$P_k = \frac{a2^{1-2\alpha_k}\Gamma(2\alpha_k)}{\Gamma(\alpha_k)\Gamma(\alpha_k + 1)} \left(\frac{\lambda_k}{b\bar{\gamma}}\right)^{\alpha_k} {}_2F_1\left(\alpha_k, \alpha_k + \frac{1}{2}; \alpha_k + 1; -\frac{\lambda_k}{b\bar{\gamma}}\right) \quad (4.23)$$

where α_k and λ_k are the fading parameters of k -th hop, a and b are modulation specific constants [106] (for BPSK, $a = 0.5$ and $b = 1$), and ${}_2F_1(\cdot)$ is the Gaussian hypergeometric function defined in [104, eq.15.1.1].

Proof. In this case, conditional SER conditioned on link SNR x is given by $P_k(x) = a \operatorname{erfc}(\sqrt{bx})$, where $\operatorname{erfc}(z) = \frac{2}{\sqrt{\pi}} \int_z^\infty e^{-t^2} dt$ is the complementary error function. Now (4.23) can be obtained by averaging $P_k(x)$ with SNR PDF using (4.22) and then solving the integral [107]. ■

Coherent BPSK maps one bit per symbol and requires the phase information for the demodulator. Although this increases demodulation complexity, the SER improves compared to DBPSK. Next, the SER of multi-level modulations is provided.

Proposition 5. *In case of quadrature and multi-level signaling, such as QPSK, MPSK, and square M -QAM modulations, k -th hop SER is given by*

$$P_k = a \frac{2^{1-2\alpha_k}\Gamma(2\alpha_k)}{\Gamma(\alpha_k)\Gamma(\alpha_k + 1)} \left(\frac{\lambda_k}{b\bar{\gamma}}\right)^{\alpha_k} {}_2F_1\left[\alpha_k, \frac{1}{2} + \alpha_k; 1 + \alpha_k; -\frac{\lambda_k}{b\bar{\gamma}}\right] - c \left[1 - \frac{4}{\pi} \sum_{n=0}^{\alpha_k-1} \left(\frac{\lambda_k}{b\bar{\gamma}}\right)^n \frac{1}{(2n+1)} {}_2F_1\left(\frac{1}{2} + n, 1 + n; \frac{3}{2} + n; -1 - \frac{\lambda_k}{b\bar{\gamma}}\right)\right] \quad (4.24)$$

where α_k and λ_k are the fading parameters of k -th hop and a , b and c are modulation specific constants (for QPSK, $a = 1$, $b = 0.5$ and $c = 0.25$) [106].

Proof. See Appendix B.2. ■

SER Analysis using the PDF of destination SNR

In addition to the upper bound of SER using per hop SERs, SER expressions based on PDF of the equivalent SNR (4.9) are also derived, which provides an exact error expression if the error is assumed to occur in the link with worst SNR. This assumption simplifies SER derivations and essentially provides a tight lower SER bound, which converges to exact SER in high SNR region. Therefore, in the following three propositions, the closed form expressions for equivalent SERs are provided.

Proposition 6. *For a class of noncoherent binary signaling, such as DBPSK and BFSK, equivalent SER is given by*

$$P_{\text{eq}} = a \sum_s p^{w(s)} q^{K-w(s)} \left(\Lambda_s \sum_{m=0}^{\hat{k}} \frac{\mu_m^s m!}{(b\bar{\gamma} + \Lambda_s)^{(m+1)}} - \sum_{m=1}^{\hat{k}} \frac{\mu_m^s m!}{(b\bar{\gamma} + \Lambda_s)^m} \right). \quad (4.25)$$

where a and b are the modulation specific constants (for DPSK, $a = 0.5$, and $b = 1$) [106].

Proof. In this case, SER can be written in the form $P_e(x) = a \exp(-bx)$. Now P_{eq} can be derived using (4.22) by replacing $f_{\gamma_k}(x)$ by $f_{\gamma_{\text{eq}}}(x)$ given in (4.9). Then the resulting expression can be simplified to (4.25) using [5, eq. 3.351.3] after some mathematical manipulations. ■

Proposition 7. *For a class of coherent binary signaling, such as BPSK and BFSK, the equivalent SER is given by*

$$P_{\text{eq}} = a \sum_s p^{w(s)} q^{K-w(s)} \left(\Lambda_s \sum_{m=0}^{\hat{k}} \frac{\mu_m^s \Gamma(m + \frac{3}{2})}{\sqrt{\pi}(m+1)(b\bar{\gamma})^{m+1}} {}_2F_1 \left(1 + m, \frac{3}{2} + m; 2 + m; -\frac{\Lambda_s}{b\bar{\gamma}} \right) - \sum_{m=1}^{\hat{k}} \frac{\mu_m^s \Gamma(m + \frac{1}{2})}{\sqrt{\pi}(b\bar{\gamma})^m} {}_2F_1 \left(m, \frac{1}{2} + m; 1 + m; -\frac{\Lambda_s}{b\bar{\gamma}} \right) \right). \quad (4.26)$$

where a and b are the modulation specific constants (for BPSK, $a = 0.5$, $b = 1$) [106].

Proof. In this case, conditional SER can be written in the form $P_e(x) = a \operatorname{erfc}(\sqrt{bx})$. Then (4.26) can be derived using (4.22) by replacing $f_{\gamma_k}(x)$ with $f_{\gamma_{\text{eq}}}(x)$. ■

Proposition 8. *In case of quadrature and multi-level signaling, such as QPSK, MPSK, and square M-QAM modulations, SER is given by*

$$P_{\text{eq}} = I_1 - I_2, \quad (4.27)$$

where the expression for I_1 is same as the P_{eq} derived in (4.26) with modified value of a and b depending upon the modulation scheme and I_2 is given by

$$I_2 = c \sum_s p^{w(s)} q^{K-w(s)} (J_1 - J_2) \quad (4.28)$$

where J_1 and J_2 are given by

$$J_1 = \sum_{m=0}^{\hat{k}} \frac{m! \mu_m^s}{\Lambda_s^m} \left(1 - \frac{4}{\pi} \sum_{n=0}^m \frac{\Lambda_s^n}{(2n+1)(b\bar{\gamma})^n} {}_2F_1 \left[\frac{1}{2} + n, 1 + n; \frac{3}{2} + n; -1 - \frac{\Lambda_s}{b\bar{\gamma}} \right] \right). \quad (4.29)$$

$$J_2 = \sum_{m=1}^{\hat{k}} \frac{m! \mu_m^s}{\Lambda_s^m} \left(1 - \frac{4}{\pi} \sum_{n=0}^{m-1} \frac{\Lambda_s^n}{(2n+1)(b\bar{\gamma})^n} {}_2F_1 \left[\frac{1}{2} + n, 1 + n; \frac{3}{2} + n; -1 - \frac{\Lambda_s}{b\bar{\gamma}} \right] \right). \quad (4.30)$$

Proof. The proof follows similar to (4.24) with averaging done over the PDF in (4.9). ■

Equation (4.27) therefore provides a generalized SER expression for a wide range of modulation schemes such as QPSK, MPSK, and square M-QAM, which are applicable in mmW communication. The computation involves Gauss hypergeometric functions, which can be easily evaluated via MATLAB.

4.4 Performance of Interference-Limited Network

Up until now, the effect of co-channel interference was ignored, and the coverage, ergodic capacity and SER were derived. This assumption is valid for mmW relay deployments where interference signals attenuate significantly due to blockages and high path losses [20]. However, network densification has emerged as a performance enabler of 5G wireless networks. In particular, ultra-dense networks with dense and massively deployed base

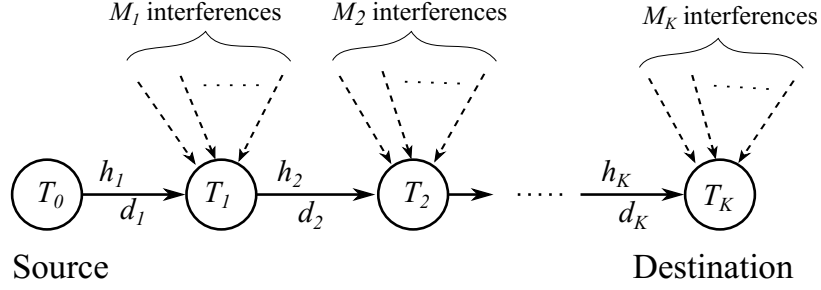


Figure 4.2: Co-channel interferences at relay and destination nodes.

stations, relays and access points can provide high data rates, better coverage, seamless connectivity and improved energy efficiency [52], [68]. However, co-channel interference then becomes the fundamental limiting factor, which must be considered in performance analysis [79].

Therefore, the interference limited regime is considered next, where the total interference is significantly higher than the additive noise. Thus the latter is neglected and the analysis focuses on the statistical distribution of SIR. To this end, two distinct cases are analyzed: (i) when interference powers are i.i.d. r.v.s and (ii) when interference powers are i.n.i.d. r.v.s. Now, the received signal model in interference limited relaying is given by

$$y_{k,l} = \sqrt{Q_{k,l}} h_{k,l} x_{k-1} + \sum_{n=1}^{M_k} \sqrt{Q_{n,k}} h_{n,k} x_{n,k} \quad (4.31)$$

where $Q_{k,l}$, $h_{k,l}$ and x_{k-1} are same as in (4.2), M_k is the total number of co-channel interferers at T_k , $Q_{n,k}$ is the average received interference power at T_k from n -th interferer, $h_{n,k}$ is the normalized fading coefficient from n -th interferer to T_k which follows a Nakagami-m distribution, $x_{n,k}$ is the transmit symbol of each interferer which is assumed Gaussian with unit mean power [55]. A schematic diagram of a multi-hop network with multiple co-channel interferers at relays and destination is given in Fig. 4.2.

4.4.1 Case 1: Interference powers are i.i.d.

In this case, k -th relay is subject to M_k number of interferers and the fading parameters of the received interference power $I_{n,k} = Q_{n,k} |h_{n,k}|^2$ are same for all n , $n \in \{1, 2, \dots, M_k\}$. Thus, $I_{n,k}$ is distributed as $I_{n,k} \sim \mathcal{G}(\alpha_{I_k}, \lambda_{I_k} / \zeta_{I_k})$ where $\zeta_{I_k} = Q_{n,k}$ is the average interference power of n -th interferer at T_k which is assumed to be equal for all n . It is apparent that the total interference power $I_k = \sum_{n=1}^{M_k} I_{n,k}$ is distributed as $I_k \sim \mathcal{G}(M_k \alpha_{I_k}, \lambda_{I_k} / \zeta_{I_k})$.

Assuming Nakagami- m fading of the desired signal, the received signal power S_k at T_k is distributed as $S_k \sim \mathcal{G}(\alpha_k, \lambda_k/\zeta_k)$, with $\zeta_k = Q_{k,l}$ being the average received signal power at T_k . Thus, the instantaneous SIR at T_k is the ratio of two independent Gamma r.v.s, i.e., $\xi_k = \frac{S_k}{I_k}$. It is well known that this ratio follows the beta prime distribution [108]. Thus, the PDF of ξ_k can be written as

$$f_{\xi_k}(x) = \frac{1}{\omega_k \bar{\xi}_k \mathcal{B}(\sigma_k, \theta_k)} \left(\frac{x}{\omega_k \bar{\xi}_k} \right)^{\sigma_k - 1} \left(1 + \frac{x}{\omega_k \bar{\xi}_k} \right)^{-\sigma_k - \theta_k}, \quad (4.32)$$

where $\sigma_k = \alpha_k$, $\theta_k = M_k \alpha_{I_k}$, $\omega_k = \frac{M_k \lambda_{I_k}}{\lambda_k}$, $\bar{\xi}_k = \frac{\zeta_k}{M_k \zeta_{I_k}}$ is the average SIR at T_k , and $\mathcal{B}(a, b) = \int_0^1 t^{a-1} (1-t)^{b-1} dt$ is the Euler's beta function. The CDF of ξ_k is given by

$$F_{\xi_k}(x) = \frac{1}{\sigma_k \mathcal{B}(\sigma_k, \theta_k)} \left(\frac{x}{\omega_k \bar{\xi}_k} \right)^{\sigma_k} {}_2F_1 \left(\sigma_k, \sigma_k + \theta_k; 1 + \sigma_k; -\frac{x}{\omega_k \bar{\xi}_k} \right). \quad (4.33)$$

Lemma 8. *For a multi-hop DF network, with independent interference statistics at each relay, the SIR coverage probability is given by*

$$P_{\text{cov}} = \sum_s p^{w(s)} q^{K-w(s)} \prod_{k=1}^K \left[1 - \frac{1}{\sigma_k \mathcal{B}(\sigma_k, \theta_k)} \left(\frac{\gamma_{\text{th}}}{\omega_k \bar{\xi}_k} \right)^{\sigma_k} \times {}_2F_1 \left(\sigma_k, \sigma_k + \theta_k; 1 + \sigma_k; -\frac{\gamma_{\text{th}}}{\omega_k \bar{\xi}_k} \right) \right] \quad (4.34)$$

where summation across s is to indicate that each hop can be in an LOS or NLOS state, similar to (4.10).

Proof. Since $P_{\text{cov}} = \prod_{k=1}^K \tilde{F}_{\xi_k}(\gamma_{\text{th}})$, by using (4.33), this follows immediately. \blacksquare

Moreover, if the distinct SIRs are identically distributed, P_{cov} has the convenient closed-form expression:

$$P_{\text{cov}} = 1 - \sum_{k=1}^K \binom{K}{k} (-1)^{k+1} \left[\frac{1}{\sigma \mathcal{B}(\sigma, \theta)} \left(\frac{\gamma_{\text{th}}}{\omega \bar{\xi}} \right)^{\sigma} {}_2F_1 \left(\sigma, \sigma + \theta; 1 + \sigma; -\frac{\gamma_{\text{th}}}{\omega \bar{\xi}} \right) \right]^k \quad (4.35)$$

where the subscript k and the summation across s are omitted since the SIR parameters at each relay are assumed identical and only the state with all hops to be in LOS is considered

to study the performance in best link condition. This provides a convenient expression for the coverage of multi-hop mmW relay network by assuming SIRs have equal statistical distribution across all the hops. Although this case may not be practical, it provides insights on the effect of fading parameters of signal and interference on the coverage. Next, some results on coverage when interference powers are not identical across the relays are presented.

4.4.2 Case 2: Interference powers are i.n.i.d.

In this case, a total of M_k interferers are considered at T_k with $M_{L,k}$ and $M_{N,k}$ respectively being the number of LOS and NLOS interferers, where $M_{L,k} + M_{N,k} = M_k$, $k \in \{1, \dots, K\}$. Consider that the interference powers at node T_k are distributed with $I_{n,k} \sim \mathcal{G}(\alpha_{n,k}, \lambda_{n,k}/\zeta_{I_{n,k}})$ where $n \in \{1, 2, \dots, M_k\}$, $\alpha_{n,k}$ and $\lambda_{n,k}$ are the channel fading parameters and $\zeta_{I_{n,k}}$ is the average interference power from n -th interferer to T_k . Similar to i.i.d. case, the desired signal power at T_k is considered to be distributed as $S_k \sim \mathcal{G}(\alpha_k, \lambda_k/\zeta_k)$.

Approximate CDF of per hop SIR

The distribution of total interference $I_k = \sum_{n=1}^{M_k} I_{n,k}$ is in general fairly complicated. Moreover, even if all $\alpha_{n,k}$'s are integers, the exact expressions, which can be derived, are very complicated and cumbersome. Therefore, a convenient assumption is that I_k is approximately Gamma. The shape and rate parameters of this r.v. can be obtained by moment matching. This method is known as the *Welch-Satterthwaite Approximation* for the sum of gamma random variables [100], [101]. The approximation is summarized in the following lemma.

Lemma 9. *Let $Y = X_1 + X_2 + \dots + X_{M_k}$, with mutually independent $X_n \sim \mathcal{G}(\alpha_n, \lambda_n)$ for $n = 1, \dots, M_k$. Then Y is approximately $\mathcal{G}(\alpha_y, \lambda_y)$, where $\alpha_y = \frac{\mu^2}{\sum_{n=1}^{M_k} \alpha_n \lambda_n^2}$, $\lambda_y = \frac{\mu}{\alpha_y}$ and $\mu = \sum_{n=1}^{M_k} \alpha_n \lambda_n$.*

Using Lemma 9, total interference I_k is approximately a $\mathcal{G}(\alpha_{I_k}, \lambda_{I_k})$ r.v., where $\alpha_{I_k} = \alpha_y$ and $\lambda_{I_k} = \lambda_y$ are obtained from Lemma 9. Now the PDF of k -th hop SIR is given by (4.32) with $\sigma_k = \alpha_k$, $\theta_k = \alpha_{I_k}$ and $\omega_k = \frac{\lambda_{I_k}}{\lambda_k}$, and the per-hop SIR CDF is given by (4.33). Now the coverage probability can be computed using (4.34). Simulations show a very close match to this analytical result (Fig. 4.3), and consequently, the error due to the Welch-Satterthwaite approximation is negligible.

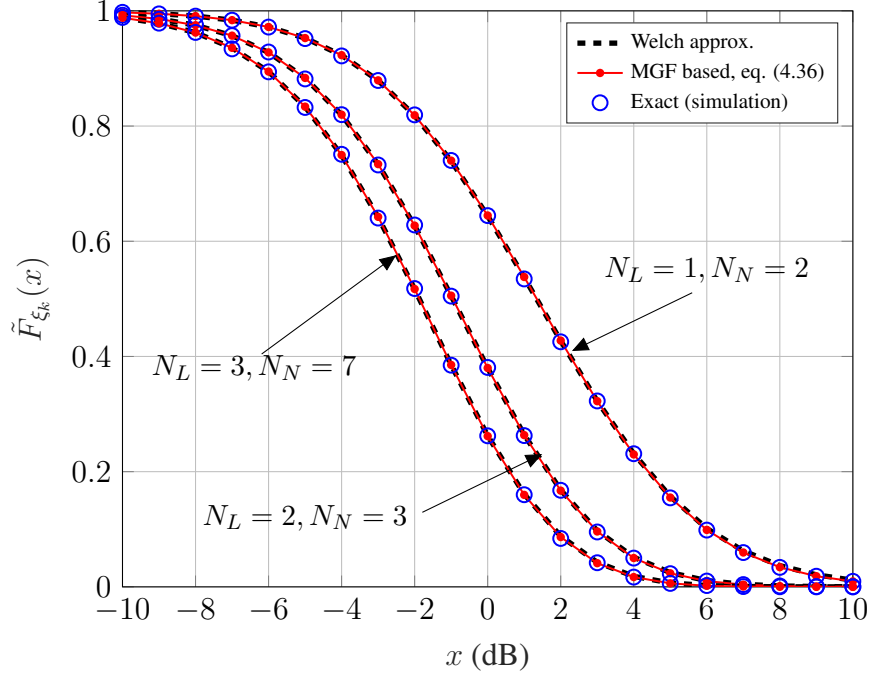


Figure 4.3: CCDF of per hop SIR plotted along x (dB) using *Welch-Satterthwaite Approximation* (Lemma 9), MGF approach (Lemma 10), and simulation. N_L and N_N denote the number of LOS and NLOS interferers, respectively, which are located at different distance to realize i.n.i.d. interference powers. The CCDF curves also refer to the per hop coverage probability along the SIR threshold of x dB.

Exact CDF of per hop SIR

Although the exact expression of the PDF of output SIR is difficult to derive in a closed form, the exact CDF of per hop SIR can be derived for any number of interferers at a given relay by considering the signal power to be Gamma distributed with integer valued shape parameter. Then, the destination SIR CDF can be written in terms of the product of individual hop SIR CDFs. To this end, in the following lemma, the exact CCDF expression for k -th hop SIR is provided.

Lemma 10. *The exact expression for the CCDF of k -th hop SIR for integer α_k is given by*

$$\tilde{F}_{\xi_k}(x) = \sum_{m=0}^{\alpha_k-1} \frac{(-1)^m (x\lambda_k/\zeta_k)^m}{m!} \mathcal{M}_{I_k}^m(x\lambda_k/\zeta_k), \quad (4.36)$$

where $\mathcal{M}_{I_k}^m(x\lambda_k/\zeta_k) = \left. \frac{d^m \mathcal{M}_{I_k}(t)}{dt^m} \right|_{t=x\lambda_k/\zeta_k}$ is the m -th moment of total interference power I_k at T_k computed at $x\lambda_k/\zeta_k$, and $\mathcal{M}_{I_k}(t) = \prod_{n=1}^{M_k} \frac{\lambda_{n,k}^{\alpha_{n,k}}}{(\lambda_{n,k} + t\zeta_{I_{n,k}})^{\alpha_{n,k}}}$ is the MGF of I_k .

Proof. The proof is given in Appendix B.3. ■

Now, using Lemma 10, the CCDF of destination SIR is given by

$$\tilde{F}_{\xi_{\text{eq}}}^{\dagger}(x) = \sum_s p^{w(s)} q^{K-w(s)} \prod_{k=1}^K \left[1 - \sum_{m=0}^{\alpha_k-1} \frac{(-1)^m}{m!} (x\lambda_k/\zeta_k)^m \mathcal{M}_{I_k}^m(x\lambda_k/\zeta_k) \right]. \quad (4.37)$$

By substituting $x = \gamma_{\text{th}}$ in (4.37), exact coverage probability can be readily obtained. However, using the CCDFs in (4.34) or (4.37) to evaluate other performance measures such as ergodic capacity and SER is difficult due to the product of K terms that complicates PDF expression of SIR.

4.4.3 Ergodic Capacity

When evaluating the exact ergodic capacity of the multi-hop network, two simplifying assumptions are made.

1. Interference powers and SIRs at all the relays are i.i.d.. The more general i.n.i.d. case requires a very complicated expansion of (4.34), and thus is left as future work.
2. All the links are in LOS state. Since the SIRs at all relays are assumed i.i.d., the link states need to be identical, i.e., either all LOS or all NLOS. Although NLOS links are viable in mmW network, the best case would be to have all LOS links. Note that, if the nodes are placed carefully, this condition is achievable. It also obviates the use of summation over s in the rest of the analysis.

Lemma 11. *The CDF of the destination SIR when per hop SIR are i.i.d. is given by*

$$F_{\xi_{\text{eq}}}(x) = \sum_{k=1}^K \binom{K}{k} \frac{(-1)^{k+1}}{(\sigma \mathcal{B}(\sigma, \theta))^k} \sum_{m=0}^{n^{\dagger}} \kappa_m \left(\frac{x}{x + \omega \bar{\xi}} \right)^{m+\sigma k} \quad (4.38)$$

where $n^{\dagger} = k(\theta - 1)$ and κ_m is the coefficient which can be computed recursively.

Proof. See Appendix B.4. ■

Lemma 12. *The PDF of destination SIR can be written as*

$$f_{\xi_{\text{eq}}}(x) = \sum_{k=1}^K \binom{K}{k} \frac{(-1)^{k+1}}{(\sigma \mathcal{B}(\sigma, \theta))^k} \sum_{m=0}^{n^{\dagger}} (m + \sigma k) \kappa_m \frac{\omega \bar{\xi}}{(x + \omega \bar{\xi})^2} \left(\frac{x}{x + \omega \bar{\xi}} \right)^{(m+\sigma k-1)}. \quad (4.39)$$

Proof. Now, (4.39) is obtained by differentiating $F_{\xi_{\text{eq}}}^i(x)$ in (4.38). ■

Having the CDF and PDF of destination SIR, ergodic and asymptotic capacities are derived next.

Exact Ergodic Capacity

Proposition 9. *The ergodic capacity of interference limited multi-hop network is given by*

$$\begin{aligned} \tilde{C} = & \frac{1}{2 \ln 2} \sum_{k=1}^K \binom{K}{k} \frac{(-1)^{k+1}}{(\sigma \mathcal{B}(\sigma, \theta))^k} \sum_{m=0}^{n^\dagger} (n+1) \kappa_m \\ & \times \left\{ \left[\frac{\sum_{j=1}^n \frac{1}{j} + \ln(\omega \bar{\xi})}{n+1} \right] + \frac{(-1)^n \ln(\omega \bar{\xi})}{n+1 (\omega \bar{\xi} - 1)^{n+1}} \right. \\ & + \sum_{k=1}^n (-1)^{k+1} \frac{\Gamma(k+1) \Gamma(n+1-k)}{k (\omega \bar{\xi})^k \Gamma(n+2)} \\ & \left. + \frac{(-1)^{n+1}}{n+1} \sum_{l=1}^n \frac{(\omega \bar{\xi} - 1)^{-l}}{l (\omega \bar{\xi})^{n+1-l}} \sum_{j=0}^{n-l} (-1)^j \binom{n-l}{j} \frac{l}{(l+j) (1 - \omega \bar{\xi})^j} \right\}, \quad (4.40) \end{aligned}$$

where $n = m + \sigma k - 1$.

Proof. See Appendix B.5. ■

Equation (4.40) provides the exact ergodic capacity as a function of average per hop SIR $\bar{\xi}$ for interference limited relays. Note that, as the number of hops increases, average per hop SIR also increases due to shorter links.

Asymptotic Capacity

To get direct insights on the capacity, Proposition 10 is provided.

Proposition 10. *As $\bar{\xi} \rightarrow \infty$, the asymptotic capacity of the multi-hop network is given by*

$$\tilde{C}_{\text{high SIR}} = \frac{1}{2 \ln 2} \left[\ln(\omega \bar{\xi}) + \sum_{k=1}^K \binom{K}{k} \frac{(-1)^{k+1}}{(\sigma \mathcal{B}(\sigma, \theta))^k} \sum_{m=0}^{n^\dagger} \kappa_m \left(\sum_{j=1}^{m+\sigma k-1} \frac{1}{j} \right) \right] \quad (4.41)$$

Proof. The proof follows similar to (4.15) and is omitted here. ■

When compared to (4.40), (4.41) includes only the first summation term in (4.40) and provides a simplified capacity expression giving insights on SIR dependence of capacity

in asymptotic region; clearly, the capacity has a dominant term of $\ln(\bar{\xi})$, which shows a logarithmic growth over the average SIR.

4.4.4 SER Analysis

To evaluate the SER in interference limited regime, the similar technique as in noise limited analysis of Section 4.3.5 are followed and (4.20) is used to evaluate the SER at the destination with new expressions for per hop SIR PDFs which are specified in the following propositions.

SER of binary noncoherent signaling

Proposition 11. *For a class of noncoherent binary signaling, such as DBPSK and FSK, k -th hop SER is given by*

$$P_k = \frac{a}{\mathcal{B}(\sigma_k, \theta_k)} \sum_{j=0}^{\theta_k-1} (-1)^j \binom{\theta_k-1}{j} \Gamma(\sigma_k + j) U(\sigma_k + j, 0, b\omega_k \bar{\xi}_k) \quad (4.42)$$

where $U(\cdot)$ is a confluent hypergeometric function of the second kind [5, 9.211.4].

Proof. The proof follows similar to (4.21) by replacing $f_{\gamma_k}(x)$ with $f_{\xi_k}(x)$. ■

Proposition 12. *For a class of noncoherent binary signaling, such as DBPSK and FSK, equivalent destination SER is given by*

$$P_{\text{eq}} = a \sum_{k=1}^K \binom{K}{k} \frac{(-1)^{k+1}}{(\sigma \mathcal{B}(\sigma, \theta))^k} \sum_{m=0}^{n^\dagger} \kappa_m (m + \sigma k)! U(m + \sigma k, 0, b\omega \bar{\xi}). \quad (4.43)$$

Proof. The proof follows similar to (4.21) by replacing $f_{\gamma_k}(x)$ with $f_{\xi_{\text{eq}}}(x)$. ■

SER of coherent binary signaling

Proposition 13. *For a class of coherent binary signaling, such as PSK and FSK, k -th hop SER is given by*

$$P_k = \frac{a}{\mathcal{B}(\sigma_k, \theta_k)} \sum_{j=0}^{\theta_k-1} \frac{(-1)^j}{\sqrt{\pi}(\sigma_k + j)} \binom{\theta_k-1}{j} \Gamma\left(\sigma_k + j + \frac{1}{2}\right) U\left(\sigma_k + j, \frac{1}{2}, b\omega_k \bar{\xi}_k\right). \quad (4.44)$$

Table 4.1: Notations and Simulation Parameters

Notation	Parameter	Value
P_T	Total transmit power	30 dBm
D	Total source to destination distance	500 m
f	Operating frequency	28 GHz
B	System bandwidth	100 MHz
ν_L, ν_N	LOS and NLOS path loss exponents	2, 3.3
m_L, m_N	Nakagami-m parameters for LOS and NLOS cases	3, 2 [3]
G_{\max}, G_{\min}	Main lobe and back lobe gains	18 dBi, -10 dBi
ϕ	half power beamwidth	30°
η_b	Blockage density	$5 \times 10^{-4} (1/m^2)$
$\mathbb{E}[L], \mathbb{E}[W]$	Average blockage length, width	15 m, 15 m
N_0	Noise power	-174 dBm/Hz + $10 \log_{10}(W) + 10$ dB

Proof. The proof follows similar to (4.23) by replacing $f_{\gamma_k}(x)$ with $f_{\xi_k}(x)$. ■

Proposition 14. *For a class of coherent binary signaling, such as PSK and FSK, equivalent destination SER is given by*

$$P_{\text{eq}} = a \sum_{k=1}^K \binom{K}{k} \frac{(-1)^{k+1}}{(\sigma \mathcal{B}(\sigma, \theta))^k} \sum_{m=0}^{n^\dagger} \frac{\kappa_m}{\sqrt{\pi}} \Gamma \left(m + \sigma k + \frac{1}{2} \right) U \left(m + \sigma k, \frac{1}{2}, b\omega \bar{\xi} \right) \quad (4.45)$$

Proof. The proof follows similar to (4.23) by replacing $f_{\gamma_k}(x)$ with $f_{\xi_{\text{eq}}}(x)$. ■

Note that, SER expressions (4.42) through (4.45) provide the SER for binary modulations such as DBPSK and BPSK. The SER of MPSK, M-QAM and other modulations are not analyzed here. For this purpose, classical MGF techniques may also be useful [109], [110]. This further analysis is left as potential future work.

4.5 Results and Discussion

In this section, the analytical results are verified with Monte-Carlo simulations. Each simulation run has 10^5 independent channel realizations. The simulation parameters are listed in Table 4.1. In all figures, curves and markers represent the analytical results and simula-

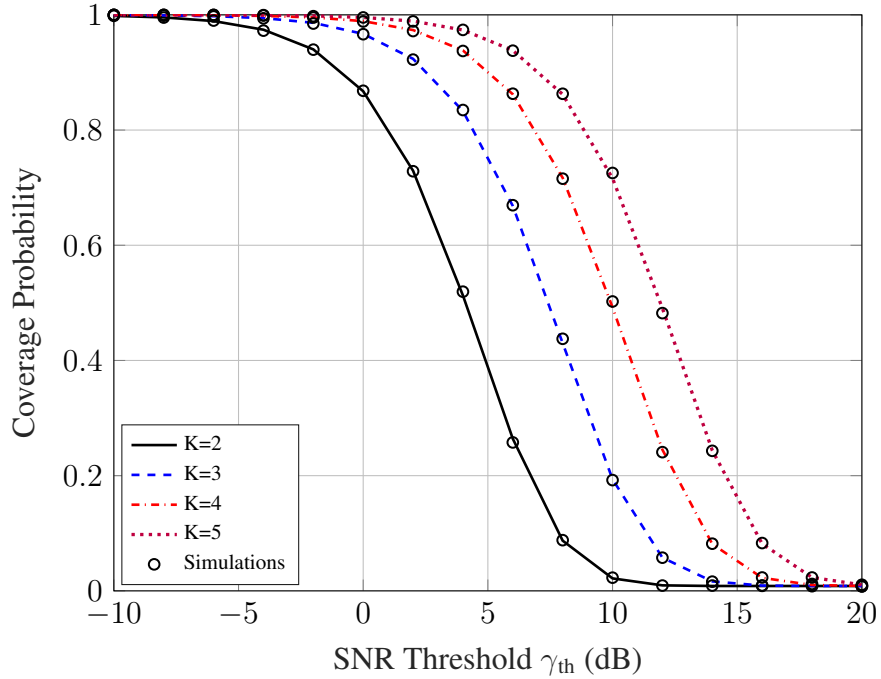


Figure 4.4: Coverage versus SNR thresholds for different K .

tion results, respectively. In all cases, the analytical and simulation results show a perfect match, verifying the correctness of the analytical derivations. The results are discussed separately for noise-limited and interference-limited regimes.

4.5.1 Noise-limited Regime

In Fig. 4.4, coverage probability in (4.10) is plotted for a varying number of hops to cover the total distance $D = 500$ meters for the noise-limited scenario. The total distance is divided equally among K hops and for the fairness in comparison, a constant total transmit power P_T is used with $\mathcal{P}_k = P_T/K$ for $k = 0, \dots, K - 1$. It is evident that the coverage improves with increasing K , which is evident by the right shift in the curves with K . For example, at $\gamma_{\text{th}} = 5$ dB, SNR coverage improves from 40% to 96% when going from $K = 2$ to $K = 5$. However, the improvement in coverage probability diminishes with increasing K .

Fig. 4.5 plots the outage probability versus average per hop SNR for different number of hops and different SNR thresholds for noise-limited case. Outage probability is evaluated using $1 - P_{\text{cov}}$ where P_{cov} is from (4.10) and is computed for a given value of average SNR and SNR threshold. In addition, it is clearly seen that the outage probability increases significantly with the increase in SNR thresholds. However, the outage increases slightly

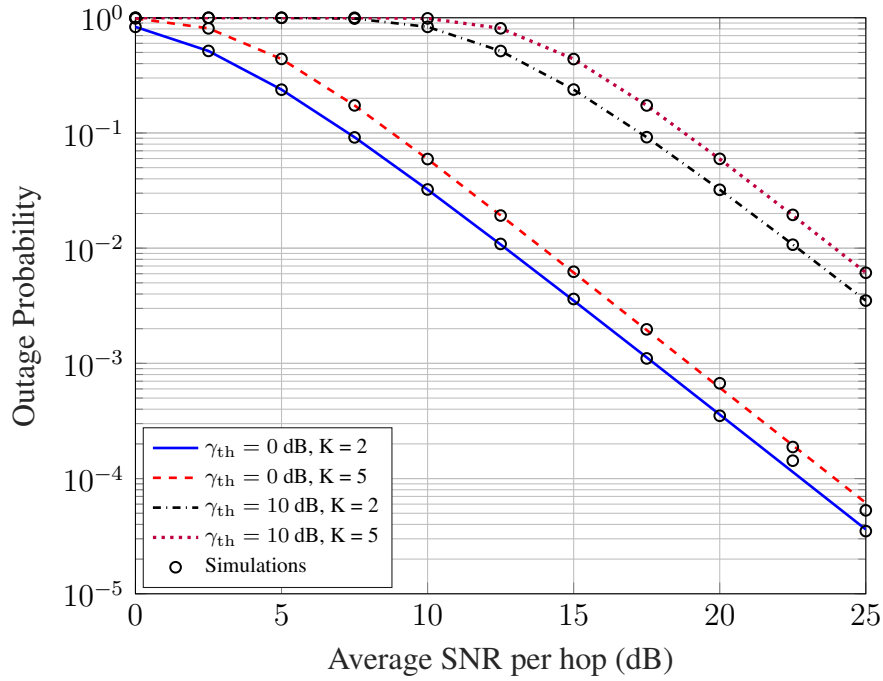


Figure 4.5: Outage Probability versus average per hop SNR for different SNR thresholds.

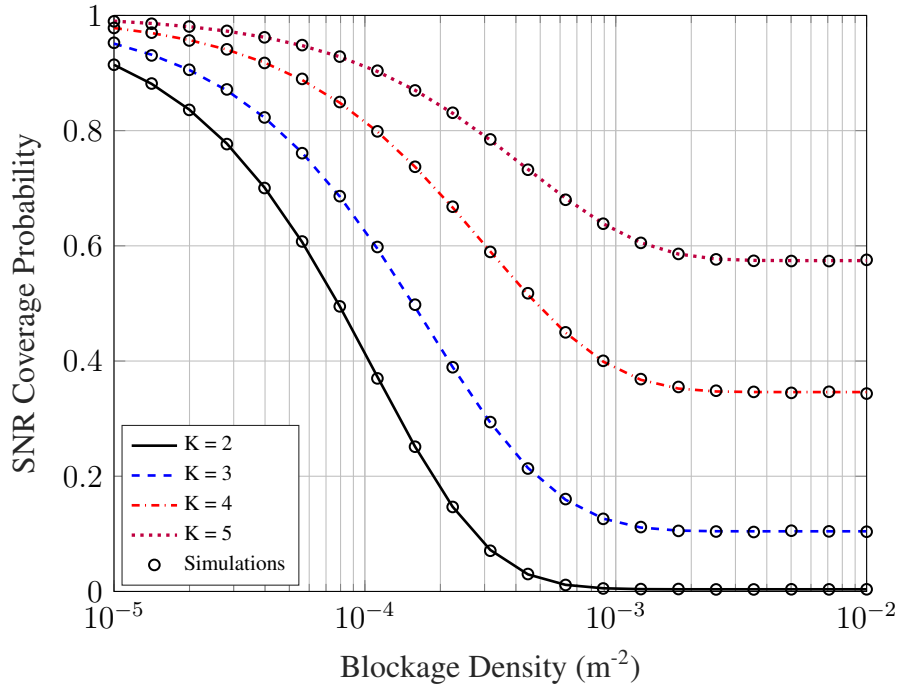


Figure 4.6: Coverage probability versus blockage density (η) at $\gamma_{th} = 10$ dB for different number of hops (K), $D = 500$ m.

with the increasing number of hops from 2 to 5. Note that, here the outage probability comparison is performed along average per hop SNR and, as a result, the increase in the number of hops appears to increase the outage probability due to the cumulative effect of outage events in each hop. However, in practice, when the number of hops is increased, average per hop SNR increases which corresponds to the decrease in outage probability (or increase in coverage probability) which is already discussed in Fig 4.4.

Fig. 4.6 plots coverage probability in (4.10) as a function of blockage density η for an SNR threshold of 10 dB. Note, in (4.10), it is used $p = e^{-\beta d}$ and $q = 1 - p$ with $\beta = \frac{2\eta(\mathbb{E}[L]+\mathbb{E}[W])}{\pi}$ (Sec. 2.1.5) and $d = D/K$. The expected length and width of blockage objects are assumed to be 15 meters for urban and semi-urban areas. Typical building dimensions are close to these values [69]. The increasing number of hops clearly improves coverage for entire range of blockage density. For example, for a blockage environment with density 10^{-4} (100 blockage objects/km²)³, coverage improves from about 40% to 90% when the number of hops increases from 2 to 5. This remarkable improvement illustrates the effectiveness of using multi-hop links to overcome mmW blockages. However, coverage probability flattens for the very highly dense distributions of objects. The reason is that all the links are then likely to be in NLOS state. The flattening point shifts right with the increased number of hops since the link distance decreases with increasing K and LOS probability is higher for a shorter link. Practically, 10^{-2} is a very high density (10,000 blockage objects/km²) and is shown here just to study the coverage in a very high density blockage environment.

To evaluate the data rate achievable with the number of hops, the rate coverage probability in (4.12) versus rate threshold is plotted for different number of hops in Fig. 4.7. As seen in the plots, the rate coverage increases by increasing the number of hops. This is because of the decreased per hop distance resulting in higher SNR. For example, 200 Mbps coverage improves from about 10% to about 87% when increasing K from 2 to 5. However, the coverage gain diminishes as K keeps increasing, which suggests that a careful choice of the number of hops must be based on the required rate coverage.

In Fig. 4.8, the ergodic capacity of the noise limited multi-hop relay link versus the average per hop SNR in (4.13) is plotted. It is assumed that co-channel relay transmission

³This blockage density is practical for a typical urban scenario.

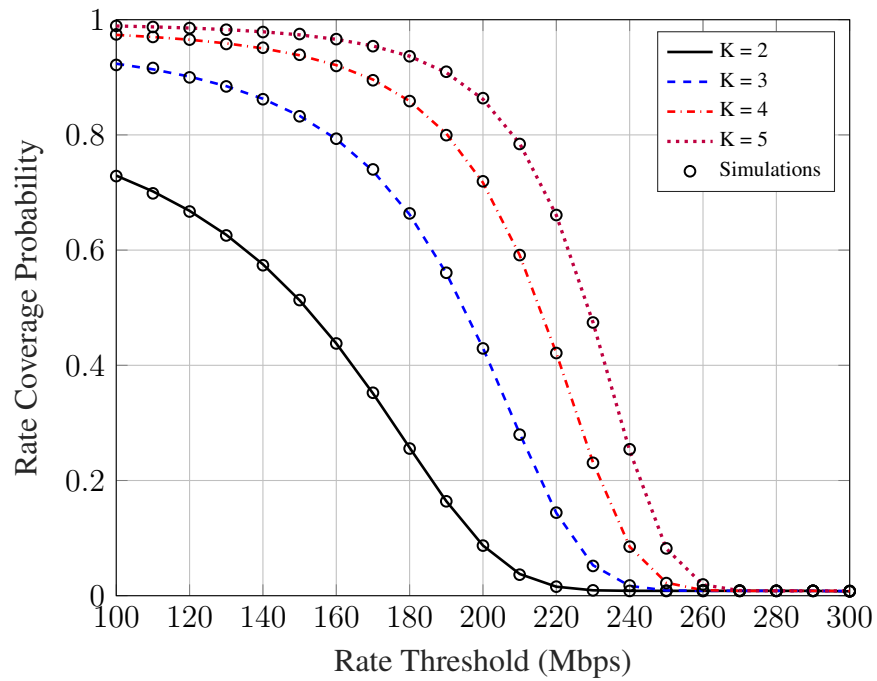


Figure 4.7: Rate coverage vs rate threshold ($D = 500$) m.

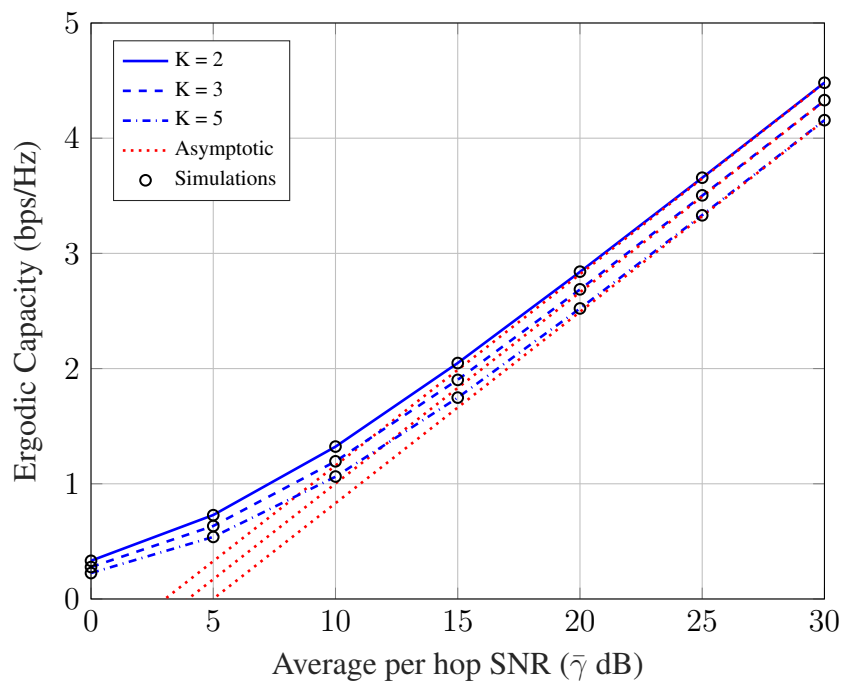


Figure 4.8: Ergodic capacity vs $\bar{\gamma}$, $K = 2, 3, 5$.

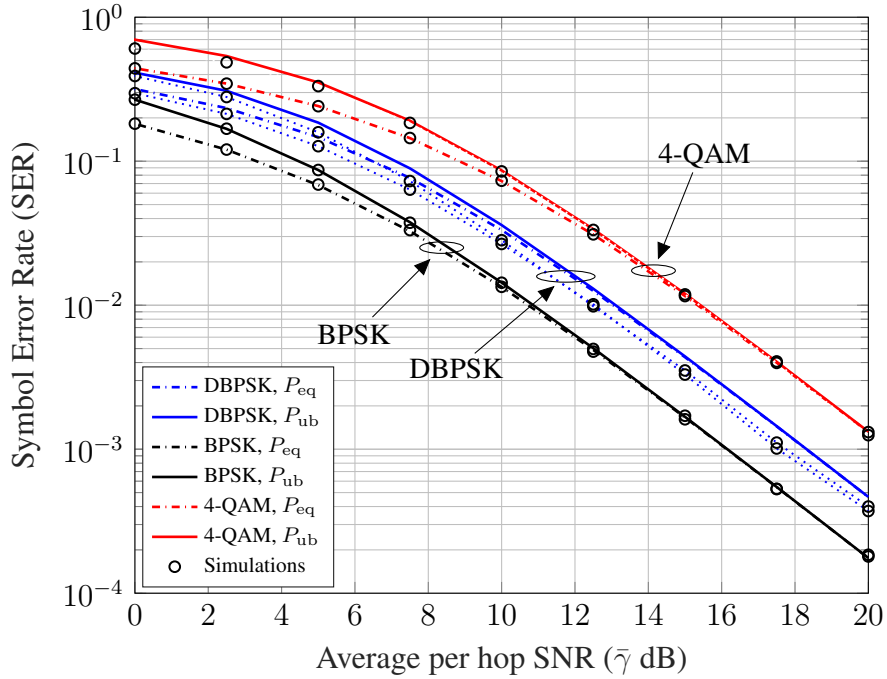


Figure 4.9: SER versus $\bar{\gamma}$ for DBPSK, BPSK and 4-QAM, $K = 3$.

is avoided only between immediate neighbors and alternately located relays can transmit in the same time slot. The plots show that, for a fixed $\bar{\gamma}$, ergodic capacity slightly decreases when the number of hops increases. As expected, the asymptotic capacity lines in (4.15) appear to converge to exact capacity for higher SNR values.

The effect of multi-hop transmission on the SERs of DBPSK, BPSK and 4-QAM versus average per hop SNR for $K = 3$ is plotted in Fig. 4.9. To compare the two classes of SER expressions which consider the error occurring in any link or error occurring in the weakest SNR link, P_{ub} and P_{eq} (Section 4.3.5) are plotted. The effect of increasing hops (not shown in the figures) shows that SER increases slightly with increasing $K = 3$ to $K = 5$ when SNR per hop is fixed. However, increasing the hops increases the average SNR per hop due to the decreased distance and higher LOS probability per hop, which can compensate for the increased SER due to multiple hops.

Fig. 4.10 plots the effect of total number of hops in ergodic capacity of the multi-hop network for different average SNRs. Clearly, the capacity is higher for higher value of $\bar{\gamma}$ and it decreases with increase in K for given $\bar{\gamma}$. However, the capacity curves do not fall sharply because it is assumed that the multiplexing gain is fixed at $1/2$ and is independent of K . This signifies the suitability of multi-hop relays in mmW networks.

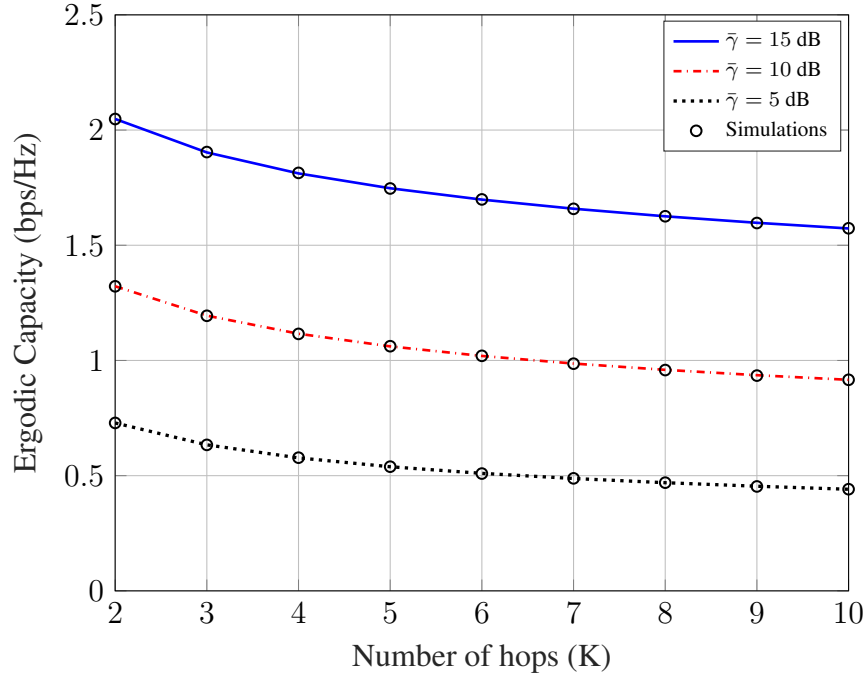


Figure 4.10: Ergodic capacity vs number of hops (K) for different average per hop SNRs.

4.5.2 Interference-limited Regime

Fig. 4.11 plots coverage probability (4.34) for a varying number of hops to cover the total distance $D = 500$ meters for interference-limited scenario. Similar to existing works [46], [96] dealing with interference-limited multi-hop links, a fixed number of interferers are considered at each relay and the destination independent of the number of hops⁴. Specifically, 5 NLOS interferers located at a distance of 100 meters from each node are assumed. The coverage improves with increasing K , which is evident by the right shift in the SIR curves with K . For example, at $\gamma_{\text{th}} = 5$ dB, SIR coverage increases from 2% to 88% when K goes from 2 to 5. This trend is due to the smaller path loss in shorter links. Simulation results for the coverage probability considering both noise and interference (labeled SINR) are also plotted. As expected, the coverage is lower in this case compared to when only interference is considered. But the SINR coverage also improves with increase in the number of hops. The gap between the SIR and SINR curves increases with K because of the following reason. When the number of hops increases, the distance of each hop decreases,

⁴This setting is reasonable due to the following reason. Consider the density of interferers is fixed, and thus, each node (a relay or the destination in the multiple-hop link) expects to receive a similar amount of interference. Thus, a given number of interferers at each relay and the destination are considered in this chapter.

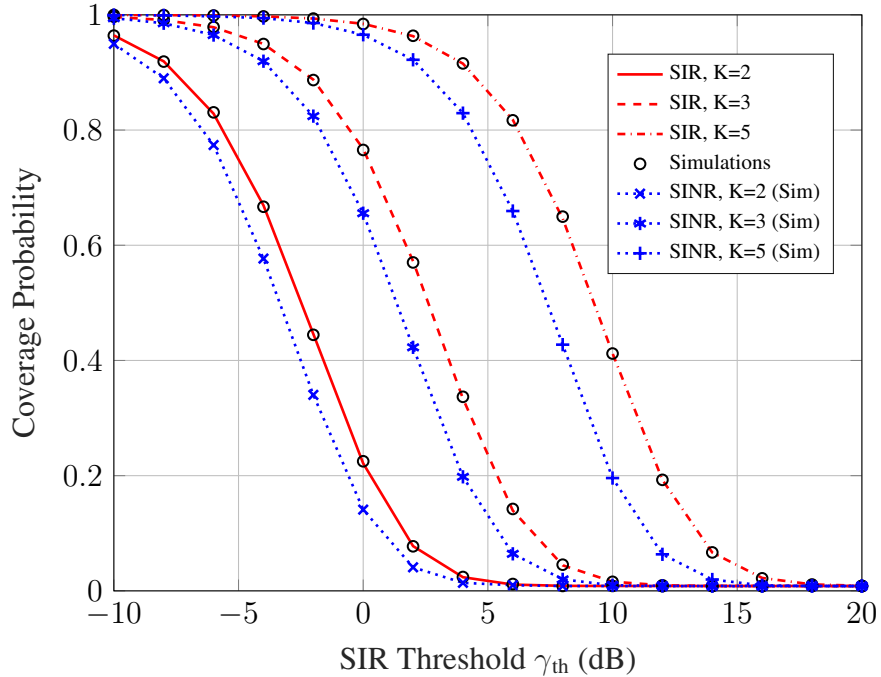


Figure 4.11: Coverage versus SIR thresholds for different K .

which means a larger received power level of desired signal at the receiver of the hop. Since each relay is impaired by a fixed number of interferers, increasing K does not affect much the interference level over a hop. Thus, when K increases, the gap between SIR and SINR for a hop becomes larger. As a result, the gap between the end-to-end SIR and end-to-end SINR also increases.

Fig. 4.12 plots the outage probability versus average per hop SIR for different number of hops and different SIR thresholds. Outage probability is evaluated using $1 - P_{\text{cov}}$ where P_{cov} is in (4.34) and is computed for a given value of average SIR and SIR threshold. It is observed that, outages are almost identical to that for noise-limited scenario. In addition, it is clearly seen that the outage probability increases significantly with the increase in SIR thresholds. However, the outage increases slightly with the increasing number of hops from 2 to 5.

In Fig. 4.13, the ergodic capacity of the interference-limited network along average SIR per hop is plotted. Similar to noise limited scenario, the capacity decreases by increasing the number of hops when plotted against the average per hop SIR. For example, at $\bar{\xi} = 10$ dB, it decreases from 1.3 bps/Hz to 1.2 bps/Hz when increasing the number of hops from 2 to 3. However, when K increases, the average SIR increases resulting the capacity to

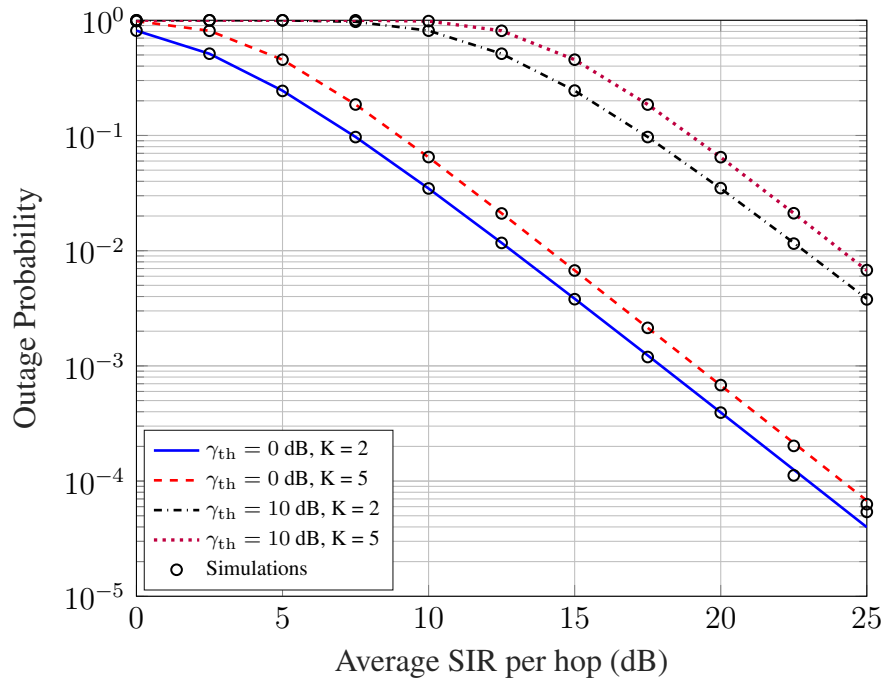


Figure 4.12: Outage Probability versus average per hop SIR for different SIR thresholds.

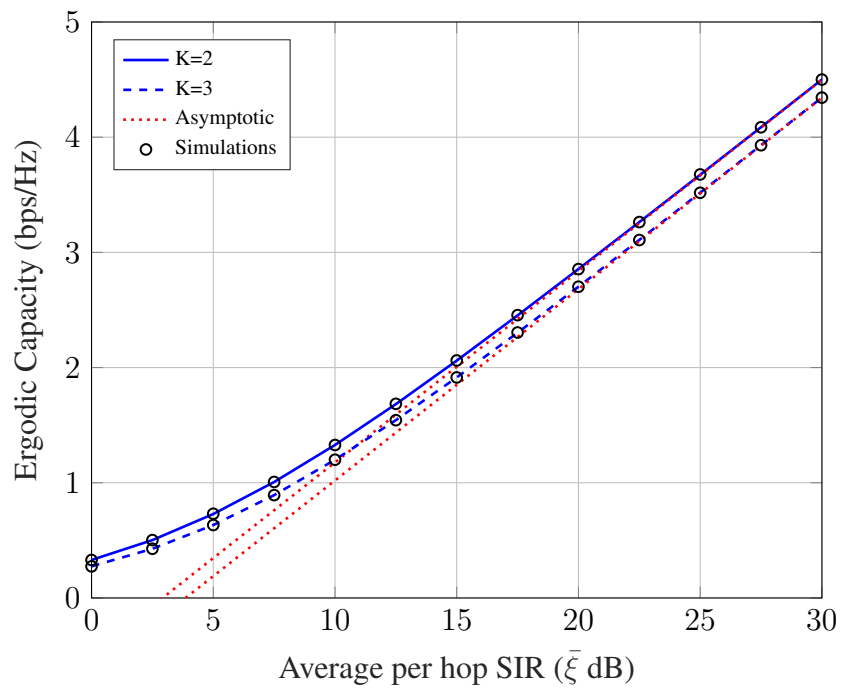


Figure 4.13: Ergodic capacity vs $\bar{\xi}$, $K = 2, 3$.

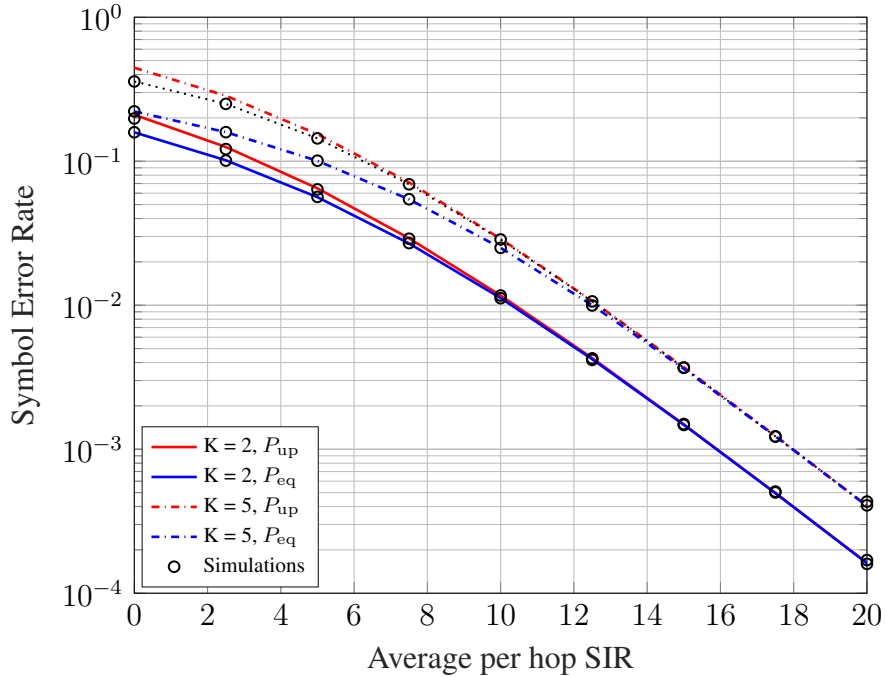


Figure 4.14: SER versus $\bar{\xi}$ for BPSK for $K = 2$ and $K = 5$.

improve.

To study an interference limited scenario, the SER versus SIR is plotted in Fig. 4.14 for BPSK for $K = 2$ and $K = 5$. SER increases along with the increase in number of hops similar to that of the noise limited case. Likewise, P_{eq} converges to P_{up} for higher SIR values.

4.6 Summary

This chapter has analyzed the coverage, capacity and symbol error rates of the mmW multi-hop link in noise-limited and interference-limited scenarios. First the distribution of equivalent SNR is derived by considering the LOS and NLOS conditions of the individual links. Then the closed-form expressions for coverage probability, rate coverage, ergodic capacity, and symbol error rates for DBPSK, BPSK and Square-QAM modulations are derived. For interference-limited scenario, first the per-hop SIR distribution considering i.i.d. and i.n.i.d. interference powers is derived. Then, the capacity and SER for DBPSK and BPSK modulations are derived. Based on the presented analysis and numerical results, following observations can be made:

- The likelihood of the destination node to achieve a sufficient SNR improves signif-

icantly when multiple hops are used. However, if the per hop SNR is fixed, outage probability and SER get increased due to cumulative effect of outage events in each hop when the number of hops increases.

- The effect of the density of blocking objects in coverage probability is significant; however, it can be compensated by increasing the number of hops.
- The noise-limited and interference-limited scenarios show similar trend of ergodic capacity (decreasing with increasing number of hops) and symbol error rates (increasing with increasing number of hops) for a given SNR/SIR. However, actual received SNR/SIR is found to increase (Fig. 4.4, Fig. 4.11) due to shorter link lengths which compensate for decreased performance caused by increased number of hops.

For future work, interference analysis considering random spatial locations of the relays and interferers can be developed. Moreover, this work can be extended to study the SER of higher order modulation schemes such as M-QAM in interference-limited scenario.

~

Chapter 5

Two-Way Relay Selection in Millimeter Wave Networks

This chapter¹ investigates the potential benefits of deploying two-way AF relays to help bidirectional data exchange between two end users in a mmW network. While the locations of the two end users are fixed, the locations of the potential relays are modeled as a homogeneous PPP. A relay is thus selected to maximize the minimum of the two users' end-to-end signal-to-noise ratios. For this system, the coverage probability is derived which shows that the considered relay selection significantly outperforms the random selection scheme in terms of coverage and average throughput.

5.1 Introduction

To overcome blockages and extend mmW links, densely placed relays have been investigated [20], [44], [81]. These works analyze coverage and rate of cellular mmW *one-way* relays, where the source nodes and relays are distributed in distinct PPPs [44]. However, the problem with one-way relays is that two end users require four time slots for a complete bidirectional data transfer, which can be accomplished in two time slots by using a two-way relay [71]. Thus, it potentially doubles spectral efficiency and has been extensively studied for conventional sub-6 GHz bands (dominant with small-scale fading) with typical issues such as channel estimation [34], [35] and performance analysis [28], [33], [111]. However, these works [28], [33]–[35], [111] and many similar sub-6 GHz contributions do not directly apply to mmW links which are fundamentally different due to directivity, path loss,

¹Chapter 5 has been published in the IEEE Communications Letters as [60].

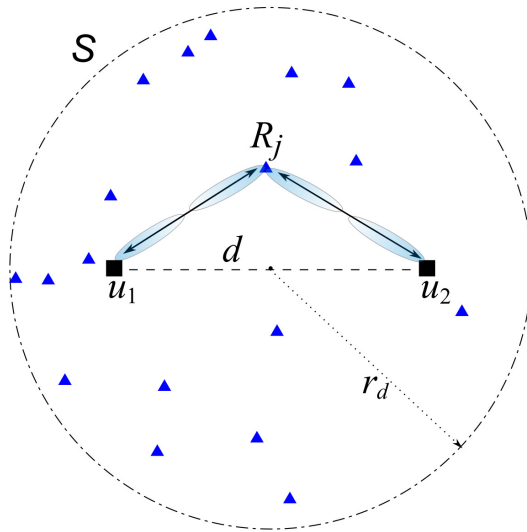


Figure 5.1: Two-way relay network. Relay R_j is selected from a set of potential relay nodes (triangles).

blockages, and the disparity of LOS and NLOS parameters [67]. These factors decrease coverage even for nearby nodes without the presence of relays [20]. To overcome impacts of these factors, the work in [81] proposes a directional mmW medium access protocol to overcome the blockage, and the work in [44] demonstrates the coverage improvement in a one-way relay aided mmW network.

Investigation of mmW two-way relaying has been lacking in the literature. Therefore, this work investigates the potential benefits of deploying two-way relays to help bidirectional data exchange between two end users. A relay is selected to maximize the minimum of the two users' end-to-end SNRs. Then the coverage probability is derived which shows that the considered relay selection significantly outperforms the random selection scheme in terms of coverage and spectral efficiency.

5.2 System Model

5.2.1 Network Modeling

Consider two-way AF relaying for two end users (namely, u_1 and u_2) at a distance d (Fig. 5.1). The locations of potential relays in the entire \mathbb{R}^2 plane form a homogeneous PPP Φ of density λ . However, due to large path losses, only the nodes inside a circular disc \mathcal{S} of radius r_d ($\gg d$), centered at the mid-point of the two users are considered. The reason is as follows. Due to heavy path loss associated with a large distance, the potential

relay nodes outside of the circular disc \mathcal{S} are unlikely to be able to provide relaying service. Thus, \mathcal{S} is essentially equivalent to entire \mathbb{R}^2 .

The homogeneous PPP Φ is a collection of points $\Phi = \{z_1, z_2, \dots\}$, $z_k \in \mathbb{R}^2$. Here $z_j, j \in \{1, 2, \dots\}$ is the location of j -th relay (R_j). The total number of relays in \mathcal{S} , N , is a Poisson r.v. with mean $\lambda\pi r_d^2$. The widely used PPP model captures the random locations of nodes and provides a tractable analysis [64]. This work assumes that the potential relay nodes are deployed without significant network planning; consequently, their locations are random. This scenario is perfectly modeled by a PPP.

All the potential relay nodes use mmW and are capable of directional beamforming. No direct link exists between u_1 and u_2 due to blockages and directivity, which necessitates the use of a relay. Also u_1 and u_2 are assumed to have the same transmit power P and the j -th relay node transmits with output power Q_j . One node can serve as a central coordinator that gets all the channel state information and performs relay selection. Channel estimation can be done using pilots and additional methods [28]. The information on direction can be efficiently obtained using the existing methods [88].

5.2.2 Path Loss, Directivity and Blockage Modeling

The path loss model in discussed in Section 2.1.2 is used which incorporates the log-normal shadowing and distance-dependent path loss. The directivity is modeled as (2.7). In this analysis, first a perfect beam alignment between the communicating nodes, i.e., $u_1 - R_j$ or $u_2 - R_j$, is considered, which provides the effective antenna gain $G_{\text{eq}} = G_{\text{max}}^2$ in a given link, and derive coverage probability. The misalignment of the beams is analyzed in Section 5.3.3.

The effect of blockages is modeled using the fixed LOS ball model [64], where two points within a distance D have a constant probability ω of being in LOS (see Section 2.1.5). The parameters ω and D are propagation environment dependent and obtained from geographic data [64].

5.2.3 SNR Modeling

Considering the j -th relay (R_j) to be used, the SNR for the $u_k - R_j$, ($k = 1, 2$) link can be written as

$$\gamma_{u_k, R_j} = P\Gamma_{u_k, R_j} \quad (5.1)$$

where Γ_{u_k, R_j} incorporates the effect of path loss, blockage, beamforming gain at the transmitter and receiver, and noise power at the receiver, and is defined as

$$\Gamma_{u_k, R_j} \triangleq \frac{G_{\text{eq}}}{N_0} \left(\frac{\omega}{L_L(u_k, R_j)} + \frac{1 - \omega}{L_N(u_k, R_j)} \right), \quad (5.2)$$

where N_0 is the noise power at the receiver, and $L_l(u_k, R_j)$ is from (2.4). The attenuation $L_l(a, b)[\text{dB}]$ can be written in linear scale as $L_l(a, b) = 10^{(\beta_l + \mathcal{X}_l)/10} \|a - b\|^{\alpha_l}$. Using the linear scale notations, (5.2) can be rewritten as

$$\Gamma_{u_k, R_j} = \underbrace{\mathcal{K}\omega e^{-\xi \mathcal{X}_L} r_{k,j}^{-\alpha_L}}_{\mathcal{Y}} + \underbrace{\mathcal{K}(1 - \omega) e^{-\xi \mathcal{X}_N} r_{k,j}^{-\alpha_N}}_{\mathcal{Z}}, \quad (5.3)$$

where $\mathcal{K} = \frac{G_{\text{eq}} 10^{-\beta/10}}{N_0}$, $\xi = \frac{\ln(10)}{10}$ is a constant used to convert dB to natural logarithm, $r_{k,j}$ is the distance between u_k ($k = 1, 2$) and relay R_j , and $e^{-\xi \mathcal{X}_L} \sim \mathcal{LN}(0, \xi^2 \sigma_L^2)$ and $e^{-\xi \mathcal{X}_N} \sim \mathcal{LN}(0, \xi^2 \sigma_N^2)$ are two independent log-normal r.v.s for LOS and NLOS links, respectively. Using the scaling property of log-normal r.v.s, the two summands in (5.3) satisfy $\mathcal{Y} \sim \mathcal{LN}(\ln(\mathcal{K}\omega r_{k,j}^{-\alpha_L}), \xi^2 \sigma_L^2)$ and $\mathcal{Z} \sim \mathcal{LN}(\ln(\mathcal{K}(1 - \omega) r_{k,j}^{-\alpha_N}), \xi^2 \sigma_N^2)$. Then, the total sum Γ_{u_k, R_j} can be approximated by a log-normal r.v. using the Fenton-Wilkinson method [112].

Using the channel reciprocity, the relay-to-user link ($R_j - u_k$, $k \in \{1, 2\}$) SNRs can be written as

$$\gamma_{R_j, u_k} = Q_j \Gamma_{u_k, R_j}.$$

The end-to-end receive SNR γ_{k, R_j} of u_k , $k \in \{1, 2\}$ when relay R_j ($j = 1, 2, \dots, N$) is used can be written as [33, eq. (2)]

$$\gamma_{k, R_j} = \frac{P Q_j \Gamma_{u_k, R_j} \Gamma_{u_{\bar{k}}, R_j}}{1 + (P + Q_j) \Gamma_{u_k, R_j} + P \Gamma_{u_{\bar{k}}, R_j}} \quad (5.4)$$

where $\{\bar{k}\} \triangleq \{1, 2\} \setminus \{k\}$.

5.3 Relay Selection

A relay is selected from Φ to maximize the reliability of both users u_1 and u_2 , i.e., maximize the minimum of the two users' end-to-end SNRs. The selection criterion may thus be stated as

$$\mathcal{R} = \underset{j}{\operatorname{arg\,max}} \min\{\gamma_{1,R_j}, \gamma_{2,R_j}\}, \quad (5.5)$$

where γ_{1,R_j} and γ_{2,R_j} are the end-to-end SNRs given in (5.4).

5.3.1 Coverage Probability

With relay selection (5.5), coverage is defined as the event that the minimum end-to-end SNR of the two users is above a predefined threshold γ_{th} . Recall that the number of nodes in \mathcal{S} , N , is a Poisson r.v. with mean $\lambda|\mathcal{S}|$, where $|\mathcal{S}| = \pi r_d^2$ is the area of \mathcal{S} . For a realization of PPP with N nodes, SNR with relay selection is given by

$$\gamma_{\mathcal{R}} = \begin{cases} \max\{\gamma_1, \gamma_2, \dots, \gamma_N\}, & \text{if } N \neq 0 \\ 0, & \text{if } N = 0 \end{cases} \quad (5.6)$$

where $\gamma_{\mathcal{R}}$ is the equivalent end-to-end SNR of selected relay \mathcal{R} , and $\gamma_j = \min\{\gamma_{1,R_j}, \gamma_{2,R_j}\}$. Subsequently, γ_j will be denoted by γ_z since it represents an arbitrary node in Φ . From the properties of PPP, given $N = k > 0$, the location z is uniformly distributed in \mathcal{S} and γ_z 's are independent. Thus, with relay selection (5.5), the coverage probability can be evaluated as

$$\begin{aligned} P_{\text{cov}} &= \mathbb{P}(\gamma_{\mathcal{R}} \geq \gamma_{\text{th}}) \\ &= 1 - \mathbb{P}\left(\max_{z \in \Phi} \gamma_z \leq \gamma_{\text{th}}\right) \\ &\stackrel{(a)}{=} 1 - \mathbb{E}_{\Phi} \left[\prod_{z \in \Phi} \mathbb{P}(\gamma_z \leq \gamma_{\text{th}}) \right] \\ &\stackrel{(b)}{=} 1 - \sum_{k=1}^{\infty} \mathbb{P}(N = k) \mathbb{E}_z \left[\prod_{z \in \Phi} F_{\gamma_z}(\gamma_{\text{th}} | N = k) \right] \\ &\stackrel{(c)}{=} 1 - \sum_{k=1}^{\infty} \frac{e^{-\lambda|\mathcal{S}|} (\lambda|\mathcal{S}|)^k}{k!} \mathbb{E}_z \left[F_{\gamma_z}(\gamma_{\text{th}}) \right]^k \end{aligned}$$

$$\begin{aligned}
&= 1 - e^{-\lambda|\mathcal{S}|} \sum_{k=1}^{\infty} \frac{(\lambda|\mathcal{S}|)^k}{k!} \nu^k \\
&= 1 - e^{-\lambda|\mathcal{S}|} (e^{\lambda|\mathcal{S}|\nu} - 1)
\end{aligned} \tag{5.7}$$

where (a) follows from independence of individual γ_z 's, in (b) the sum starts from $k = 1$ since it is assumed that $N = k > 0$, (c) uses the probability for Poisson distribution, and ν is the outage probability of a randomly located relay uniformly distributed over \mathcal{S} and is given by [76]

$$\nu = \mathbb{E}_z \left[F_{\gamma_z}(\gamma_{\text{th}}) \right] = \frac{1}{|\mathcal{S}|} \int_0^{2\pi} \int_0^{r_d} F_{\gamma_z}(\gamma_{\text{th}}) r dr d\theta \tag{5.8}$$

where given z , $F_{\gamma_z}(\gamma_{\text{th}})$ is the conditional CDF of end-to-end SNR γ_z . The value of ν is then obtained numerically by averaging $F_{\gamma_z}(\gamma_{\text{th}})$ over Φ .

5.3.2 CDF expression of γ_z

Expression of $F_{\gamma_z}(\gamma_{\text{th}})$ is needed to compute the outage probability ν in (5.8). To derive $F_{\gamma_z}(\gamma_{\text{th}})$, the location of R_j is conditioned to be z . Specifically, first the conditional CDF $F_{\gamma_z}(\gamma_{\text{th}})$ of minimum end-to-end SNR $\gamma_j = \min\{\gamma_{1,R_j}, \gamma_{2,R_j}\}$ conditioned on the location z derived, and then its expected value is computed as in (5.8). For simplicity, the conditional notation is omitted.

Let $X \triangleq \Gamma_{u_1, R_j}$ and $Y \triangleq \Gamma_{u_2, R_j}$, where $X \sim \mathcal{LN}(\mu_x, \sigma_x^2)$ and $Y \sim \mathcal{LN}(\mu_y, \sigma_y^2)$. Now the CDF of $\min\{\gamma_{1,R_j}, \gamma_{2,R_j}\}$ can be written as [28]

$$\begin{aligned}
F_{\gamma}(\gamma_{\text{th}}) &= 1 - \mathbb{P}(\min\{\gamma_{1,R_j}, \gamma_{2,R_j}\} > \gamma_{\text{th}}) \\
&= 1 - \underbrace{\mathbb{P}(\gamma_{2,R_j} > \gamma_{\text{th}}, X < Y)}_{Pr_1} - \underbrace{\mathbb{P}(\gamma_{1,R_j} > \gamma_{\text{th}}, X > Y)}_{Pr_2}.
\end{aligned} \tag{5.9}$$

Here Pr_1 is given by

$$\begin{aligned}
Pr_1 &= \mathbb{P}\left(\frac{PQ_jXY}{PX + (P + Q_j)Y + 1} > \gamma_{\text{th}}, X < Y\right) \\
&= \int_a^{\infty} \mathbb{P}\left(y > \max\left\{x, \frac{(1 + Px)\gamma_{\text{th}}}{PQ_jx - (P + Q_j)\gamma_{\text{th}}}\right\}\right) f_X(x) dx \\
&= \int_a^b \mathbb{P}\left(y > \frac{(1 + Px)\gamma_{\text{th}}}{PQ_jx - (P + Q_j)\gamma_{\text{th}}}\right) f_X(x) dx + \int_b^{\infty} \mathbb{P}(y > x) f_X(x) dx
\end{aligned}$$

$$= \int_a^b \int_{c_1}^{\infty} f_Y(y) f_X(x) dy dx + \int_b^{\infty} \int_x^{\infty} f_Y(y) f_X(x) dy dx, \quad (5.10)$$

where $c_1 = \frac{(1+Px)\gamma_{th}}{PQ_jx - (P+Q_j)\gamma_{th}}$, $a = \frac{P+Q_j}{PQ_j}\gamma_{th}$, and $b = \frac{(2P+Q_j)\gamma_{th} + \sqrt{(2P+Q_j)^2\gamma_{th}^2 + 4PQ_j\gamma_{th}}}{2PQ_j}$.

Similarly, Pr_2 can be derived as

$$\begin{aligned} Pr_2 &= \mathbb{P}\left(\frac{PQ_jXY}{(P+Q_j)X + PY + 1} > \gamma_{th}, X > Y\right) \\ &= \int_b^{\infty} \mathbb{P}\left(y > \frac{(1+(P+Q_j)x)\gamma_{th}}{PQ_jx - P\gamma_{th}}, y < x\right) f_X(x) dx \\ &= \int_b^{\infty} \int_{c_2}^x f_Y(y) f_X(x) dy dx \end{aligned} \quad (5.11)$$

where $c_2 = \frac{(1+(P+Q_j)x)\gamma_{th}}{PQ_jx - P\gamma_{th}}$. Now, by substituting (5.10) and (5.11) in (5.9), $F_\gamma(\gamma_{th})$ is given by

$$\begin{aligned} F_\gamma(\gamma_{th}) &= 1 - \int_a^b \int_{c_1}^{\infty} f_Y(y) dy f_X(x) dx - \int_b^{\infty} \int_{c_2}^{\infty} f_Y(y) dy f_X(x) dx \\ &= 1 - \int_a^b Q\left(\frac{\ln c_1 - \mu_y}{\sigma_y}\right) \frac{1}{\sqrt{2\pi}x\sigma_x} \exp\left(-\frac{(\ln x - \mu_x)^2}{2\sigma_x^2}\right) dx \\ &\quad - \int_b^{\infty} Q\left(\frac{\ln c_2 - \mu_y}{\sigma_y}\right) \frac{1}{\sqrt{2\pi}x\sigma_x} \exp\left(-\frac{(\ln x - \mu_x)^2}{2\sigma_x^2}\right) dx \end{aligned} \quad (5.12)$$

where $Q(\cdot)$ is the upper tail probability of the standard Gaussian distribution. Now by substituting $\frac{\ln x - \mu_x}{\sqrt{2}\sigma_x} = u$ in the resulting expression, $F_\gamma(\gamma_{th})$ can be written as

$$F_\gamma(\gamma_{th}) = 1 - \frac{1}{\sqrt{\pi}} \int_{a'}^{b'} Q\left(\frac{\ln c'_1 - \mu_y}{\sqrt{2}\sigma_y}\right) e^{-u^2} du - \frac{1}{\sqrt{\pi}} \int_{b'}^{\infty} Q\left(\frac{\ln c'_2 - \mu_y}{\sqrt{2}\sigma_y}\right) e^{-u^2} du \quad (5.13)$$

where $a' = \frac{\ln a - \mu_x}{\sqrt{2}\sigma_x}$, $b' = \frac{\ln b - \mu_x}{\sqrt{2}\sigma_x}$, and c'_1 and c'_2 are obtained by substituting $x = e^{(\mu_x + \sqrt{2}\sigma_x u)}$ in c_1 and c_2 , respectively. The integrals in (5.13) can now be calculated with one sided Gauss-Hermite Quadrature rule [113], i.e.,

$$\int_{t_1}^{t_2} f(u) e^{-u^2} du = \int_0^{t_2} f(u) e^{-u^2} du - \int_0^{t_1} f(u) e^{-u^2} du$$

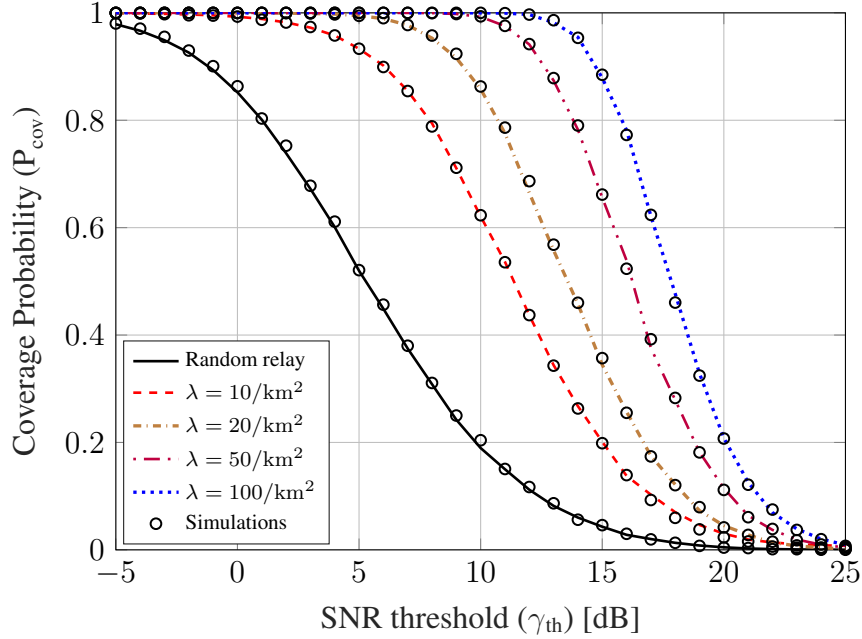


Figure 5.2: Coverage vs. SNR threshold for several relay densities.

$$= \sum_{i=1}^M w_{2,i} f(u_{2,i}) - \sum_{i=1}^M w_{1,i} f(u_{1,i}) \quad (5.14)$$

where $f(u)$ represents the Q-function in each integral of (5.13), the weights $w_{k,i}$ and abscissas $u_{k,i}$ are real numbers calculated based on [113] for range of 0 and t_k , $k \in \{1, 2\}$. Here, M is the number of abscissas used to calculate the integral, which gives the trade-off in accuracy and computation time. Here, $M = 5$ is found to be sufficiently close to the simulation results. In calculating the sum in (5.14), only the abscissas that fall in the domain of integral are used and the rest are ignored.

5.3.3 Coverage Probability with Beam Alignment Errors

In Section 5.2.2, coverage (5.7) is derived for no beam alignment errors. However, in practice, perfect beam alignment may be difficult to achieve. Therefore, the case with beam alignment error is considered next. From Section 2.1.4, the effective antenna gains $G_{\text{eq}1}$ for the $u_1 - R_j$ link and $G_{\text{eq}2}$ for the $u_2 - R_j$ link have the PDF given in (2.8). Next, considering that the two links are independent, the overall coverage probability P_{cov} is given by (3.31) with $P_{\text{cov},\text{SRD}}(\cdot, \cdot)$ replaced by $P_{\text{cov}}(\cdot, \cdot)$.

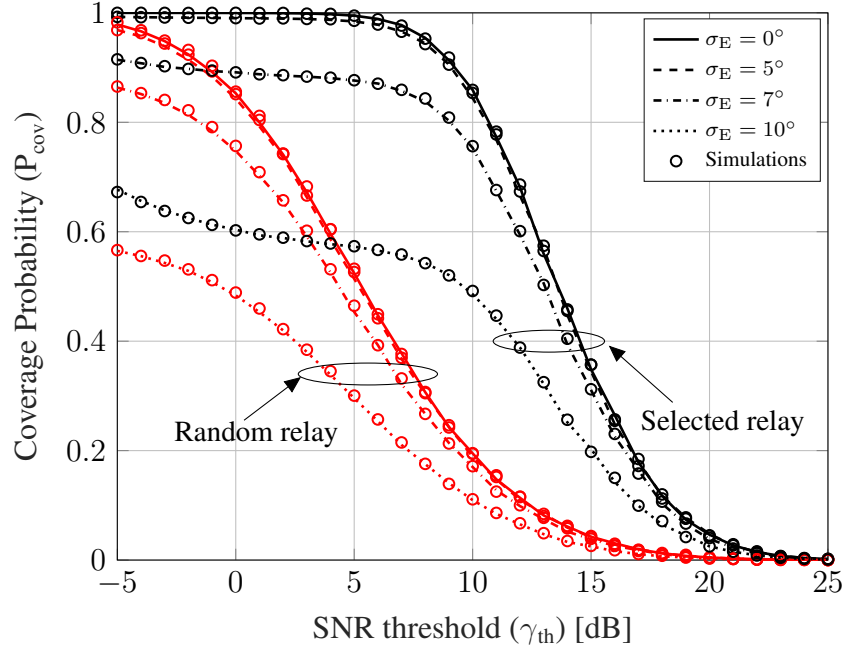


Figure 5.3: Coverage vs. SNR threshold for different beam alignment errors (σ_E), when $\phi = 30^\circ$ and $\lambda = 20/\text{km}^2$.

5.4 Numerical Results and Simulations

In this section, the analytical results are verified with Monte-Carlo simulation (10^5 independent PPP realizations). It is considered that a carrier frequency of 73 GHz with bandwidth $B = 1$ GHz is used and all nodes have directional antennas with gains $G_{\max} = 18\text{dB}$ and $G_{\min} = -10\text{dB}$. Other parameters are set as follows: $\alpha_L = 2$, $\alpha_N = 3.3$, $\sigma_L = 5.2$ dB and $\sigma_N = 7.6$ dB [64]. The transmit power of 30 dBm is used for all the nodes, i.e., u_1 and u_2 and the selected relay. In the figures, the curves represent analysis, and the markers are for simulated results. Clearly, analytical results match exactly with simulations, verifying the correctness of the analysis.

Fig. 5.2 plots coverage probability versus the SNR threshold for the selected relay in (5.5) and that of a random relay, for various node densities. It can be observed that as the node density increases from $10/\text{km}^2$ to $100/\text{km}^2$, the coverage improves from 20% to 90% for a 15 dB threshold. Fig. 5.3 plots the effect of beam alignment error on coverage probability. It can be observed that for small beam alignment error (σ_E) of up to 5 degrees, the performance is close to that of perfect beam alignment case. However, when σ_E increases to 7 degrees, the coverage probability decreases for both the random relay selection and the

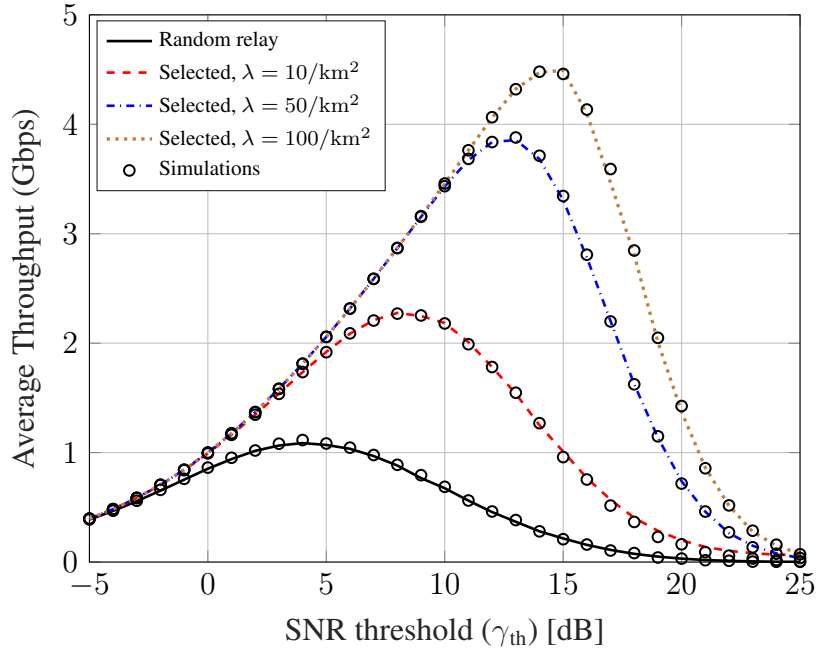


Figure 5.4: Average user throughput for different SNR thresholds.

best relay selection and it decreases significantly when σ_E reaches 10 degrees.

Fig. 5.4 shows the effect of relay density on average user throughput, which is calculated as $C = BP_{\text{cov}} \log_2(1 + \gamma_{\text{th}})$. The achieved throughput with a random relay is always less than that of the optimally selected relay per (5.5), and increasing the relay density increases the throughput of the system.

5.5 Summary

The problem of two-way AF mmW relay selection is studied in this chapter. The challenge is to improve the bidirectional communication between two fixed end users. The locations of potential relay nodes are modeled as a homogeneous PPP. The best relay is selected to maximize the minimum end-to-end SNR (for u_1 and u_2). The exact CDF of the minimum end-to-end SNR with a random relay is derived first, and used it to get the coverage probability of relay selection (5.5). It is found that relay selection (5.5) provides significantly better coverage and spectral efficiency compared to the random selection scheme. Increasing the node density also improves coverage due to spatial diversity. Overall, two-way relay selection in mmW networks appears to offer significant benefits.

~

Chapter 6

Coverage Analysis of Cooperative NOMA in Millimeter Wave Networks

This chapter analyzes the coverage probability of a cooperative non-orthogonal multiple access (NOMA) mmW network consisting of source (S) and destination (D) pair without a direct link between them. A relay (R) is selected from a set of users distributed as a homogeneous Poisson point process (PPP). The selection process has two steps. First, the users that meet a rate threshold are selected to be the decoding set. Second, from the decoding set, a relay is selected that is nearest to S or nearest to D . The S to R channel is NOMA. Although user locations form a homogeneous PPP, the decoding set is an inhomogeneous PPP. Therefore, by characterizing its spatial density (location dependent) the coverage probability is derived. It is shown that compared to orthogonal multiple access, NOMA provides higher coverage for these two relay-selection schemes. The coverage probability of random relay selection is also derived to quantify the benefits of relay selection in mmW NOMA.

6.1 Introduction

NOMA is a paradigm shift from traditional orthogonal multiple access (OMA) because it allows multiple users to share the same resource block. This creates a potential trade-off between interference and spectral efficiency, which is achieved via power domain multiplexing and successive interference cancellation [57]. Compared to OMA, NOMA offers higher sum rates, lower outage and improved fairness. Since mmW NOMA networks facilitate higher spectral efficiency and an abundance of spectrum, their coverage and rate performance with beam misalignment [114] and outage performance with random beam-

forming [58] have been analyzed. On the other hand, high path losses and blockage, which shrink the coverage area in mmW communications [20], can be mitigated via the use of relays [44], [55], [59]. In this situation, NOMA can improve the spectral efficiency of relays, and relays in turn can mitigate blockages and extend the link distance. Thus, the best of both spectral efficiency and coverage can be achieved. This use of relays leads to cooperative NOMA.

In cooperative NOMA, a user with a strong channel relays the data to a user with weaker channel, which improves outage and sum rate performance significantly [61]. Although studied extensively for sub-GHz bands (see [61], [62] and references therein), an analysis of cooperative mmW NOMA has remained absent thus far. This letter fills this gap by characterizing the ability of destination (D) to achieve a sufficient signal-to-noise ratio (SNR) and the ability of both relay (R) and D to meet the rate requirements for a simple cooperative NOMA mmW network. In this network, R is selected from a pool of user nodes, and there is no direct link from source S to D . In the context of cellular networks, S may be thought as a base-station, the pool as a collection of the cell users and D as a cell-edge user. The selected user of the pool will act as R . So R -to- D channel is a direct device-to-device channel [115]. Here, S has separate data symbols to transmit to both R and D . For this, OMA would require a total of three time slots: one time slot to transmit R 's data, and two time slots to transmit D 's data via R . In contrast, if NOMA is used, superimposed data of R and D can be transmitted in first time slot, and R can transmit D 's data in the next slot, decreasing the required number of time slots from three to two, which improves spectral efficiency.

6.2 System Model

Consider a source (S), a destination (D) and a set of users which are distributed in a circular disc \mathcal{D} of radius \mathcal{R} as a homogeneous Poisson point process (PPP) Φ with a density λ . No direct link from S to D is assumed, and a relay R is selected from active users that are receiving data from S . Here, only the relays that are in line of sight (LOS) from S and D are considered because non line of sight path losses exceed 20 dB or more over LOS links [20]. A link of length d becomes LOS with probability of $e^{-\beta d}$ where $\beta = \frac{2\mu(\mathbb{E}[L]+\mathbb{E}[W])}{\pi}$ is a blockage parameter in which μ is the blockage density, and $\mathbb{E}[L]$ and $\mathbb{E}[W]$ respectively,

are the average length and width of the blockage objects [69]. In this case, S simultaneously transmits x_R and x_D , intended for R and D , respectively, using NOMA with power scaling factors a_R and a_D where $a_R^2 + a_D^2 = 1$. The required data rate at D is considered lower than that at R , and consequently, it is required that $a_R < a_D$ [57]. In the first time-slot, S transmits the superimposed symbols to the selected relay (relay selection in Section 6.3). The received signal at R can be written as

$$y_R = h_{SR}(a_R x_R + a_D x_D) \sqrt{P_S G_S G_R \Psi} d_{SR}^{-\alpha/2} + w_R \quad (6.1)$$

where h_{SR} is small scale fading in $S - R$ link, P_S is the total transmit power at S , G_S and G_R are the directional antenna gains at S and R , respectively, $\Psi = \frac{c}{4\pi f}$ is a path loss at 1 meter distance and c and f are the speed of light in free space and the operating mmW frequency, d_{SR} is the distance between S and R , α is the path loss exponent, and w_R is the additive white Gaussian noise (AWGN) at R . Now, R first decodes x_D by treating the x_R term as interference, which will result in the signal to interference-plus-noise ratio (SINR) of [57]

$$\gamma_{R,D} = \frac{P_S \Psi G_S G_R h_{SR}^2 d_{SR}^{-\alpha} a_D^2}{P_S \Psi G_S G_R h_{SR}^2 d_{SR}^{-\alpha} a_R^2 + N_0}. \quad (6.2)$$

Next, with error free decoding, R removes the x_D term from y_R and decodes its own symbol x_R . The SNR at R to decode x_R is thus

$$\gamma_{R,R} = \frac{P_S \Psi G_S G_R h_{SR}^2 d_{SR}^{-\alpha} a_R^2}{N_0}. \quad (6.3)$$

Next, R forwards x_D to D . The received signal at D is

$$y_D = h_{RD} x_D \sqrt{P_R G_R G_D \Psi} d_{RD}^{-\alpha/2} + w_D, \quad (6.4)$$

where h_{RD} is small scale fading in $R - D$ link, P_R is the transmit power of R , G_D is the directional antenna gain at D , d_{RD} is the distance between R and D , and w_D is the AWGN at D . Now, the received SNR at D is given by

$$\gamma_D = \frac{P_R \Psi G_R G_D h_{RD}^2 d_{RD}^{-\alpha}}{N_0}. \quad (6.5)$$

The fading parameters h_{SR} and h_{RD} are assumed to be Nakagami- m distributed. Thus, channel power gains $|h_{SR}|^2$ and $|h_{RD}|^2$ are Gamma random variables (r.v.) with probability density function (PDF) $f_X(x) = \frac{\nu^m}{\Gamma(m)} x^{m-1} e^{-\nu x}$, $x > 0$, with shape parameter $m \geq 1$ and rate parameter $\nu > 0$.

6.3 Coverage Analysis

Coverage is the probability that both R and D meet their individual data rate requirements R_R and R_D , respectively. Thus, SINR or SNR thresholds of $\tau_R = 2^{2R_R} - 1$ and $\tau_D = 2^{2R_D} - 1$ must be met while decoding the data of R and D , respectively. Therefore, coverage depends on two events - (1) a relay can successfully decode its own message and the message for D in the first time slot, and (2) in the second time slot, D successfully decodes its message from R .

6.3.1 Relay Selection

Since multiple nodes are capable of decoding and forwarding data to D , selecting the best among them improves coverage. Therefore, several relay selection strategies are analyzed and compared for their coverage performances.

Selection scheme 1 (\mathcal{S}_1): Nearest to source relay selection

Consider the source S to be at origin, and D is at $(L, 0)$ in polar coordinate system and an arbitrary relay is located at (r, θ) . With this, the location dependent distance between an arbitrary relay to D is $d_{RD} = \sqrt{r^2 - 2rL \cos(\theta) + L^2} \triangleq \rho$, and denote $d_{SR} = r$. This scheme works as follows: first, a set of nodes that can decode S 's message to D and successfully transmit it to D is selected. This set is called the decoding set, which is an inhomogeneous PPP $\hat{\Phi}_1$ because it is a subset of Φ and the selection of its members is influenced by path loss and blockage, i.e., selection is not random. The density function of the inhomogeneous PPP $\hat{\Phi}_1$, $\hat{\lambda}_1(r, \theta)$, is described in Lemma 13. Second, a relay is selected from the the decoding set.

Lemma 13. *The density function of the decoding set $\hat{\Phi}_1$ is characterized by*

$$\hat{\lambda}_1(r, \theta) = \lambda e^{-\beta(r+\rho)} \exp(-\nu(\xi_D r^\alpha + \zeta_D \rho^\alpha)) \sum_{n=0}^{m-1} \sum_{k=0}^{m-1} \frac{\nu^{n+k}}{n! k!} \xi_D^n \zeta_D^k r^{n\alpha} \rho^{k\alpha}, \quad (6.6)$$

where $\xi_D = \frac{\tau_D N_0}{P_S \Psi G_S G_R (a_D^2 - a_R^2 \tau_D)}$ and $\zeta_D = \frac{\tau_D N_0}{P_R \Psi G_R G_D}$.

Proof. A relay in Φ is retained in $\hat{\Phi}_1$ if it can decode the message for D in the first time slot and can successfully deliver this message to D in the second time slot. Let P_1 be the probability that a relay meets the above criteria, which can be written mathematically as

$$\begin{aligned}
P_1 &= \mathbb{P}(\gamma_{R,D} \geq \tau_D, \gamma_D \geq \tau_D) \\
&\stackrel{(a)}{=} \mathbb{P}(\gamma_{R,D} \geq \tau_D) \mathbb{P}(\gamma_D \geq \tau_D) \\
&\stackrel{(b)}{=} \mathbb{P}(h_{SR}^2 \geq \xi_D r^\alpha) \mathbb{P}(h_{RD}^2 \geq \zeta_D \rho^\alpha) \\
&\stackrel{(c)}{=} \exp(-\nu(\xi_D r^\alpha + \zeta_D \rho^\alpha)) \sum_{n=0}^{m-1} \sum_{k=0}^{m-1} \frac{\nu^{n+k}}{n! k!} \xi_D^n \zeta_D^k r^{n\alpha} \rho^{k\alpha}, \tag{6.7}
\end{aligned}$$

where (a) is due to the independence of two events, (b) is obtained using (6.2) and (6.5), and (c) is obtained using the complimentary cumulative distribution function (CCDF) of Gamma r.v. with an integer-valued shape parameter m . It is also assumed $a_D^2 > a_R^2 \tau_D$, otherwise the coverage probability will be automatically zero. This assumption is widely used in the analysis of NOMA networks [61], [62]. Now, using the LOS probabilities of $e^{-\beta r}$ and $e^{-\beta \rho}$ in $S - R$ and $R - D$ links, respectively, and by thinning Φ with P_1 , (6.6) is obtained. ■

The average size of the decoding set $\hat{\Phi}_1$ is given by

$$\hat{\Lambda}_{D,1} = \int_{\theta=0}^{2\pi} \int_{r=0}^{\mathcal{R}} \hat{\lambda}_1(r, \theta) r dr d\theta. \tag{6.8}$$

The relay from this set that is closest to S is selected. This selection achieves the maximum average SNR at R . To derive coverage probability, distribution of the distance of the selected relay from $\hat{\Phi}_1$ from S is required, which is given in Lemma 14.

Lemma 14. *The PDF of the distance of the nearest relay $\hat{\Phi}_1$ from S is given by*

$$f_r(z) = z \hat{\lambda}_1(z, \theta) \exp\left(-\int_{\theta=0}^{2\pi} \int_{r=0}^z \hat{\lambda}_1(r, \theta) r dr d\theta\right). \tag{6.9}$$

Proof. Let z be the distance from S to the nearest relay in $\hat{\Phi}_1$. This means no relay is located within a circle centered at S with radius z , which corresponds to the void probability

of the PPP $\hat{\Phi}_1$, given by

$$\tilde{F}_r(z) = \mathbb{P}(r > z) = \exp\left(-\int_{\theta=0}^{2\pi} \int_{r=0}^z \hat{\lambda}_1(r, \theta) r dr d\theta\right). \quad (6.10)$$

Now, using $f_r(z) = -\frac{\tilde{F}_r(z)}{dz}$, (6.9) is obtained. \blacksquare

Theorem 5. *The coverage probability of the selection scheme \mathcal{S}_1 is given by*

$$\begin{aligned} P_{\text{cov}}^{\mathcal{S}_1} &= \lambda \sum_{j=0}^{m-1} \sum_{k=0}^{m-1} \sum_{n=0}^{m-1} \frac{\nu^{j+k+n}}{j! k! n!} \xi_R^j \xi_D^n \zeta_D^k \int_{\theta=0}^{2\pi} \int_{z=0}^{\mathcal{R}} e^{-\beta(z+\rho_z)} e^{-\nu((\xi_D+\xi_R)z^\alpha + \zeta_D \rho_z^\alpha)} z^{\alpha(j+n)} \rho_z^{\alpha k} \\ &\quad \times \exp\left(-\lambda \sum_{n=0}^{m-1} \sum_{k=0}^{m-1} \frac{\nu^{n+k}}{n! k!} \xi_D^n \zeta_D^k r^{\alpha n} \rho^{\alpha k} \int_{\theta=0}^{2\pi} \int_{r=0}^z e^{-\beta(r+\rho)} e^{-\nu(\xi_D r^\alpha + \zeta_D \rho^\alpha)} r dr d\theta\right) \\ &\quad \times z dz d\theta, \end{aligned} \quad (6.11)$$

where $\rho_z = \sqrt{z^2 - 2zL \cos(\phi) + L^2}$.

Proof. Here, coverage is the probability that the selected relay from $\hat{\Phi}_1$ meets the SNR threshold τ_R . Mathematically,

$$\begin{aligned} P_{\text{cov}}^{\mathcal{S}_1} &= \mathbb{P}(\gamma_{R,R} \geq \tau_R) = \mathbb{P}\left(h_{SR}^2 \geq \frac{\tau_R N_0 r^\alpha}{P_S \Psi G_S G_R}\right) \\ &= \mathbb{E}_r \left[\exp(-\nu \xi_R r^\alpha) \sum_{j=0}^{m-1} \frac{\nu^j}{j!} (\xi_R r^\alpha)^j \right] \end{aligned} \quad (6.12)$$

where $\xi_R = \frac{\tau_R N_0}{P_S \Psi G_S G_R}$. Now, by taking the expectation in (6.12) over $f_r(z)$ in (6.9), (6.11) is obtained. \blacksquare

Selection scheme 2 (\mathcal{S}_2): Nearest to destination relay selection

To make the analysis tractable, the origin is shifted to the location of D so that S is located at (L, π) in polar coordinates. An arbitrary relay is located at (l, ϕ) and its distance from S is given by $d_{SR} = \sqrt{l^2 + 2lL \cos(\phi) + L^2} \triangleq \delta$, and denote $d_{RD} = l$. This displacement of origin does not affect the performance when radius \mathcal{R} of user disc \mathcal{D} is much larger than L , and is used just to aid the tractability of the analysis. Here, a decoding set is formed again. In this case, the decoding set includes the nodes that can meet the rate requirements of R

and D in the first hop. This means, the conditions $\gamma_{R,D} \geq \tau_D$ and $\gamma_{R,R} \geq \tau_R$ are met by the decoding set of relays which forms an inhomogeneous PPP, denoted by $\hat{\Phi}_2$ with a density function $\hat{\lambda}_2(l, \phi)$ given in Lemma 3.

Lemma 15. *The density function of the decoding set $\hat{\Phi}_2$ is given by*

$$\hat{\lambda}_2(l, \phi) = \lambda e^{-\beta\delta} e^{-\nu\eta\delta^\alpha} \sum_{n=0}^{m-1} \frac{\nu^n}{n!} \eta^n \delta^{n\alpha}, \quad (6.13)$$

where $\eta = \xi_D$ if $\frac{\tau_D}{1 + \tau_D} < a_D^2 \leq \frac{\tau_D(1 + \tau_R)}{\tau_R(1 + \tau_D)}$ and $\eta = \xi_R$ if $\frac{\tau_D(1 + \tau_R)}{\tau_R(1 + \tau_D)} \leq a_D^2 < 1$.

Proof. Let P_2 be the probability that a relay in Φ is retained in $\hat{\Phi}_2$, which can be written mathematically as

$$\begin{aligned} P_2 &= \mathbb{P}(\gamma_{R,D} \geq \tau_D, \gamma_{R,R} \geq \tau_R) \\ &= \mathbb{P}(h_{SR}^2 \geq \xi_D \delta^\alpha, h_{SR}^2 \geq \xi_R \delta^\alpha) \\ &= \mathbb{P}(h_{SR}^2 \geq \delta^\alpha \max\{\xi_D, \xi_R\}). \end{aligned} \quad (6.14)$$

Here, if the power allocation factors a_R and a_D are fixed, closed form expression of P_2 can be derived. Since it is assumed that $a_D^2 > a_R^2 \tau_D$, a_D must satisfy $a_D^2 > \frac{\tau_D}{1 + \tau_D}$, and the coverage is zero for $0 \leq a_D^2 \leq \frac{\tau_D}{1 + \tau_D}$. It can be shown by simple mathematical manipulations that $\xi_D > \xi_R$ if a_D satisfies $\frac{\tau_D}{1 + \tau_D} < a_D^2 \leq \frac{\tau_D(1 + \tau_R)}{\tau_R(1 + \tau_D)}$, and $\xi_D < \xi_R$ if a_D satisfies $\frac{\tau_D(1 + \tau_R)}{\tau_R(1 + \tau_D)} \leq a_D^2 < 1$. Then, using the CCDF of Gamma r.v., P_2 can be written as

$$P_2 = \exp(-\nu\eta\delta^\alpha) \sum_{n=0}^{m-1} \frac{\nu^n}{n!} \eta^n \delta^{n\alpha}. \quad (6.15)$$

Now, using the LOS probabilities of $e^{-\beta\delta}$ in $S - R$ link, and by thinning Φ with P_2 , (6.13) is obtained. ■

Then, the average number of relays in $\hat{\Phi}_2$ is given by

$$\hat{\Lambda}_{D,2} = \lambda \sum_{n=0}^{m-1} \frac{(\nu\eta)^n}{n!} \int_{\phi=0}^{2\pi} \int_{l=0}^{\mathcal{R}} e^{-\beta\delta - \nu\eta\delta^\alpha} \delta^{n\alpha} l dl d\phi. \quad (6.16)$$

Next, an LOS relay is selected from $\hat{\Phi}_2$ that is closest to D . This is equivalent to selecting a relay that provides a maximum average SNR at D . In Theorem 6, the coverage probability of this selection scheme is provided.

Theorem 6. *The coverage probability of the selection scheme \mathcal{S}_2 is given by*

$$P_{\text{cov}}^{\mathcal{S}_2} = \lambda \sum_{j=0}^{m-1} \sum_{n=0}^{m-1} \frac{\nu^{j+n}}{j! n!} \zeta_D^j \eta^n \int_{\phi=0}^{2\pi} \int_{z=0}^{\mathcal{R}} e^{-\nu(\zeta_D z^\alpha + \eta \delta_z^\alpha)} e^{-\beta(z+\delta_z)} z^{\alpha j} \delta_z^{\alpha n} \\ \times \exp \left(-\lambda \sum_{n=0}^{m-1} \frac{(\nu \eta)^n}{n!} \int_{\phi=0}^{2\pi} \int_{l=0}^z e^{-\beta(l+\delta)} e^{-\nu \eta \delta^\alpha} \delta^{\alpha n} l dl d\phi \right) z dz d\phi, \quad (6.17)$$

where $\delta_z = \sqrt{z^2 + 2zL \cos(\phi) + L^2}$.

Proof. Here, to achieve the coverage, the selected relay from $\hat{\Phi}_2$ must meet $\gamma_D \geq \tau_D$. Therefore, $P_{\text{cov}}^{\mathcal{S}_2}$ can be written as

$$P_{\text{cov}}^{\mathcal{S}_2} = \mathbb{P}(\gamma_D \geq \tau_D) = \mathbb{P} \left(h_{RD}^2 \geq \frac{\tau_D N_0 l^\alpha}{P_R \Psi G_S G_R} \right) \\ = \mathbb{E}_l \left[\exp(-\nu \zeta_D l^\alpha) \sum_{j=0}^{m-1} \frac{\nu^j}{j!} (\zeta_D l^\alpha)^j \right]. \quad (6.18)$$

Now, taking the expectation in (6.18) with the PDF of distance of the nearest relay in $\hat{\Phi}_2$ from D , given by $f_l(z) = z e^{-\beta z} \hat{\lambda}_2(z, \phi) \exp \left(-\int_{\phi=0}^{2\pi} \int_{l=0}^z e^{-\beta l} \hat{\lambda}_2(l, \phi) l dl d\phi \right)$, (6.17) is obtained. The $f_l(z)$ expression can be derived similar to (6.9). ■

Selection Scheme 3 (\mathcal{S}_3): Random relay selection

Since the selection schemes \mathcal{S}_1 and \mathcal{S}_2 require knowledge of distance or location information, the immediate question is what the performance loss is if such information is not available. To answer it, random relay selection from the decoding set is considered. Coverage probability of it is given in Theorem 7.

Theorem 7. *When a relay is selected at random from $\hat{\Phi}_2$, the coverage probability is given*

by

$$P_{\text{cov}}^{\mathcal{S}_3} = \frac{\lambda \left(1 - e^{-\hat{\Lambda}_{\mathcal{D},2}}\right)}{\hat{\Lambda}_{\mathcal{D},2}} \sum_{j=0}^{m-1} \sum_{n=0}^{m-1} \frac{\nu^{n+j}}{n! j!} \eta^n \zeta_D^j \int_{\phi=0}^{2\pi} \int_{l=0}^{\mathcal{R}} l^{\alpha j+1} \delta^{\alpha n} e^{-\beta(l+\delta)} e^{-\nu(\eta\delta^\alpha + \zeta_D l^\alpha)} dl d\phi. \quad (6.19)$$

Proof. The proof follows from the proof of Theorem 6 where the expectation over $\hat{\Phi}_2$ is taken with the PDF of the location of a randomly selected relay, which is given by $f_X(x) = \frac{\hat{\lambda}_2(l,\phi)}{\hat{\Lambda}_{\mathcal{D},2}}$. Now, applying the LOS probability of $e^{-\beta l}$ in $R - D$ link, (6.19) is obtained in which the term $(1 - e^{-\hat{\Lambda}_{\mathcal{D},2}})$ is included due to the coverage being zero if no relay exists in $\hat{\Phi}_2$. ■

6.4 Numerical Results

Here the derived analytical results are verified via 10^5 Monte-Carlo simulations per run. The simulation parameters are set as follow: $G_S = G_R = G_D = 18$ dBi, $a_R = 0.25$, $\alpha = 2$, $\mathcal{R} = 1000$ m, $L = 200$ m, $\lambda = 5 \times 10^{-5}/\text{m}^2$, $\mu = 2 \times 10^{-4}$, $\mathbb{E}[L] = \mathbb{E}[W] = 15$ m, unless otherwise specified. For comparison, OMA transmission with same rate requirements at R and D that uses best-worst relay selection criteria is also simulated [27].

Fig. 6.1 plots coverage expressions (6.11), (6.17) and (6.19) for NOMA and OMA. This figure shows that \mathcal{S}_2 scheme (i.e., closest-to-destination relay selection) provides the best coverage followed closely by \mathcal{S}_1 scheme (i.e., closest-to-source relay selection). However, with random relay selection, the coverage probability decreases after an initial increase when transmit power increases. The reason is that for large transmit powers, the decoding set has relay nodes farther away from D . If such a node is picked randomly, then the resulting $R - D$ link is less likely to be LOS, reducing coverage at D .

To study the effect of relay density on the coverage, Fig. 6.2 plots the coverage probabilities (6.11), (6.17) and (6.19) along the relay density for two values of blockage densities $\mu = \{2 \times 10^{-4}/\text{m}^2, 5 \times 10^{-4}/\text{m}^2\}$. Here, the coverage for \mathcal{S}_1 , \mathcal{S}_2 and OMA improve with increasing relay density λ . Note also that, these coverages shift to lower values when the blockage density μ is increased. This suggests that if μ increases, λ should be increased to maintain the same coverage. For a random relay, coverage flattens for higher λ because its selection is independent of density as long as at least one relay exists in the decoding set, a

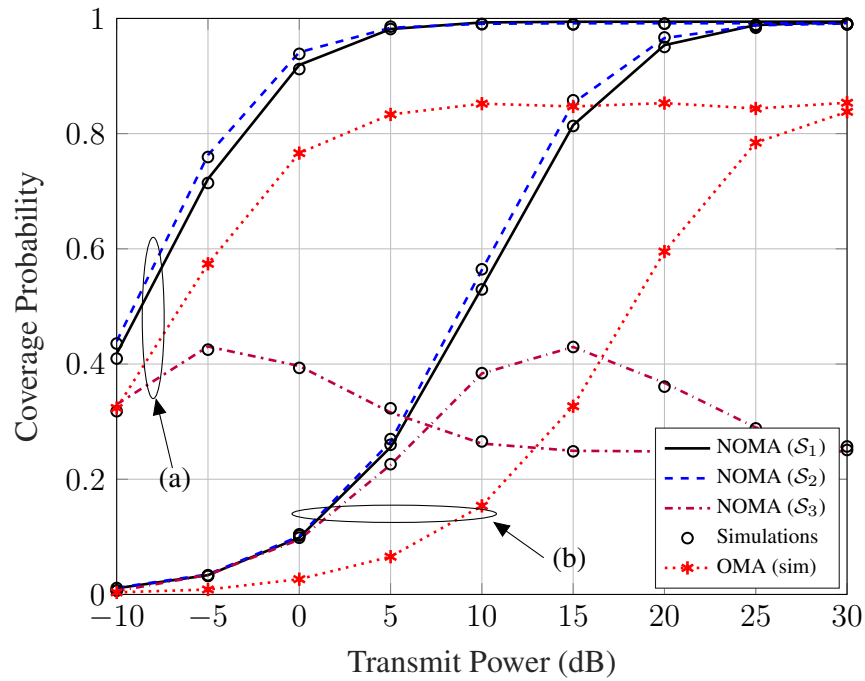


Figure 6.1: Coverage probability vs transmit power for NOMA using $\mathcal{S}_1, \mathcal{S}_2$ and \mathcal{S}_3 and OMA, where the curves (a) are for $\{R_D, R_R\} = \{1, 3\}$ bps/Hz, and (b) for $\{R_D, R_R\} = \{1.9, 6\}$ bps/Hz.

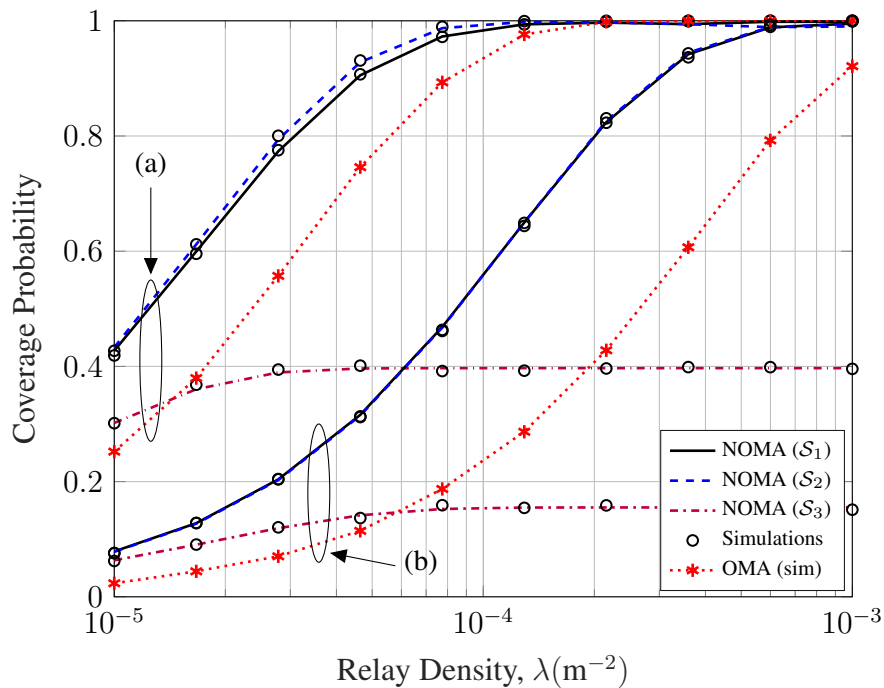


Figure 6.2: Coverage probability vs relay density for rate thresholds $\{R_D, R_R\} = \{1, 3\}$ bps/Hz with $P_S = P_R = 0$ dB. The curves (a) are for $\mu = 2 \times 10^{-4}/\text{m}^2$, and (b) are for $\mu = 5 \times 10^{-4}/\text{m}^2$.

phenomenon also reported in Chapters 3.

6.5 Summary

This letter has derived coverage probability of three mmW cooperative NOMA relay selection schemes. It is found that both closest-to-source and closest-to-destination relay selections perform closely and both outperform OMA. However, coverage due to a random relay may be worse than that of OMA depending on the transmit power level and relay density.

~

Chapter 7

Conclusion and Future Research Directions

7.1 Conclusion and Summary of Contributions

The use of mmW band is a key to address the exponential data growth in 5G networks with new services and data intensive applications. Although in principle the abundance of spectrum facilitates the development of higher data rate links, high path losses and blockages in mmW bands must be addressed before they can be used for highly reliable commercial 5G networks. High path losses can be compensated via large antenna arrays that allow for directional beamforming. However, the blockage problem due to high penetration losses across walls and other objects and poor diffraction around the corners remains a key challenge in utilizing mmW spectrum in cellular networks.

Motivated by this, improving the coverage against the blockages and enhancing the link rates and spectral efficiency are considered and examined for relay networks. The use of wireless relays offer coverage, reliability and capacity improvements for sub-6 GHz networks and hence have already been included in 3GPP Release-14 for LTE-A standard. Therefore, this thesis investigated several mmW relay problems, specifically, one-way, two-way, multi-hop, and NOMA relays. The specific contributions of this thesis are as follows:

- In Chapter 3, performance of the mmW DF relays using tools from stochastic geometry was analyzed. The locations of radio nodes were modeled as a two-dimensional homogeneous PPP in \mathbb{R}^2 . Then a subset of these nodes was chosen as the decoding set and it was found that the spatial point process of the decoding set follows an inhomogeneous PPP. Then a relay is selected from the decoding set and the coverage was analyzed for three cases: without using a relay, best relay selection, and randomly

picked relay. It was found that the relay deployment significantly improved the coverage performance, especially with the best relay selection. Also, the increase in relay deployment density improved the coverage significantly. The analysis was also extended to study the effect of beam alignment errors, the effect of power splitting, rate coverage probability, and spectral efficiency.

- Chapter 4 analyzed the performance of a multi-hop mmW DF relay network by allowing each link to be in LOS or NLOS state. And each state is characterized by a distinct Nakagami m parameter. In the noise-limited case, the distribution of destination SNR was derived first, which was then used to derive the closed-form coverage probability, ergodic capacity, and SER. However, for the interference-limited case, if the interference powers at a relay are i.i.d., per-hop SIR follows beta-prime distribution. However, if the interference powers are i.n.i.d., computation of the per-hop and destination SIR distribution is highly complicated. To circumvent this problem, the *Welch-Satterthwaite Approximation* for the sum of Gamma variables was used to derive the distribution of the per-hop SIR. Subsequently, coverage, capacity and SERs were derived. For both noise-limited and interference-limited scenarios, coverage probability improves significantly with the use of multiple hops. However, it should be noted that, for a fixed per hop SNR (or SIR), outage probability and SER increase due to cumulative effect of outage events in each hop when the number of hops increases.
- Chapter 5 investigated the potential benefits of deploying two-way AF relays to assist bidirectional data exchange between two end users in a mmW network. To account for the spatial randomness of node locations, potential relays were assumed to follow homogeneous PPP distribution. Then, a relay that maximizes the minimum of end-to-end SNR for two users was selected. The coverage probability achieved by this selection was derived and the results demonstrated that the selected relay significantly improved the coverage and spectral efficiency. For comparison, the coverage with a randomly selected relay was also plotted which provided substantially lower coverage. The increase in relay density deployment also increased the coverage.
- Chapter 6 studied a cooperative NOMA in mmW network where a user receiving data

from transmitter forwards it to a farther destination which lacks the coverage. While the source and destination locations were fixed, a relay was selected from the users whose locations follow a homogeneous PPP. First, a set of users that meet certain rate threshold were selected in a decoding set. Then, a relay from this set was selected using two criteria: (i) nearest to source, and (ii) nearest to destination. Then, coverage probability of these mmW cooperative NOMA relay selection schemes were derived which demonstrated that, compared to orthogonal multiple access, NOMA provides higher coverage and rates with relay selection schemes (i) and (ii). The coverage with a randomly selected relay was also derived to quantify the benefits of relay selection in mmW NOMA.

There are significant implications of this thesis research in future mmW network deployments and industry applications. For example, the coverage probability results in Chapter 3 can be used to decide the cell size and relay deployment density to achieve the required rate or SNR at a typical user in a given blockage scenario. Similarly, if more than two hops are required to provide the coverage to a user in a far-reaching or blocked region, results from multi-hop relay analysis in Chapter 4 can be used to decide number of hops required to provide the coverage to such users also impaired by co-channel transmissions. Similarly, two-way relay selection presented in Chapter 5 can be used to associate a given user to a base station where the base station acts as a relay and uses mmW frequencies in both access and backhaul links. In addition, the results from cooperative mmW NOMA presented in Chapter 6 provide useful insights on required transmit power level to achieve a given rate at concurrently served two NOMA users and in understanding the required active user density to make coverage viable at a blocked node by using an active user device.

7.2 Future Research Directions

The thesis research can be extended in several research directions.

- In Chapter 3, the noise limited regime was analyzed because co-channel interference becomes negligible when mmW nodes are deployed at low spatial densities and when co-channel signals are also subject to high path losses and blockages. However, with highly dense network deployments, co-channel interference is the limiting

factor [116]. Moreover, Chapter 3 assumes the availability of perfect channel state information and direction information (e.g., angles of arrival and so on). In practical systems, this information is estimated by using incoming signals and by transmitting exogenous signals (e.g., pilots). Thus, future work includes the analysis of co-channel interference and the quantification of performance losses due to imperfect channel and directional estimates.

- In Chapter 4, for the interference limited scenario, symbol error rates of two binary modulations were analyzed. Extending this analysis to additional modulation schemes such as QPSK and M-QAM is a potential research topic.
- In Chapter 4, the relay is subject to a fixed number of interferers, each located at a fixed distance from the relay. However, in practice, neither their numbers nor their distances are fixed. For example, interfering nodes can be mobile and their transmissions are asynchronous with the relay. Another possibility is that the interfering node has a different transmit cycle than the desired transmitter, thereby causing interference only during part of transmission time. Therefore, future works include the analysis spatially random interferer locations. For this, the random node locations can be modeled as a point process and the tools from stochastic geometry can be used to derive the performance measures such as coverage and rate.

~

Appendix A

Derivations for Chapter 3

A.1 Proof of Lemma 4

The CCDF of the distance from the destination to the selected relay conditioned on a relay from $\hat{\Phi}_L$ being selected can be written as

$$\begin{aligned}
 \bar{G}_{r_L}(z) &= \mathbb{P}\left(\text{No LOS relay is closer than } z \text{ given that} \right. \\
 &\quad \left. \text{no NLOS relay is closer than } r_L^{\frac{\alpha_L}{\alpha_N}}\right) \\
 &= \mathbb{P}\left(r_L > z \mid r_N > r_L^{\frac{\alpha_L}{\alpha_N}}\right) \\
 &= \frac{\mathbb{P}\left(r_N > r_L^{\frac{\alpha_L}{\alpha_N}}, r_L > z\right)}{\mathbb{P}\left(r_N > r_L^{\frac{\alpha_L}{\alpha_N}}\right)} \\
 &= \frac{\int_z^\infty \mathbb{P}\left(r_N > r_L^{\frac{\alpha_L}{\alpha_N}} \mid r_L = v\right) f_{r_L}(v) dv}{\int_0^\infty \mathbb{P}\left(r_N > r_L^{\frac{\alpha_L}{\alpha_N}} \mid r_L = v\right) f_{r_L}(v) dv} \\
 &\stackrel{(b)}{=} \frac{\int_z^\infty \exp\left(-\Lambda_N\left([0, v^{\frac{\alpha_L}{\alpha_N}}]\right)\right) f_{r_L}(v) dv}{A_L}, \tag{A.1}
 \end{aligned}$$

where in (b) the void probability for PPP $\hat{\Phi}_N$ is used, where

$$\Lambda_N([0, v^{\frac{\alpha_L}{\alpha_N}}]) = \int_{r=0}^{v^{\frac{\alpha_L}{\alpha_N}}} \int_{\theta=0}^{2\pi} (1 - p_L(r)) \hat{\lambda}(x) r d\theta dr \tag{A.2}$$

is the expected number of NLOS relays in $\mathcal{B}(0, v^{\frac{\alpha_L}{\alpha_N}})$. Now, the required distance distribution in (3.21) is obtained using $g_{r_L}(z) = -\frac{d\bar{G}_{r_L}(z)}{dz}$. The derivation for $g_{r_N}(z)$ in (3.22) follows similarly.

~

Appendix B

Derivations for Chapter 4

B.1 Proof of Lemma 7

Proof. Since $\tilde{F}_{X_{\min}}(x) = \prod_k \tilde{F}_{X_k}(x)$, $\alpha_k \in \mathbb{N}$, and $\tilde{F}_{X_k}(x) = e^{-\lambda_k x} \sum_{n=0}^{\alpha_k-1} \frac{(\lambda_k x)^n}{n!}$, $\tilde{F}_{\gamma_{\text{eq}}}(x)$ can be written as

$$\tilde{F}_{\gamma_{\text{eq}}}(x) = e^{-(\lambda_1 + \dots + \lambda_K)x} \underbrace{\prod_{k=1}^K \sum_{n=0}^{\alpha_k-1} \frac{(\lambda_k x)^n}{n!}}_P, \quad 0 \leq x < \infty, \quad (\text{B.1})$$

where the product term P can be expanded as

$$P = \sum_{n_1=0}^{\alpha_1-1} a_{1n_1} x^{n_1} \cdot \sum_{n_2=0}^{\alpha_2-1} a_{2n_2} x^{n_2} \dots \sum_{n_K=0}^{\alpha_K-1} a_{Kn} x^{n_K} \quad (\text{B.2})$$

where $a_{kn} = \frac{\lambda_k^n}{n!}$, $k = 1, 2, \dots, K$. The above expression is the product of K number of $(\alpha_k - 1)$ -th degree polynomials which can be readily computed using the convolution of coefficients. Clearly, P is a polynomial in x of degree $\sum \alpha_k - K$. By symbolically multiplying the K polynomials of P and collecting all the terms corresponding to the coefficient of x^m , Lemma 7 is obtained. ■

B.2 Proof of Proposition 8

For QPSK, MPSK, and Square-QAM modulations, conditional SER can be written in the form $P_k(x) = a \operatorname{erfc}(\sqrt{bx}) - c \operatorname{erfc}^2(\sqrt{bx})$. Now P_k is given by averaging over k -th hop

SNR PDF as

$$\begin{aligned} P_k &= \int_0^\infty \left(a \operatorname{erfc}(\sqrt{bx}) - c \operatorname{erfc}^2(\sqrt{bx}) \right) f_{\gamma_k}(x) dx \\ &= I_1 - I_2 \end{aligned} \quad (\text{B.3})$$

where $f_{\gamma_k}(x)$ is same as in (4.22), and the first integral I_1 is same as (4.26) in Proposition 4 with a and b depending on modulation scheme. The second integral I_2 is given by

$$I_2 = \frac{c}{\Gamma(\alpha_k)} \left(\frac{\lambda_k}{\bar{\gamma}} \right)^{\alpha_k} \int_0^\infty x^{m-1} e^{-\frac{\lambda_k}{\bar{\gamma}} x} \operatorname{erfc}^2(\sqrt{bx}) dx. \quad (\text{B.4})$$

Now with the help of [117, eq.(28)] and after some mathematical manipulations, I_2 can be written as

$$I_2 = c \left[1 - \frac{4}{\pi} \sum_{n=0}^{\alpha_k-1} \left(\frac{\lambda_k}{b\bar{\gamma}} \right)^n \frac{1}{(2n+1)} {}_2F_1 \left(\frac{1}{2} + n, 1 + n; \frac{3}{2} + n; -1 - \frac{\lambda_k}{b\bar{\gamma}} \right) \right]. \quad (\text{B.5})$$

Finally substituting I_1 and I_2 , (4.24) is obtained.

B.3 Proof of Lemma 10

Consider $S_k \sim \mathcal{G}(\alpha_k, \lambda_k/\zeta_k)$ be the desired signal power and the interference powers are distributed with $I_{n,k} \sim \mathcal{G}(\alpha_{n,k}, \lambda_{n,k}/\zeta_{I_{n,k}})$ where $n \in \{1, 2, \dots, M_k\}$ with total of M_k interferers at T_k . Now the CCDF of ξ_k is given by

$$\begin{aligned} \tilde{F}_{\xi_k}(x) &= \mathbb{P}(\xi_k > x) = \mathbb{P}\left(\frac{S_k}{I_k} > x\right) \\ &= \mathbb{P}(S_k > xI_k) = \mathbb{E}_{I_k} \left[\frac{\Gamma(\alpha_k, xI_k\lambda_k/\zeta_k)}{\Gamma(\alpha_k)} \right] \\ &= \mathbb{E}_{I_k} \left[e^{-xI_k\lambda_k/\zeta_k} \sum_{m=0}^{\alpha_k-1} \frac{(xI_k\lambda_k/\zeta_k)^m}{m!} \right] \\ &= \sum_{m=0}^{\alpha_k-1} \frac{1}{m!} \mathbb{E}_{I_k} \left[(xI_k\lambda_k/\zeta_k)^m e^{-(xI_k\lambda_k/\zeta_k)} \right] \\ &= \sum_{m=0}^{\alpha_k-1} \frac{(-1)^m (x\lambda_k/\zeta_k)^m}{m!} \mathcal{M}_{I_k}^m(x\lambda_k/\zeta_k) \end{aligned} \quad (\text{B.6})$$

where $I_k = \sum_{n=1}^{M_k} I_{n,k}$ is the total interference power at T_k and the m -th moment of I_k , $\mathcal{M}_{I_k}^m(t)$ can be obtained using the MGF of I_k which is given by

$$\begin{aligned}\mathcal{M}_{I_k}(t) &= \mathbb{E} [e^{-tI_k}] = \mathbb{E} \left[e^{-t \sum_{n=1}^{M_k} I_{n,k}} \right] \\ &= \prod_{n=1}^{M_k} \frac{\lambda_{n,k}^{\alpha_{n,k}}}{(\lambda_{n,k} + t\zeta_{I_{n,k}})^{\alpha_{n,k}}},\end{aligned}\tag{B.7}$$

where the product in last equality is using the property of MGF of sum of independent gamma random variables.

B.4 Proof of Lemma 11

Using (4.35) for identical per hop SIRs, the CDF of e2e SIR can be written as

$$\begin{aligned}F_{\xi_{\text{eq}}}(x) &= \sum_{k=1}^K \binom{K}{k} (-1)^{k+1} \left[\frac{1}{\sigma \mathcal{B}(\sigma, \theta)} \left(\frac{x}{\omega \xi} \right)^\sigma \right. \\ &\quad \left. \times {}_2F_1 \left(\sigma, \sigma + \theta, 1 + \sigma, -\frac{x}{\omega \xi} \right) \right]^k\end{aligned}\tag{B.8}$$

Now, using the transformation formula for hypergeometric function [5, 9.131.1], (B.8) can be rewritten as

$$F_{\xi_{\text{eq}}}(x) = \sum_{k=1}^K \binom{K}{k} \frac{(-1)^{k+1}}{(\sigma \mathcal{B}(\sigma, \theta))^k} \left(\frac{x}{x + \omega \xi} \right)^{\sigma k} \left[{}_2F_1 \left(\sigma, -(\theta - 1); 1 + \sigma; \frac{x}{x + \omega \xi} \right) \right]^k\tag{B.9}$$

Now, because its second argument is a negative integer, the hypergeometric function in (B.9) truncates after the θ -th term. Thus, it can be conveniently written as a finite series as follows:

$${}_2F_1 \left(\sigma, -(\theta - 1); 1 + \sigma; \frac{x}{x + \omega \xi} \right) = \sum_{j=0}^{\theta-1} \delta_j \left(\frac{x}{x + \omega \xi} \right)^j\tag{B.10}$$

where δ_j is given by

$$\delta_j = (-1)^j \binom{\theta - 1}{j} \left(\frac{\sigma}{\sigma + j} \right).$$

Now substituting (B.10) in (B.9), the k -th power of the sum in (B.10) needs to be computed. Note that this product results in a polynomial of degree $k(\theta - 1)$, where the polynomial coefficients can be computed as a convolution sum of the individual coefficients. With this, the polynomial representation becomes

$$\left[\sum_{j=0}^{\theta-1} \delta_j \left(\frac{x}{x + \omega \bar{\xi}} \right)^j \right]^k = \sum_{m=0}^{n^\dagger} \kappa_m \left(\frac{x}{x + \omega \bar{\xi}} \right)^m \quad (\text{B.11})$$

where $n^\dagger = k(\theta - 1)$ and κ_m are the polynomial coefficients computed using convolution. Now substituting (B.11) into (B.9), (4.38) is obtained.

B.5 Proof of Proposition 9

Proof. By averaging the instantaneous capacity over the e2e SIR PDF in (4.39), ergodic capacity can be written as

$$\tilde{C} = \frac{1}{K \ln 2} \sum_{k=1}^K \binom{K}{k} \frac{(-1)^{k+1}}{(\sigma \mathcal{B}(\sigma, \theta))^k} \sum_{m=0}^{n^\dagger} (n+1) \kappa_m I_n(a) \quad (\text{B.12})$$

where $n = m + \sigma k - 1$, $a = \omega \bar{\xi}$, and $I_n(a)$ is given by

$$I_n(a) = \int_0^\infty \ln(1 + ax) \frac{x^n}{(x+1)^{n+2}} dx \quad (\text{B.13})$$

where $a > 1$. To develop closed-form $I_n(a)$, (B.13) is transformed as a Mellin integral [118]

$$I_n(a) = \frac{1}{2\pi j} \int_{c-j\infty}^{c+j\infty} \underbrace{\frac{\Gamma(s)\Gamma(1+s)\Gamma(1-s)\Gamma(n+1-s)}{sa^s\Gamma(n+2)}}_{=F(s)} ds \quad (\text{B.14})$$

where $-1 < c < 0$. For future use, integration path $\mathcal{C}_1 = c + jx, -\infty < x < \infty$ is defined. In order to exactly evaluate (B.14), complex contour integration technique is used. The following is the main tool needed. Let $f(z)$ be a complex function which is analytic inside and on a closed curve \mathcal{C} except for a countable numbers of singularities inside \mathcal{C} at z_1, z_2, \dots . The residue theorem establishes the value of the counter clockwise line integral

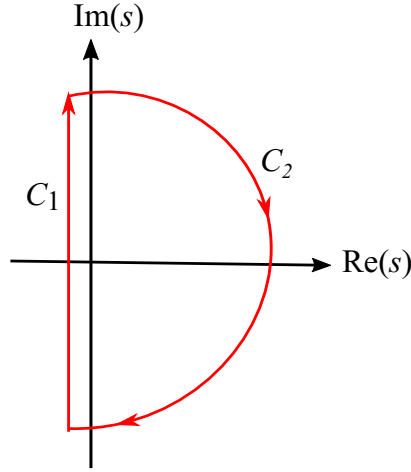


Figure B.1: Integration contour.

of $f(z)$ over \mathcal{C} as follows:

$$\frac{1}{2\pi i} \oint_{\mathcal{C}} f(z) dz = \sum_{k=1}^n \text{Res}_{z=z_k} f(z) \quad (\text{B.15})$$

where an l -th order residue at $z = a$ is given by

$$\text{Res}_{z=a} = \lim_{z \rightarrow a} \left[\frac{1}{(l-1)!} \frac{d^{l-1}}{dz^{l-1}} ((z-a)^l f(z)) \right]. \quad (\text{B.16})$$

To apply (B.15) to evaluate $I_n(a)$, a closed contour \mathcal{C} must be chosen first. The vertical integration line in (B.14) can be closed by an infinite radius semi-circle on the right half plane (Fig. B.1). Thus, $\mathcal{C} = \mathcal{C}_1 \cup \mathcal{C}_2$ where $\mathcal{C}_2 = re^{\theta}$ with $r \rightarrow \infty$ and $-\pi/2 \leq \theta \leq \pi/2$. Inside \mathcal{C} , $F(s)$ has infinite number of poles. The residues must be summed together according to (B.15). However, the line integral is in clockwise direction. Thus, $I_n(a)$ can be written as

$$I_n(a) = - \sum_{k=0}^{\infty} \text{Res}_{s=k} F(s). \quad (\text{B.17})$$

Since $F(s)$ contains several $\Gamma(\cdot)$ terms, an understanding of the poles of $\Gamma(s)$ itself is warranted. By using integration by parts, it can be shown that $\Gamma(s) = \int_1^{\infty} t^{s-1} e^{-t} dt + \sum_{k=0}^{\infty} \frac{1}{k!(s+k)}$. This expression shows that $\Gamma(s)$ has first order poles at $s = 0, -1, -2, \dots$. By adapting this fact, next, all the residues of $F(s)$ are evaluated systematically. There are three cases to be considered:

1. **The pole at $s = 0$.** This is a second order pole. To see that, note that near $s = 0$,

$F(s) \approx \frac{c\Gamma(s)}{s}$ where c is a constant. Thus, since $\Gamma(s)$ has a first-order pole at $s = 0$, $F(s)$ has a second order pole. The residue of this pole are evaluated using (B.16) to give

$$\text{Res}_{s=0} F(s) = - \left[\frac{\Psi(n+1) + \gamma + \ln(a)}{n+1} \right]$$

where $\Psi(z) = \frac{d}{dz} \ln \Gamma(z)$ is the Digamma function.

2. **The poles at $s = 1, 2, \dots, n$.** These are generated from $\Gamma(1-s)$ and they do not coincide with any other poles. Hence, they are first-order poles. Thus, this is evaluated using (B.16) to give for $k = 1, 2, \dots, n$,

$$\text{Res}_{s=k} F(s) = (-1)^k \left[\frac{\Gamma(k+1)\Gamma(n+1-k)}{ka^k\Gamma(n+2)} \right].$$

3. **The poles at $s = n+1, n+2, \dots$.** These are second-order poles due to the product $\Gamma(1-s)\Gamma(n+1-s)$. Their residues are evaluated using (B.16) as

$$\text{Res}_{s=k} F(s) = \lim_{s \rightarrow k} \frac{d}{ds} (s-k)^2 F(s) \quad k = n+1, \dots$$

By simplifying this, the residues for $k = n+1, n+2, \dots$ are given by

$$\text{Res}_{s=k} F(s) = \frac{(-1)^n \Gamma(k) [\Psi(k) - \Psi(k-n) - \ln a]}{a^k \Gamma(k-n) \Gamma(n+2)}.$$

By adding all the residues in (B.17), $I_n(a)$ is written as

$$\begin{aligned} I_n(a) = & \left[\frac{\Psi(n+1) + \gamma + \ln(a)}{n+1} \right] + \sum_{k=1}^n (-1)^{k+1} \frac{\Gamma(k+1)\Gamma(n+1-k)}{ka^k\Gamma(n+2)} \\ & + (-1)^{n+1} \sum_{k=n+1}^{\infty} \frac{\Gamma(k) [\Psi(k) - \Psi(k-n) - \ln a]}{a^k \Gamma(k-n) \Gamma(n+2)}. \end{aligned} \quad (\text{B.18})$$

The sum index k in the second sum is replaced by $k+n+1$ and the three Gamma terms by a binomial coefficient. Thus, (63) can be further simplified as

$$I_n(a) = \left[\frac{\Psi(n+1) + \gamma + \ln(a)}{n+1} \right] + \sum_{k=1}^n (-1)^{k+1} \frac{\Gamma(k+1)\Gamma(n+1-k)}{ka^k\Gamma(n+2)}$$

$$+ \frac{(-1)^{n+1}}{n+1} \sum_{k=0}^{\infty} \binom{n+k}{k} \frac{[\Psi(k+n+1) - \Psi(k+1) - \ln a]}{a^{k+n+1}}. \quad (\text{B.19})$$

Since it is known that $\sum_{k=0}^{\infty} \binom{n+k}{k} x^k = \frac{1}{(1-x)^{n+1}}$ for $|x| < 1$, (B.19) can be further simplified as

$$I_n(a) = \left[\frac{\sum_{k=1}^n \frac{1}{k} + \ln(a)}{n+1} \right] + \frac{(-1)^n}{n+1} \frac{\ln(a)}{(a-1)^{n+1}} + \sum_{k=1}^n (-1)^{k+1} \frac{\Gamma(k+1)\Gamma(n+1-k)}{ka^k\Gamma(n+2)} + \frac{(-1)^{n+1}}{n+1} \sum_{k=0}^{\infty} \binom{n+k}{k} \frac{[\Psi(k+n+1) - \Psi(k+1)]}{a^{k+n+1}}. \quad (\text{B.20})$$

Since $\Gamma(z+1) = z\Gamma(z)$, it can be obtained that $\ln \Gamma(z+1) = \ln z + \ln \Gamma(z)$. Thus, by differentiating this, it is given that $\Psi(z+1) = \frac{1}{z} + \Psi(z)$. Then by repeatedly applying this recursion, it is found that $\Psi(k+n+1) = \Psi(k+1) + \sum_{l=1}^n \frac{1}{k+l}$. By using this, (B.20) can be further simplified as

$$I_n(a) = \left[\frac{\sum_{k=1}^n \frac{1}{k} + \ln(a)}{n+1} \right] + \frac{(-1)^n}{n+1} \frac{\ln(a)}{(a-1)^{n+1}} + \sum_{k=1}^n (-1)^{k+1} \frac{\Gamma(k+1)\Gamma(n+1-k)}{ka^k\Gamma(n+2)} + \frac{(-1)^{n+1}}{n+1} \sum_{k=0}^{\infty} \binom{n+k}{k} \frac{[\sum_{l=1}^n \frac{1}{k+l}]}{a^{k+n+1}}. \quad (\text{B.21})$$

Note that $\frac{1}{k+l} = \int_0^1 t^{l+k-1} dt$, by substituting this in the infinite sum of (B.21), it is found that

$$\begin{aligned} \sum_{k=0}^{\infty} \binom{n+k}{k} \frac{1}{a^{k+n+1}} &= \int_0^1 t^{l-1} \sum_{k=0}^{\infty} \binom{n+k}{k} \frac{t^k}{a^{k+n+1}} dt \\ &\stackrel{(a)}{=} \int_0^1 \frac{t^{l-1}}{(a-t)^{n+1}} dt \\ &\stackrel{(b)}{=} \frac{1}{la^{n+1}} {}_2F_1 \left(n+1, l; l+1; \frac{1}{a} \right) \\ &\stackrel{(c)}{=} \frac{(a-1)^{-l}}{la^{n+1-l}} {}_2F_1 \left(l, l-n; l+1; \frac{1}{1-a} \right) \\ &\stackrel{(d)}{=} \frac{(a-1)^{-l}}{la^{n+1-l}} \sum_{j=0}^{n-l} (-1)^j \binom{n-l}{j} \frac{l}{(l+j)(1-a)^j} \end{aligned} \quad (\text{B.22})$$

where in (a), the binomial expansion for a negative integer power is used, (b) is obtained

from [5, 3.194.1], (c) is due to transformation formula for hypergeometric function [5, 9.131.1], and (d) follows from the fact that the hypergeometric series ${}_2F_1(\alpha, \beta; \gamma; z)$ terminates if either α or β is a nonpositive integer: ${}_2F_1(\alpha, -m; \gamma; z) = \sum_{j=0}^m (-1)^j \binom{m}{j} \frac{(\alpha)_j}{(\gamma)_j} z^j$ where $(q)_j = \frac{\Gamma(q+j)}{\Gamma(q)}$ is the Pochhammer symbol. Now, by substituting (B.22) in (B.21), $I_n(a)$ is given by

$$\begin{aligned}
I_n(a) = & \left[\frac{\sum_{k=1}^n \frac{1}{k} + \ln(a)}{n+1} \right] + \frac{(-1)^n}{n+1} \frac{\ln(a)}{(a-1)^{n+1}} \sum_{k=1}^n (-1)^{k+1} \frac{\Gamma(k+1)\Gamma(n+1-k)}{ka^k\Gamma(n+2)} \\
& + \frac{(-1)^{n+1}}{n+1} \sum_{l=1}^n \frac{(a-1)^{-l}}{la^{n+1-l}} \sum_{j=0}^{n-l} (-1)^j \binom{n-l}{j} \frac{l}{(l+j)(1-a)^j}. \tag{B.23}
\end{aligned}$$

Finally, substituting (B.23) in (B.12), (4.40) is obtained. ■

~

Bibliography

- [1] Ericsson Inc., “Ericsson Mobility Report,” Nov. 2018. [Online]. Available: <https://www.ericsson.com/assets/local/mobility-report/documents/2018/ericsson-mobility-report-november-2018.pdf>
- [2] E. Dahlman, S. Parkvall, and J. Skold, *5G NR: The Next Generation Wireless Access Technology*. Academic Press, 2018.
- [3] T. Bai and R. W. Heath, “Coverage and rate analysis for millimeter-wave cellular networks,” *IEEE Trans. Wireless Commun.*, vol. 14, no. 2, pp. 1100–1114, Feb. 2015.
- [4] J. G. Andrews, T. Bai, M. N. Kulkarni, A. Alkhateeb, A. K. Gupta, and R. W. Heath, “Modeling and analyzing millimeter wave cellular systems,” *IEEE Trans. Commun.*, vol. 65, no. 1, pp. 403–430, Jan. 2017.
- [5] I. S. Gradshteyn and I. M. Ryzhik, *Table of Integrals, Series, and Products*. Academic press, 2014.
- [6] Z. Pi and F. Khan, “An introduction to millimeter-wave mobile broadband systems,” *IEEE Commun. Mag.*, vol. 49, no. 6, pp. 101–107, June 2011.
- [7] S. Sesia, M. Baker, and I. Toufik, *LTE-The UMTS Long Term Evolution: From Theory to Practice*. John Wiley & Sons, 2011.
- [8] 3GPP, “Technical specification group services and system aspects; release 15 description; summary of rel-15 work items (Release 15),” in *3GPP TR 21.915 V0.6.0, Tech Rep.*, Feb. 2019.
- [9] J. G. Andrews, S. Buzzi, W. Choi, S. V. Hanly, A. Lozano, A. C. Soong, and J. C. Zhang, “What will 5G be?” *IEEE J. Sel. Areas Commun.*, vol. 32, no. 6, pp. 1065–1082, Jun. 2014.

- [10] C.-X. Wang, F. Haider, X. Gao, X.-H. You, Y. Yang, D. Yuan, H. Aggoune, H. Haas, S. Fletcher, and E. Hepsaydir, “Cellular architecture and key technologies for 5G wireless communication networks,” *IEEE Commun. Mag.*, vol. 52, no. 2, pp. 122–130, Feb. 2014.
- [11] T. Kim, J. Park, J.-Y. Seol, S. Jeong, J. Cho, and W. Roh, “Tens of Gbps support with mmwave beamforming systems for next generation communications,” in *Proc. IEEE Globecom*, 2013, pp. 3685–3690.
- [12] International Telecommunication Union, “IMT vision–framework and overall objectives of the future development of IMT for 2020 and beyond,” *Recommendation ITU-R M.2083-0*, Sep. 2015.
- [13] F. Boccardi, R. W. Heath, A. Lozano, T. L. Marzetta, and P. Popovski, “Five disruptive technology directions for 5G,” *IEEE Commun. Mag.*, vol. 52, no. 2, pp. 74–80, Feb. 2014.
- [14] N. Bhushan, J. Li, D. Malladi, R. Gilmore, D. Brenner, A. Damnjanovic, R. Sukhavasi, C. Patel, and S. Geirhofer, “Network densification: the dominant theme for wireless evolution into 5G,” *IEEE Commun. Mag.*, vol. 52, no. 2, pp. 82–89, Feb. 2014.
- [15] A. Ghosh, N. Mangalvedhe, R. Ratasuk, B. Mondal, M. Cudak, E. Visotsky, T. A. Thomas, J. G. Andrews, P. Xia, H. S. Jo *et al.*, “Heterogeneous cellular networks: From theory to practice,” *IEEE Commun. Mag.*, vol. 50, no. 6, Jun 2012.
- [16] E. G. Larsson, O. Edfors, F. Tufvesson, and T. L. Marzetta, “Massive mimo for next generation wireless systems,” *IEEE Commun. Mag.*, vol. 52, no. 2, pp. 186–195, Feb. 2014.
- [17] T. Rappaport, R. Heath, R. Daniels, and J. Murdock, *Millimeter Wave Wireless Communications*. Prentice Hall, 2015.
- [18] W. Roh, J.-Y. Seol, J. Park, B. Lee, J. Lee, Y. Kim, J. Cho, K. Cheun, and F. Aryanfar, “Millimeter-wave beamforming as an enabling technology for 5G cellular communications: theoretical feasibility and prototype results,” *IEEE Commun. Mag.*, vol. 52, no. 2, pp. 106–113, Feb. 2014.
- [19] T. S. Rappaport, S. Sun, R. Mayzus, H. Zhao, Y. Azar, K. Wang, G. N. Wong, J. K. Schulz, M. Samimi, and F. Gutierrez, “Millimeter wave mobile communications for 5G cellular: It will work!” *IEEE Access*, vol. 1, pp. 335–349, May 2013.

- [20] S. Rangan, T. S. Rappaport, and E. Erkip, “Millimeter-wave cellular wireless networks: Potentials and challenges,” *Proc. of the IEEE*, vol. 102, no. 3, pp. 366–385, Mar. 2014.
- [21] S. Han, I. Chih-Lin, Z. Xu, and C. Rowell, “Large-scale antenna systems with hybrid analog and digital beamforming for millimeter wave 5G,” *IEEE Commun. Mag.*, vol. 53, no. 1, pp. 186–194, Jan. 2015.
- [22] T. S. Rappaport, G. R. MacCartney, M. K. Samimi, and S. Sun, “Wideband millimeter-wave propagation measurements and channel models for future wireless communication system design,” *IEEE Trans. Commun.*, vol. 63, no. 9, pp. 3029–3056, Sep. 2015.
- [23] IEEE Standard Association, “Amendment 2: Millimeter-wave-based Alternative Physical Layer Extension,” in *Part 15.3: Wireless Medium Access Control (MAC) and Physical Layer (PHY) Specifications for High Rate Wireless Personal Area Networks (WPANs)*, Oct. 2009.
- [24] ———, “IEEE 802.11ad, Amendment 3: Enhancements for Very High Throughput in the 60 GHz Band,” in *Part 11: Wireless LAN Medium Access Control (MAC) and Physical Layer (PHY) Specifications*, Dec. 2012.
- [25] J. Hoydis, M. Kobayashi, and M. Debbah, “Green small-cell networks: A cost- and energy-efficient way of meeting the future traffic demands,” *IEEE Veh. Technol. Mag.*, vol. 6, no. 1, pp. 37–43, Mar. 2011.
- [26] J. N. Laneman, D. N. Tse, and G. W. Wornell, “Cooperative diversity in wireless networks: Efficient protocols and outage behavior,” *IEEE Trans. Inf. Theory*, vol. 50, no. 12, pp. 3062–3080, Dec. 2004.
- [27] Y. Jing and H. Jafarkhani, “Single and multiple relay selection schemes and their achievable diversity orders,” *IEEE Trans. Wireless Commun.*, vol. 8, no. 3, pp. 1414–1423, Mar. 2009.
- [28] S. Atapattu, Y. Jing, H. Jiang, and C. Tellambura, “Relay selection and performance analysis in multiple-user networks,” *IEEE J. Sel. Areas Commun.*, vol. 31, no. 8, pp. 1517–1529, Aug. 2013.
- [29] 3GPP, “Technical specification group radio access network; evolved universal terrestrial radio access (E-UTRA); relay radio transmission and reception (Release 14),” in *3GPP TS 36.116 V14.0.0, Tech Rep.*, Mar. 2017.

- [30] Z. Ding, X. Lei, G. K. Karagiannidis, R. Schober, J. Yuan, and V. K. Bhargava, "A survey on non-orthogonal multiple access for 5G networks: Research challenges and future trends," *IEEE J. Sel. Areas Commun.*, vol. 35, no. 10, pp. 2181–2195, Oct. 2017.
- [31] Z. Ding, M. Peng, and H. V. Poor, "Cooperative non-orthogonal multiple access in 5G systems," *IEEE Commun. Lett.*, vol. 19, no. 8, pp. 1462–1465, Aug. 2015.
- [32] ComSoc Technology Blog. Huawei and NTT Docomo "5G" mmWave field trial in Tokyo. [Online]. Available: <http://techblog.comsoc.org/2017/12/07/huawei-and-ntt-docomo-5g-mmwave-field-trial-in-downtown-tokyo/>
- [33] Y. Jing, "A relay selection scheme for two-way amplify-and-forward relay networks," in *Proc. 2009 Int. Conf. on Wireless Commun. Signal Process., (WCSP)*, Nov. 2009, pp. 1–5.
- [34] G. Wang, F. Gao, W. Chen, and C. Tellambura, "Channel estimation and training design for two-way relay networks in time-selective fading environments," *IEEE Trans. Wireless Commun.*, vol. 10, no. 8, pp. 2681–2691, Aug. 2011.
- [35] G. Wang, F. Gao, Y.-C. Wu, and C. Tellambura, "Joint CFO and channel estimation for OFDM-based two-way relay networks," *IEEE Trans. Wireless Commun.*, vol. 10, no. 2, pp. 456–465, Feb. 2011.
- [36] S. Atapattu, Y. Jing, H. Jiang, and C. Tellambura, "Relay selection schemes and performance analysis approximations for two-way networks," *IEEE Trans. Commun.*, vol. 61, no. 3, pp. 987–998, Mar. 2013.
- [37] S. S. Ikki and M. H. Ahmed, "Performance analysis of adaptive decode-and-forward cooperative diversity networks with best-relay selection," *IEEE Trans. Commun.*, vol. 58, no. 1, pp. 68–72, Jan. 2010.
- [38] D. Senaratne and C. Tellambura, "Unified exact performance analysis of two-hop amplify-and-forward relaying in Nakagami fading," *IEEE Trans. Veh. Technol.*, vol. 59, no. 3, pp. 1529–1534, Mar. 2010.
- [39] G. Amarasuriya, M. Ardakani, and C. Tellambura, "Output-threshold multiple-relay-selection scheme for cooperative wireless networks," *IEEE Trans. Veh. Technol.*, vol. 59, no. 6, pp. 3091–3097, Jul. 2010.

- [40] X. Gong, S. A. Vorobyov, and C. Tellambura, "Joint bandwidth and power allocation with admission control in wireless multi-user networks with and without relaying," *IEEE Trans. Signal Process.*, vol. 59, no. 4, pp. 1801–1813, Apr. 2011.
- [41] V. N. Q. Bao, T. Q. Duong, and C. Tellambura, "On the performance of cognitive underlay multihop networks with imperfect channel state information," *IEEE Trans. Commun.*, vol. 61, no. 12, pp. 4864–4873, Dec. 2013.
- [42] H. Wang, S. Ma, and T.-S. Ng, "On performance of cooperative communication systems with spatial random relays," *IEEE Trans. Commun.*, vol. 59, no. 4, pp. 1190–1199, Apr. 2011.
- [43] H. Wang, S. Ma, T.-S. Ng, and H. V. Poor, "A general analytical approach for opportunistic cooperative systems with spatially random relays," *IEEE Trans. Wireless Commun.*, vol. 10, no. 12, pp. 4122–4129, Dec. 2011.
- [44] S. Biswas, S. Vuppala, J. Xue, and T. Ratnarajah, "On the performance of relay aided millimeter wave networks," *IEEE J. Sel. Topics Signal Process.*, vol. 10, no. 3, pp. 576–588, Apr. 2016.
- [45] M. O. Hasna and M.-S. Alouini, "Outage probability of multihop transmission over Nakagami fading channels," *IEEE Commun. Lett.*, vol. 7, no. 5, pp. 216–218, May 2003.
- [46] S. S. Ikki and S. Aissa, "Multihop wireless relaying systems in the presence of cochannel interferences: Performance analysis and design optimization," *IEEE Trans. Veh. Technol.*, vol. 61, no. 2, pp. 566–573, Feb. 2012.
- [47] V. A. Aalo, G. P. Efthymoglou, T. Soithong, M. Alwakeel, and S. Alwakeel, "Performance analysis of multi-hop amplify-and-forward relaying systems in Rayleigh fading channels with a Poisson interference field," *IEEE Trans. Wireless Commun.*, vol. 13, no. 1, pp. 24–35, Jan. 2014.
- [48] J. Qiao, L. X. Cai, and X. Shen, "Multi-hop concurrent transmission in millimeter wave WPANs with directional antenna," in *Proc. IEEE Int. Conf. on Commun. (ICC)*, June 2010, pp. 1–5.
- [49] J. Kim and A. F. Molisch, "Quality-aware millimeter-wave device-to-device multi-hop routing for 5G cellular networks," in *proc. IEEE Int. Conf. on Commun. (ICC)*, June 2014, pp. 5251–5256.

- [50] B. Sahoo, C.-H. Yao, and H.-Y. Wei, "Millimeter-wave multi-hop wireless backhauling for 5G cellular networks," in *85th Veh. Tech. Conf. (VTC)*. IEEE, June 2017.
- [51] J. García-Rois, F. Gómez-Cuba, M. R. Akdeniz, F. J. González-Castaño, J. C. Burguillo, S. Rangan, and B. Lorenzo, "On the analysis of scheduling in dynamic duplex multihop mmwave cellular systems," *IEEE Trans. Wireless Commun.*, vol. 14, no. 11, pp. 6028–6042, Nov. 2015.
- [52] X. Lin and J. G. Andrews, "Connectivity of millimeter wave networks with multi-hop relaying," *IEEE Wireless Commun. Lett.*, vol. 4, no. 2, pp. 209–212, Apr. 2015.
- [53] O. Semiari, W. Saad, M. Bennis, and Z. Dawy, "Inter-operator resource management for millimeter wave, multi-hop backhaul networks," *IEEE Trans. Wireless Commun.*, vol. 16, no. 8, pp. 5258–5272, Aug. 2017.
- [54] H. Miao and M. Faerber, "Self-organized multi-hop millimeter-wave backhaul network: Beam alignment and dynamic routing," in *proc. IEEE Europ. Conf. on Networks and Commun. (EuCNC)*, June 2015, pp. 275–279.
- [55] A. Chelli, K. Kansanen, M.-S. Alouini, and I. Balasingham, "On bit error probability and power optimization in multihop millimeter wave relay systems," *IEEE Access*, vol. 6, pp. 3794–3808, Jan. 2018.
- [56] L. Dai, B. Wang, Y. Yuan, S. Han, I. Chih-Lin, and Z. Wang, "Non-orthogonal multiple access for 5G: solutions, challenges, opportunities, and future research trends," *IEEE Commun. Mag.*, vol. 53, no. 9, pp. 74–81, Sep. 2015.
- [57] Y. Saito, Y. Kishiyama, A. Benjebbour, T. Nakamura, A. Li, and K. Higuchi, "Non-orthogonal multiple access (NOMA) for cellular future radio access," in *77th IEEE VTC-Spring*. IEEE, 2013, pp. 1–5.
- [58] Z. Ding, P. Fan, and H. V. Poor, "Random beamforming in millimeter-wave NOMA networks," *IEEE Access*, vol. 5, pp. 7667–7681, Feb. 2017.
- [59] K. Belbase, Z. Zhang, H. Jiang, and C. Tellambura, "Coverage analysis of millimeter wave decode-and-forward networks with best relay selection," *IEEE Access*, vol. 6, pp. 22 670–22 683, 2018.
- [60] K. Belbase, C. Tellambura, and H. Jiang, "Two-way relay selection for millimeter wave networks," *IEEE Commun. Lett.*, vol. 22, no. 1, pp. 201–204, Jan. 2018.

- [61] Z. Ding, H. Dai, and H. V. Poor, "Relay selection for cooperative NOMA," *IEEE Wireless Commun. Lett.*, vol. 5, no. 4, pp. 416–419, Aug. 2016.
- [62] L. Zhang, J. Liu, M. Xiao, G. Wu, Y.-C. Liang, and S. Li, "Performance analysis and optimization in downlink NOMA systems with cooperative full-duplex relaying," *IEEE J. Sel. Areas Commun.*, vol. 35, no. 10, pp. 2398–2412, Oct. 2017.
- [63] A. Alkhateeb, O. El Ayach, G. Leus, and R. W. Heath, "Channel estimation and hybrid precoding for millimeter wave cellular systems," *IEEE J. Sel. Topics Signal Process.*, vol. 8, no. 5, pp. 831–846, Oct. 2014.
- [64] S. Singh, M. N. Kulkarni, A. Ghosh, and J. G. Andrews, "Tractable model for rate in self-backhauled millimeter wave cellular networks," *IEEE J. Sel. Areas Commun.*, vol. 33, no. 10, pp. 2196–2211, May 2015.
- [65] A. Alkhateeb, Y.-H. Nam, M. S. Rahman, J. Zhang, and R. W. Heath, "Initial beam association in millimeter wave cellular systems: Analysis and design insights," *IEEE Trans. Wireless Commun.*, vol. 16, no. 5, pp. 2807–2821, May 2017.
- [66] A. Goldsmith, *Wireless Communications*. Cambridge University Press, 2005.
- [67] M. R. Akdeniz, Y. Liu, M. K. Samimi, S. Sun, S. Rangan, T. S. Rappaport, and E. Erkip, "Millimeter wave channel modeling and cellular capacity evaluation," *IEEE J. Sel. Areas Commun.*, vol. 32, no. 6, pp. 1164–1179, June 2014.
- [68] E. Turgut and M. C. Gursoy, "Coverage in heterogeneous downlink millimeter wave cellular networks," *IEEE Trans. Commun.*, vol. 65, no. 10, pp. 4463–4477, Oct. 2017.
- [69] T. Bai, R. Vaze, and R. W. Heath, "Analysis of blockage effects on urban cellular networks," *IEEE Trans. Wireless Commun.*, vol. 13, no. 9, pp. 5070–5083, June 2014.
- [70] M. O. Hasna and M.-S. Alouini, "End-to-end performance of transmission systems with relays over Rayleigh-fading channels," *IEEE Trans. Wireless Commun.*, vol. 2, no. 6, pp. 1126–1131, Nov. 2003.
- [71] C. E. Shannon, "Two-way communication channels," in *Proc. 4th Berkeley Symp. Math. Stat. Prob.*, vol. 1. Citeseer, 1961, pp. 611–644.

- [72] M. O. Hasna and M.-S. Alouini, "End-to-end outage probability of multihop relayed transmissions over lognormal shadowed channels," *The Arabian Journ. for Sci. and Engg.*, vol. 28, no. 2C, pp. 35–44, 2003.
- [73] J. G. Andrews, F. Baccelli, and R. K. Ganti, "A tractable approach to coverage and rate in cellular networks," *IEEE Trans. Commun.*, vol. 59, no. 11, pp. 3122–3134, Nov. 2011.
- [74] M. Haenggi, J. G. Andrews, F. Baccelli, O. Dousse, and M. Franceschetti, "Stochastic geometry and random graphs for the analysis and design of wireless networks," *IEEE J. Sel. Areas Commun.*, vol. 27, no. 7, Sep. 2009.
- [75] S. N. Chiu, D. Stoyan, W. S. Kendall, and J. Mecke, *Stochastic Geometry and its Applications*. John Wiley & Sons, 2013.
- [76] M. Haenggi, *Stochastic Geometry for Wireless Networks*. Cambridge University Press, 2012.
- [77] J. F. C. Kingman, *Poisson Processes*. Clarendon Press, 1992, vol. 3.
- [78] K. Belbase, H. Jiang, and C. Tellambura, "Coverage analysis of decode-and-forward relaying in millimeter wave networks," in *Proc. IEEE Intern. Conf. on Commun. (ICC)*, May 2018.
- [79] A. Thornburg, T. Bai, and R. W. Heath Jr, "Performance analysis of outdoor mmWave ad hoc networks," *IEEE Trans. Signal Process.*, vol. 64, no. 15, pp. 4065–4079, Aug. 2016.
- [80] M. Giordani, M. Mezzavilla, and M. Zorzi, "Initial access in 5G mmwave cellular networks," *IEEE Commun. Mag.*, vol. 54, no. 11, pp. 40–47, Nov. 2016.
- [81] S. Singh, F. Ziliotto, U. Madhow, E. Belding, and M. Rodwell, "Blockage and directivity in 60 GHz wireless personal area networks: From cross-layer model to multihop MAC design," *IEEE J. Sel. Areas Commun.*, vol. 27, no. 8, pp. 1400–1413, Oct. 2009.
- [82] V. Sakarellos, D. Skraparlis, A. Panagopoulos, and J. Kanellopoulos, "Optimum placement of radio relays in millimeter-wave wireless dual-hop networks," *IEEE Antennas Propag. Mag.*, vol. 51, no. 2, pp. 190–199, Apr. 2009.

- [83] S. Wu, R. Atat, N. Mastronarde, and L. Liu, "Coverage analysis of D2D relay-assisted millimeter-wave cellular networks," in *Proc. IEEE WCNC*, 2017, pp. 1–6.
- [84] Y. Dhungana and C. Tellambura, "Outage probability of underlay cognitive relay networks with spatially random nodes," in *Proc. IEEE Globecom*, 2014, pp. 3597–3602.
- [85] A. Behnad, A. M. Rabiei, and N. C. Beaulieu, "Performance analysis of opportunistic relaying in a Poisson field of amplify-and-forward relays," *IEEE Trans. Commun.*, vol. 61, no. 1, pp. 97–107, Jan. 2013.
- [86] Z. Lin, Y. Li, S. Wen, Y. Gao, X. Zhang, and D. Yang, "Stochastic geometry analysis of achievable transmission capacity for relay-assisted device-to-device networks," in *Proc. IEEE ICC*, 2014, pp. 2251–2256.
- [87] W. Lu and M. Di Renzo, "Performance evaluation of relay-aided cellular networks by using stochastic geometry," in *Proc. 19th IEEE CAMAD Workshop*, 2014, pp. 265–269.
- [88] J. Wang, "Beam codebook based beamforming protocol for multi-Gbps millimeter-wave WPAN systems," *IEEE J. Sel. Areas Commun.*, vol. 27, no. 8, pp. 1390–1399, Oct. 2009.
- [89] E. Koyuncu, Y. Jing, and H. Jafarkhani, "Distributed beamforming in wireless relay networks with quantized feedback," *IEEE J. Sel. Areas Commun.*, vol. 26, no. 8, pp. 1429–1439, Oct. 2008.
- [90] A. Shahmansoori, G. E. Garcia, G. Destino, G. Seco-Granados, and H. Wymeersch, "5G position and orientation estimation through millimeter wave MIMO," in *IEEE Globecom Workshops*, 2015.
- [91] K. Belbase, C. Tellambura, and H. Jiang, "Coverage, capacity, and error rate analysis of multi-hop millimeter-wave decode and forward relaying," submitted to *IEEE Access*.
- [92] L. Kong, L. Ye, F. Wu, M. Tao, G. Chen, and A. V. Vasilakos, "Autonomous relay for millimeter-wave wireless communications," *IEEE J. Sel. Areas Commun.*, vol. 35, no. 9, pp. 2127–2136, Sep. 2017.

- [93] G. Yang and M. Xiao, “Performance analysis of millimeter-wave relaying: Impacts of beamwidth and self-interference,” *IEEE Trans. Commun.*, vol. 66, no. 2, pp. 589–600, Feb. 2018.
- [94] T. S. Rappaport, Y. Xing, G. R. MacCartney, A. F. Molisch, E. Mellios, and J. Zhang, “Overview of millimeter wave communications for fifth-generation (5G) wireless networks—with a focus on propagation models,” *IEEE Trans. Antennas Propag.*, vol. 65, no. 12, pp. 6213–6230, Dec. 2017.
- [95] G. K. Karagiannidis, “Performance bounds of multihop wireless communications with blind relays over generalized fading channels,” *IEEE Trans. Wireless Commun.*, vol. 5, no. 3, pp. 498–503, Mar. 2006.
- [96] T. Soithong, V. A. Aalo, G. P. Efthymoglou, and C. Chayawan, “Performance of multihop relay systems with co-channel interference in Rayleigh fading channels,” *IEEE Commun. Lett.*, vol. 15, no. 8, pp. 836–838, Aug. 2011.
- [97] G. Amarasuriya, C. Tellambura, and M. Ardakani, “Asymptotically-exact performance bounds of AF multi-hop relaying over Nakagami fading,” *IEEE Trans. Commun.*, vol. 59, no. 4, pp. 962–967, Apr. 2011.
- [98] R. Mesleh, S. S. Ikki, O. Amin, and S. Boussakta, “Analysis and optimization of AF multi-hop over Nakagami-m fading channels in the presence of CCI,” in *Proc. IEEE 24th Int. Symp. on PIMRC*, 2013, pp. 2021–2026.
- [99] A. A. AbdelNabi, F. S. Al-Qahtani, M. Shaqfeh, S. S. Ikki, and H. M. Alnuweiri, “Performance analysis of MIMO multi-hop system with TAS/MRC in Poisson field of interferers,” *IEEE Trans. Commun.*, vol. 64, no. 2, pp. 525–540, Feb. 2016.
- [100] F. E. Satterthwaite, “An approximate distribution of estimates of variance components,” *Biometrics bulletin*, vol. 2, no. 6, pp. 110–114, Dec. 1946.
- [101] B. L. Welch, “The generalization of “student’s” problem when several different population variances are involved,” *Biometrika*, vol. 34, no. 1/2, pp. 28–35, Jan. 1947.
- [102] H. Shokri-Ghadikolaei and C. Fischione, “Millimeter wave ad hoc networks: Noise-limited or interference-limited?” in *Proc. IEEE Globecom Workshops (GC Wkshps)*. IEEE, 2015, pp. 1–7.

- [103] T. Wang, A. Cano, G. B. Giannakis, and J. N. Laneman, “High-performance cooperative demodulation with decode-and-forward relays,” *IEEE Trans. Commun.*, vol. 55, no. 7, pp. 1427–1438, Jul. 2007.
- [104] M. Abramowitz and I. A. Stegun, *Handbook of Mathematical Functions: with Formulas, Graphs, and Mathematical Tables*. Courier Corp., Nov. 1964, vol. 55.
- [105] V. N. Q. Bao and H. Y. Kong, “Error probability performance for multi-hop decode-and-forward relaying over Rayleigh fading channels,” in *11th IEEE ICACT*, vol. 3, 2009, pp. 1512–1516.
- [106] A. Annamalai, C. Tellambura, and V. K. Bhargava, “Equal-gain diversity receiver performance in wireless channels,” *IEEE Trans. Commun.*, vol. 48, no. 10, pp. 1732–1745, Oct. 2000.
- [107] Wolfram Research, Inc., “Mathematica Online.” [Online]. Available: <https://www.wolfram.com>
- [108] L. Norman, S. Kotz, and N. Balakrishnan, *Continuous Univariate Distributions*. Wiley, 1995, vol. 2.
- [109] C. Tellambura, A. Annamalai, and V. K. Bhargava, “Closed form and infinite series solutions for the MGF of a dual-diversity selection combiner output in bivariate nakagami fading,” *IEEE Trans. Commun.*, vol. 51, no. 4, pp. 539–542, 2003.
- [110] C. Tellambura, “Evaluation of the exact union bound for trellis-coded modulations over fading channels,” *IEEE Trans. Commun.*, vol. 44, no. 12, pp. 1693–1699, 1996.
- [111] H. X. Nguyen, H. H. Nguyen, and T. Le-Ngoc, “Diversity analysis of relay selection schemes for two-way wireless relay networks,” *Springer Wireless Personal Communications*, vol. 59, no. 2, pp. 173–189, Jan. 2010.
- [112] L. Fenton, “The sum of log-normal probability distributions in scatter transmission systems,” *IRE Trans. Commun.*, vol. 8, no. 1, pp. 57–67, Mar. 1960.
- [113] N. M. Steen, G. D. Byrne, and E. Gelbard, “Gaussian quadratures for the integrals $\int_0^\infty \exp(-x^2)f(x)dx$ and $\int_0^b \exp(-x^2)f(x)dx$,” *Mathematics of Computation*, vol. 23, no. 107, pp. 661–671, May 1969.
- [114] Y. Zhou, V. W. Wong, and R. Schober, “Coverage and rate analysis of millimeter wave NOMA networks with beam misalignment,” *IEEE Trans. Commun.*, vol. 17, no. 12, pp. 8211–8227, Dec. 2018.

- [115] Z. Zhang, Z. Ma, M. Xiao, Z. Ding, and P. Fan, "Full-duplex device-to-device-aided cooperative nonorthogonal multiple access," *IEEE Trans. Veh. Technol.*, vol. 66, no. 5, pp. 4467–4471, May 2017.
- [116] H. Shokri-Ghadikolaei and C. Fischione, "The transitional behavior of interference in millimeter wave networks and its impact on medium access control," *IEEE Trans. Commun.*, vol. 64, no. 2, pp. 723–740, Feb. 2016.
- [117] A. Annamalai, C. Tellambura, and V. K. Bhargava, "Exact evaluation of maximal-ratio and equal-gain diversity receivers for M-ary QAM on Nakagami fading channels," *IEEE Trans. Commun.*, vol. 47, no. 9, pp. 1335–1344, Sep. 1999.
- [118] Y. Dhungana and C. Tellambura, "Uniform approximations for wireless performance in fading channels," *IEEE Trans. Commun.*, vol. 61, no. 11, pp. 4768–4779, Oct. 2013.